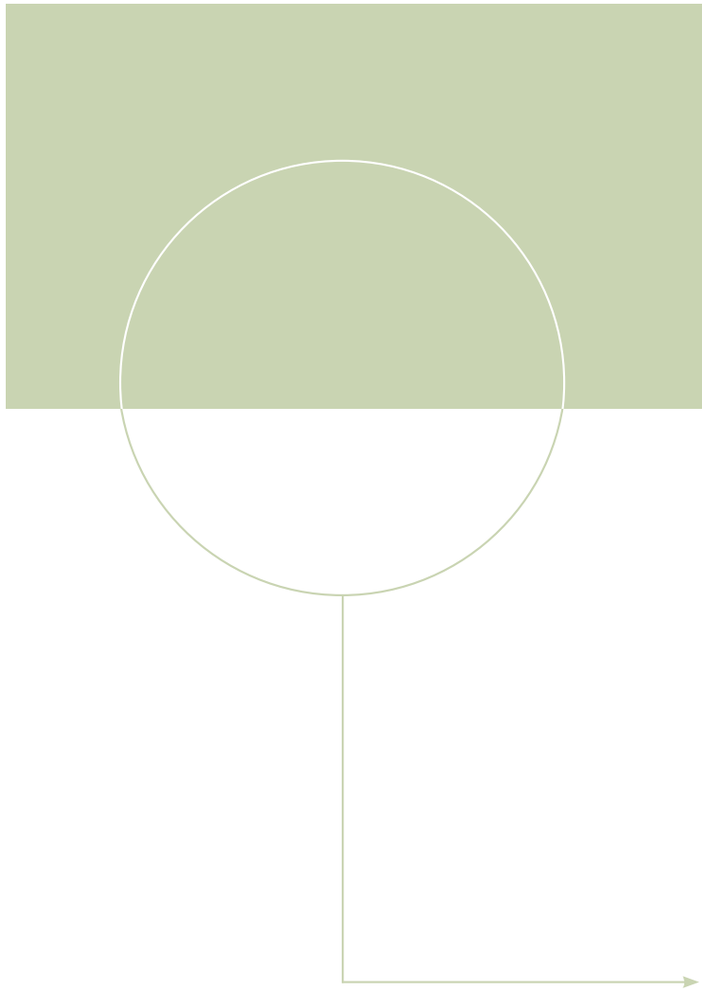

Master's thesis

2019

Sara Hegdahl Åsly

NTNU
Norwegian University of
Science and Technology
Faculty of Information Technology and Electrical
Engineering
Department of Engineering Cybernetics

Sara Hegdahl Åsly

# Supervised learning for classification of EEG signals evoked by visual exposure to RGB colors

June 2019

NTNU
Norwegian University of
Science and Technology

NTNU
Norwegian University of
Science and Technology

NTNU

Norwegian University of
Science and Technology

# Supervised learning for classification of EEG signals evoked by visual exposure to RGB colors

Sara Hegdahl Åsly

Master of Cybernetics and Robotics
Submission date: June 2019
Supervisor: Marta Molinas
Co-supervisor: Luis Alfredo Moctezuma
Alejandro A. Torres-Garcia

Norwegian University of Science and Technology
Department of Engineering Cybernetics

# *Abstract*

This thesis has investigated the possibility to classify EEG signals produced by visual exposure to red, green and blue (RGB) colors, thought to provide rapid control and decreased learning times brain-computer interface (BCI) applications. An in-house experiment with 17 participants was designed and conducted. Analytic and empirical signal analysis methods were studied using event-related potential (ERP), short time Fourier transform (STFT), and empirical mode decomposition (EMD). Two classification methods have been explored. The first method used features from intrinsic mode functions (IMFs) obtained with EMD as inputs for machine learning (ML) algorithms, reaching accuracies of 0.37 and 0.63 for a generic and subject-specific model, respectively. Classification accuracy of gray and any of the RGB colors were up to 0.99. The second method used EEG signals as input to a convolutional neural network (CNN), obtaining a maximum accuracy of 0.46 across all subjects.

All accuracies are above the chance level of 0.33 for three class classification, which indicates that the methods can partly describe the colors in EEG signals. The study concludes that generic models for classification of RGB colors are challenging, and subject-tailored models are preferred for practical applications. Although the model performances were not ideal, it is believed that the dataset collected and the results presented encourage to further research.

# *Abstract - Norwegian*

Denne masteroppgaven har undersøkt muligheten for å klassifisere EEG-signaler fremstilt av visuell eksponering for rød, grønn og blå (RGB) farge, noe som anatas å gi kort responstid og redusert læringstid for hjerne-datamaskin-grensesnitt-applikasjoner (BCI). Et eksperiment med 17 deltakere ble designet og gjennomført. Analytiske og empiriske signalanalysemetoder ble undersøkt ved hjelp av hendelsesrelatert potensial (ERP), kort Fourier-transformasjon (STFT) og *empirical mode decomposition* (EMD). To klassifikasjonsmetoder ble benyttet. Den første metoden bruker egenskaper som finnes i *intrinsic mode functions* (IMF) fra EMD som inndata til algoritmer for maskinlæring (ML), og oppnår en nøyaktighet på henholdhvis $0,37$ og $0,63$ for en generisk og individ-tilpasset modell. Klassifikasjonsnøyaktigheten mellom grå og RGB-fargene var opp til $0,99$. Den andre metoden bruker EEG-signalerer som inndata til et konvolusjonelt nevralt nettverk (CNN), og oppnår en nøyaktighet på $0,46$ over alle individer.

Alle nøyaktigheter er over 0.33, som er den tilfeldige nøyaktigheten for klassifisering av tre klasser, noe som indikerer at metodene delvis kan beskrive farger i EEG-signaler. Studien konkluderer med at generiske modeller for klassifisering av RGB-farger er utfordrende, og individ-tilpassede modeller foretrekkes for praktisk anvendelse. Selv om resultatene ikke var ideelle, vil datasettet og resultatene gi grunnlag for videre forskning.

# *Acknowledgements*

I want to express my gratitude to Marta Molinas for introducing me to the topic, and for providing excellent supervision along the way. She has given me opportunities and trust, for which I am truly grateful.

My special thanks go to Luis Alfredo Moctezuma, for regularly giving programming guidance and valuable feedback on my thesis - he deserves credit (and none of the blame). I would also like to acknowledge Alejandro A. Torres-García for his guidance and ideas. Thanks to everyone who participated in the experiment; it demands real courage to wear that electrode cap.

As always, thanks to my dad for his never-ending amusement for science, and his unique insights to my master project. His exciting experiments and intriguing questions have, and forever will, motivate me to learn new things.

Finally, with my whole heart, I thank you, Idir Berg Ould-Saada, for help with machine learning and mental motivation throughout all aspects of my master degree.

Trondheim, June 9. 2019 Sara Åsly

# *Preface*

This master thesis completes a Master of Technology at the Department of Engineering Cybernetics, Norwegian University of Science and Technology (NTNU) in the spring of 2019. The project is supervised by Professor M. Molinas (NTNU), who is responsible for concept formation and introduction to the EMD signal analysis tool. I am the lead investigator, responsible for all major areas of data collection, analysis, and manuscript composition.

The software and experiment execution referred to in Ch. 5, was done by myself with the assistance of L. A. Moctezuma and A. A. Torres-Garca. S. Rasheed (University of Milan) provided a complementary dataset. The feature extraction method in Sec. 4.2.1 is based on work by L. A. Moctezuma, who also provided feature theory. The deep learning architecture in Sec. 4.2.2 is developed by the Army Research Laboratory, adjusted to meet the requirements for our dataset.

The results in Ch. 6, and concluding analysis in Ch. 8 are my original work. State-of-the-art literature in Ch. 3 is introduced by M. Molinas, L. A. Moctezuma, A. A. Torres-Garca and myself, formulated by me. Portions of Ch. 1-2 are presented in my Semester project "The effect of RGB color stimuli on the human brain: finding a unique descriptor in EEG recordings" (NTNU, 2018). The topics are covered in my master thesis, as I believe it can be useful to perceive the full picture for new readers.

Parts of Sec. 6.3 has been published as S. Åsly, L.A. Moctezuma, M. Gilde, and M.Molinas, "Towards EEG based signals classification of RGB color based stimuli" and will be presented at the 8th Graz Brain-Computer Interface Conference 2019.

The main contribution of this thesis is experiment design, conduction, subjects recruitment, and data collection. I genuinely hope it will serve useful for future researchers addressing the topic of unique neural signature of color perception in the human brain.

I had no prior experience with EEG signals, nor data analysis when starting this project; hopefully, my master thesis reflects the variety of knowledge I have gained the past year.

# Contents

# List of Tables

# List of Figures

# Abbreviations

**API** application programming interface. 36, 38

**BCI** brain-computer interface. 1–4, 20, 21, 35, 38, 67, 68

**CNN** convolutional neural network. 19, 22, 23, 29, 30, 61, 62, 65, 68, 69, 86

**DFT** discrete Fourier transform. 11

**DL** deep learning. 19, 22, 26, 61, 69

**DT** decision tree. 18, 29

**EEG** electroencephalography. 1–3, 5, 8, 9, 11, 12, 14, 15, 17, 19–24, 26, 27, 29–31, 36–39, 42, 43, 56, 61, 67, 68

**EEMD** ensemble empirical mode decomposition. 14

**EMD** empirical mode decomposition. 3, 12–14, 21, 24, 27, 43, 50, 53–56, 60, 65, 67, 69, 70

**EMG** electromyogram. 24, 39

**EOG** electrooculogram. 24, 39

**ERP** event-related potential. 3, 10, 11, 20, 25, 43, 45, 47, 57

**ERSP** event-related spectral perturbations. 20, 21

**ESD** electrostatic discharge. 35

**FFT** fast Fourier transform. 11

**fMRI** functional magnetic resonance imaging. 5

**fNIRS** functional near-infrared spectroscopy. 20

**FT** Fourier transform. 11, 12

**GDS** g.tec Device Service. 38

**HFD** Higuchi fractal dimension. 15, 16

**HHT** Hilbert-Huang transform. 13, 14

**HT** Hilbert transform. 13

**ICA** independent component analysis. 20, 25, 43, 69

**IMF** intrinsic mode function. x, 12–15, 24, 27, 28, 43, 50–55, 60, 61, 67, 70

**k-NN** $k$-nearest neighbors. 18, 29

**LGN** lateral geniculate nucleus. 8

**ML** machine-learning. 3, 17–19, 26, 29, 67

**NB** naive Bayes. 19, 29, 58

**NN** neural network. 17, 19, 22, 24, 65, 66, 86

**OCR** optical character recognition. 22

**PFD** Petrosian fractal dimensions. 15

**RF** random forest. 18, 29, 58

**RGB** red, green and blue. 2, 3, 5, 7, 17, 20–22, 24, 27, 32, 34, 39, 40, 48, 56, 57, 60, 61, 67–69

**STFT** short time Fourier transform. 3, 12, 43, 48, 49, 67, 69

**SVM** support vector machine. 18, 20, 21, 29

# Chapter 1

# Introduction

Color vision in mammals is useful for object detection and identification during various tasks, such as recognizing ripe fruit on a tree. Humans ability to identify colors based on light waves entering the eye is a complex task, successfully solved by the human brain and the visual system.

Brain activity produces electrical activity that can be recorded from the scalp, from the cortical surface, or from within the brain. These signals can be captured with invasive or non-invasive methods, i.e., whether the sensors are set-up after a craniotomy or not [1]. Electroencephalography (EEG) has become a well-known technique for monitoring and recording brain activity, due to its high temporal resolution, relatively low cost, high portability, and few risks to the user [2]. In the field of neurology and neurophysiology, EEG is practiced in hospitals to investigate various conditions such as fainting, epilepsy, coma, personality change, sleep disorder, and after various traumas. Monitoring brain signals is considered a mature field that is now also being spun out into commercial products, that can be used for reaching mindfulness and identifying mental states [3][4].

By recording brain signals, a specific cognitive state can be sent from a person to a computer without the use of speech, gestures, or writing. A computer can then translate brain activity into desired commands for an external device or the computer itself. Such an application practiced in real time is called a brain-computer interface (BCI), and the principle is illustrated in Fig. 1.1. Brain activity is recorded with electrodes, and the signals are classified using pre-trained algorithms. A learning algorithm has to be trained to learn the properties of the different signals to detect those properties in unknown signals. Classification refers to the task of identifying to which category a new observation belongs. Trained

algorithms are, therefore, capable of separating the different mental states of the user, and can decide on which action to execute.

A BCI application can be controlled using various neuro-paradigms, such as imagining a movement or visual stimuli. Naturally, colors produce dedicated brain responses, and an intriguing question is if EEG recordings contain components capable of distinguishing colors from each other. These components could then be used to determine which color a person sees, which would allow accurate control of any electro-mechanic device. This particular area of using colors to produce the control signals for BCI applications remains unclear, and few researchers have addressed the topic, despite its simplistic nature compared to other neuro-paradigms.

The brain responds to color faster than any other stimuli. Visually evoked signals are observed as short as 200 $ms$ after stimuli, enabling quick control, as compared to slower processes such as imagined movement observed 700 $ms$ after imagining start [5]. Moreover, exposure to visual stimuli does not require the user to provoke mental actively; just let the visual system passively produce the control signals. Consequently, color controlled BCIs is thought to reduce learning times for the user.

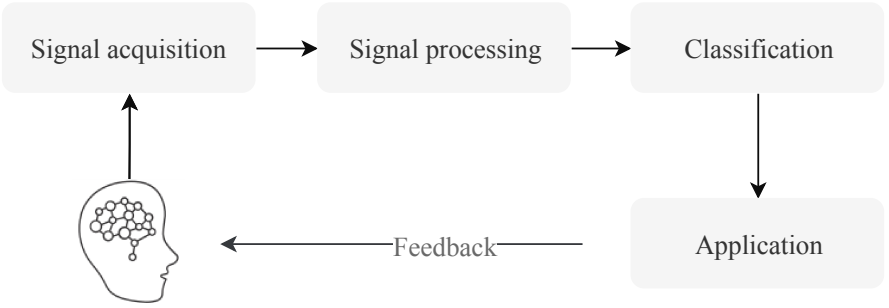


FIGURE 1.1: Design and operation of a BCI system.

## 1.1 Problem description

The overall purpose of this research is to investigate color related characteristics in EEG signals. As this research constitutes an almost new approach for working with EEG and color stimuli, the study addresses a wide range of relevant topics, such as facts about the visual system, and state-of-the-art research on the topic of color perception in the human brain. These areas are, therefore, addressed and discussed.

Using knowledge from the topics mentioned above, this works aims to classify EEG signals produced by visual stimuli to red, green and blue (RGB) color.

The problem is approached by investigating signal analysis methods, used both for visual inspection and computational methods. The methods used are event-related potential (ERP), short time Fourier transform (STFT) and empirical mode decomposition (EMD). A first step is to test if it is possible to distinguish the RGB colors from gray color, and the second step is to classify the RGB colors from each other. A variety of methods will be examined and questioned in the search for the optimal approach.

The evaluation of techniques requires a suitable dataset, consisting of EEG signals produced by subjects being exposed to RGB colors. An essential part of this work is, therefore, to design, implement, and record such a dataset.

### 1.1.1 Research Questions

The following research questions will be addressed:

1. Is it possible to distinguish EEG signals produced by red, green or blue color exposure by visual inspection of transformations (ERP, STFT and EMD) applied to the EEG signals?
2. Is it possible to distinguish between RGB colors and gray color from EEG signals using machine-learning (ML)?
3. Can information contained in EEG data be used to train ML models and efficiently differentiate between RGB colors?

### 1.1.2 Motivation

This work is the first effort towards the design of a reliable real-time classification of EEG signals produced by looking at a color, which could enable physically disabled people with cognitive functions to control their environment. Real-time classification refers to the capability to perform a classification task and give a rapid response to a user, which is required for any practical application. For instance, a user can open and close doors by looking at colored signs, as illustrated in Fig. 1.2. Even though the commercialization of a BCI application is beyond the scope of this work, it surely provides an underlying motivation.

## 1.2 Report structure

This report gives a comprehensive overview of knowledge and tools to design, execute, and analyze brain dynamics caused by visual stimuli to RGB. A selection

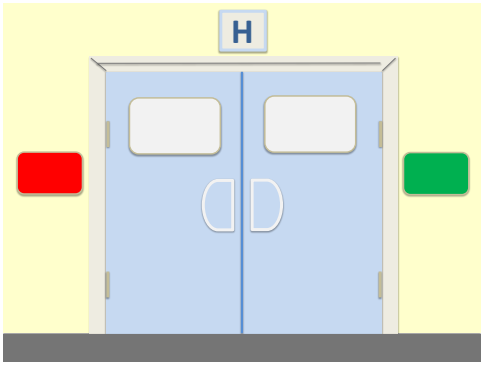


FIGURE 1.2: Example of real-time application with dedicated colored signs.

of background theory related to the visual system and the brain, as well as signal analysis methods are summed in Ch. 2. State-of-the-art research is addressed in Ch. 3. The methods used for feature extraction and classification for this project are outlined in Ch. 4. Ch. 5 presents the experimental paradigm used for data collection, as well as the hardware and software employed. In Ch. 6 the results are presented and discussed. Finally, Ch. 7 summarizes the whole thesis, and Ch. 8 concludes and provides a discussion for the next steps in the process of developing a BCI system based on color perception.

# Chapter 2

# Background

*Understanding the underlying processes in the brain is central to the discipline of brain signal experiments. The objective of this chapter* [1] *is to provide background knowledge considered useful for the design and execution of RGB experiments.*

## 2.1 The human brain and the visual system

The visual system converts light into electric signals. These signals enable a visual understanding of objects in the surroundings, while simultaneously provoke, for instance, feelings and memories. This process is an extremely complex task, far beyond the capabilities of the most advanced computer vision systems. A general understanding of how the human brain and the visual system work is necessary for both experimental design and interpreting the findings.

Information regarding the processes in the human brain can be recorded with EEG electrodes. The rest of this section is dedicated to briefly introduce the major concepts and functions of the human brain and the visual system.

### 2.1.1 The human brain

The human brain receives information from the senses and controls thoughts and movements. Technologies such as functional magnetic resonance imaging (fMRI) have been used to analyze the blood response in different areas of the brain as a result of external stimuli [7]. Such studies have enabled scientists to divide the brain into different parts and regions, according to their function. Some of the main brain regions are presented in Fig. 2.1 [8].

[1] Note that this chapter is an updated version of the background presented in the author's work described in [6]

- **Frontal lobe** (red) has mostly executive functions such as personality, emotions, higher thinking skills, and movement control.
- **Temporal lobe** (yellow), processes hearing and other senses, and helps with language and reading.
- **Parterial lobe** (blue) is involved with senses, attention, and language.
- **Occipital lobe** (green) is related to vision, including the recognition of shapes and colors.

These are just a few of the parts and functions of the brain. Other deeper parts are, for instance, controlling adrenaline and sleep. Processes are constantly happening in the brain, some of which are impossible to control.

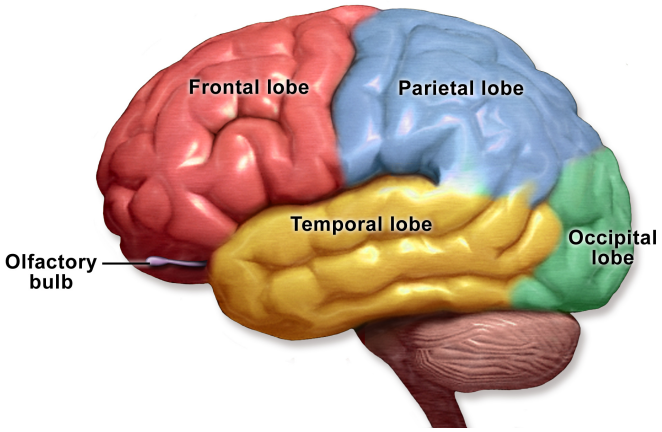


FIGURE 2.1: Main human brain regions.

#### 2.1.1.1 How brains process information

Neurons in the brain receive, processes and transmit information through electrical and chemical signals. The processing of information mostly happens in the outer layer of the brain, the cerebral cortex. The brain consists of nerve cells, called neurons. A neuron contains a cell body (soma), holding the cell nucleus. An axon and several dendrites branch out of the cell body. Neurons are connected with synapses, and when a neuron receives a potential, a movement of ions is produced throughout the membrane, which creates a current that propagates in the head. [9].

### 2.1.2 The visual system

The process of vision starts when light enters the eye through the pupil. Humans can detect light waves of different frequencies and amplitudes. The portion of the

electromagnetic spectrum the human eye can detect is called the visible spectrum and includes wavelengths in the range $380-740\,nm$ [10]. The wavelength of a light wave determines its color, and the amplitude relates to its brightens. Hence, blue light with low amplitude will appear dull, while higher amplitude and intensity will make the color look bright [11].

The main parts of the human eye are illustrated in Fig. 2.2 [12]. The iris, surrounding the pupil, contracts, or expands the pupil to control the level of illumination to enter the eye (1). Light reaches the light-sensitive tissue lining the back of the eye, called the retina, and is absorbed by photoreceptors (2). The photoreceptors transform the light energy into nerve impulses that the human brain interprets. The signal is passed to neural cells (3), moves through the optic nerve before the information is sent to the brain (5).

There exist two types of photoreceptors; rods and cones. Cones detect fine detail in color, and distinct cones are sensitive to RGB. The rods, on the other hand, are light sensitive, but do only register a scale of gray with poor resolution - and will, for instance, be used to recognize the shape of large objects in dark surroundings. The photoreceptors are all connected with synapses to the bipolar neurons which transfers information to the ganglions. The action potentials created by the ganglion cells are connected to the optic nerve, which transfers the signals to the thalamus before they continue back to the occipital lobe, where the visual cortex is located. In the context of color perception, a significant area of interest (in addition to the eye itself) is as the name suggests, the visual cortex.

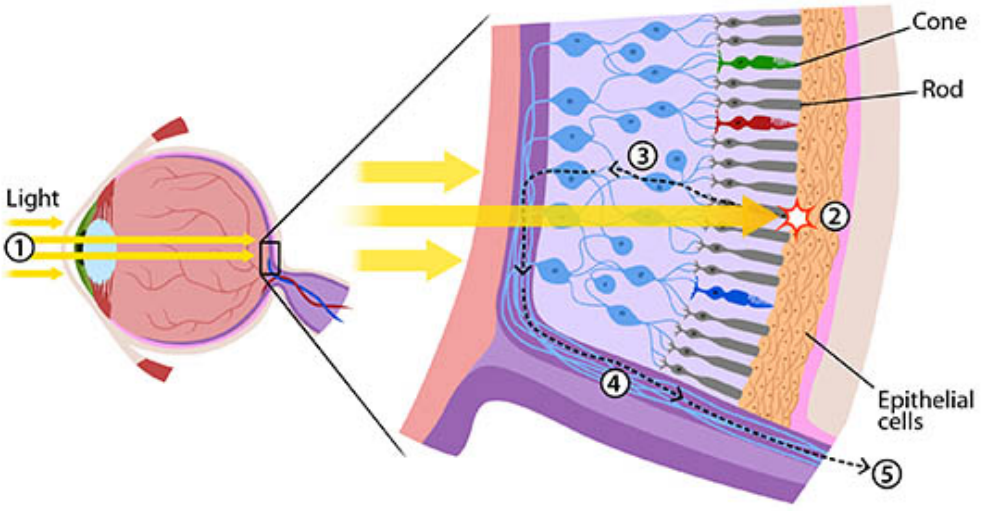


FIGURE 2.2: Working of the eye.

#### 2.1.2.1 Neural processing of the visual signal

Most of the pioneering work on the visual system was done in [13][14][15]. The following is a much-simplified version of the findings.

There are more than 100 million light receptors in each retina; still, the two optic nerves contain only 1 million fibers, and essential processing is done locally in the retina. The signal passes through bipolar and ganglion cells, before the modified signal passes through the optic nerve to the lateral geniculate nucleus (LGN) where the signal is distributed to various parts of the visual cortex [16].

A recent study by two neuroscientists shares more information about the type of processing going on in the eyeball, before transmission to the brain [17]. Visual abilities are already set up in the bipolar cells, right after the first synapse of the visual system [18]. The retina breaks the visual world into several parallel channels before transmission to the visual cortex.

The different types of ganglion cells, responsible for local processing in the retina were first described in [19]. Further research has shown that two of these ganglions are responsible for high temporal precision and high spatial acuity, in other words, speed, and *sharpness*, in primate vision [20].

**Suppression of redundant data - data compression**

It has intuitively been assumed that the visual system generates a continuous stream of images. However, it has recently been demonstrated that redundant data is suppressed to save energy by frequently forwarding image differences [17]. The visual system will not update unchanged images to the brain. The visual receptor cells become fatigued very quickly, and hence, they turn off altogether after a few seconds unless there is a change in stimuli [16].

## 2.2 Electroencephalography

The following subsections provides important terms and concepts related to EEG.

A general advantage of using EEG is the ability to examine brain activity unfolding in real time. In this project, EEG was preferred due to its relatively low cost, accessibility, and that it can easily be managed without significant arrangements and special lab setups. One can record EEG signals using wet or dry electrodes; wet electrodes require adding a conductive substance, such as a gel, while dry electrodes achieve acceptable contact without any additions, resulting in a more straightforward experiment procedure. One of the significant disadvantages of

EEG is that it is hard to figure out where in the brain the electrical activity is originated.

EEG is a well know technique for recording brain signals from the scalp [21][22]. Even though the current generated by a single neuron in the human brain is undetectable, a collection of them can produce time-dependent electric fields that are measurable via EEG electrodes. More precisely, EEG is a measure of the electric potential difference between a point on the scalp and a reference electrode. The positioning of the reference electrode is important when designing EEG experiments.

### 2.2.1 Electrode placement

Electrodes are commonly positioned on the scalp according to the international 10-20 system or the 10-10 system [23]. The numbers refer to the fact that the distance between adjacent electrodes is either 10% or 20% of the total front-back or right-left distance of the scalp [24]. Each position has identification letters to identify the lobe and a number to a corresponding hemisphere position, as shown in Tab. 2.1.

TABLE 2.1: Brain lobes and associated electrode label.

| **Electrode** | **Lobe** |
|---|---|
| F | Frontal |
| T | Temporal |
| C | Central* |
| P | Parietal |
| O | Occipital |

Electrode positions from top and side view are presented in Fig. 2.3[2]. The electrodes are labeled with the letter representing the respective brain lobe and numbered according to its position. Even numbers refer right hemisphere (blue), and odd numbers refer to the left hemisphere (red). Electrodes placed on the midline, zero, are denoted with "z" (green and black).

### 2.2.2 Frequency bands of the brain

Brain waves have been grouped according to their frequencies, referred to as the frequency bands of the brain. These frequency bands are normally sorted from lower to higher frequencies, namely delta ($\delta$), theta ($\theta$), alpha ($\alpha$), beta ($\beta$), and

[2]Illustrations used with written consent from Trans Cranial Technologies ltd

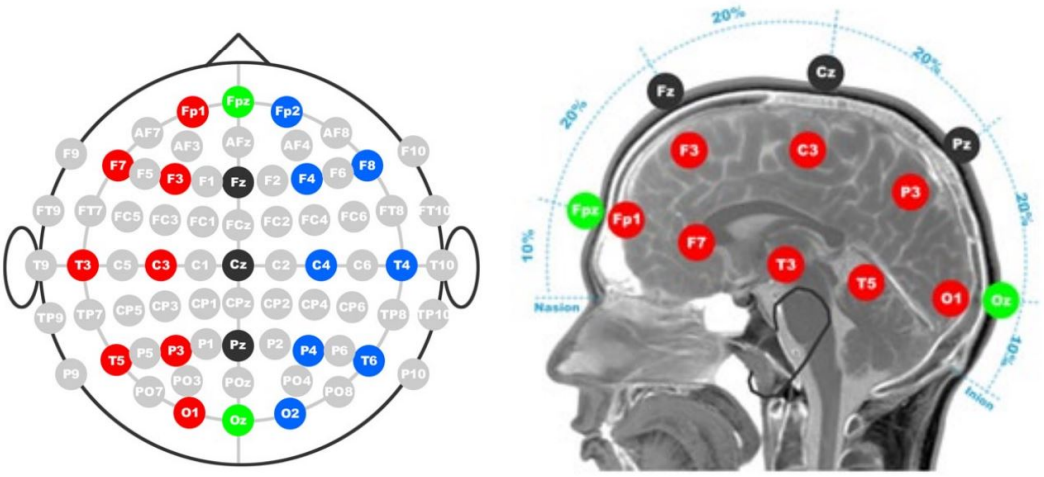


FIGURE 2.3: Top and lateral view of EEG electrode placement, according to the international 10-20 system.

gamma ($\gamma$) waves [21]. The different frequency bands are given together with their associated mental state in Tab. 2.2 [25]. Besides, when studied in more detail, different brain rhythms are related to certain cognitive processes. Delta waves are used to analyze sleep [26]. Theta waves are associated with memory and cognitive workload [27]. Alpha waves are dominant in when in a calm state, and they have been linked to inhibition and attention [28]. Beta waves are observed to be stronger during the planning or execution of movements [29]. Finally, gamma waves are associated with memory and learning [30][31].

TABLE 2.2: Frequency bands of the brain.

| **Brain rhythm** | **Frequency** | **Associated with** |
|---|---|---|
| **Delta wave** ($\delta$) | $0.5 - 4Hz$ | Deep sleep |
| **Theta wave** ($\theta$) | $4 - 8Hz$ | Day dreaming and meditation |
| **Alpha wave** ($\alpha$) | $8 - 12Hz$ | Awake, but relaxed |
| **Beta wave** ($\beta$) | $12 - 30Hz$ | Awake and thinking |
| **Gamma wave** ($\gamma$) | $> 30Hz$ | Deep focus |

### 2.2.3 Event related potentials

ERPs are small voltages that arise on the scalp as a response to specific sensory, cognitive or motor event or stimuli that are time- and phase-locked. ERPs has been used to evaluate the brain functioning and response. ERPs produces several well-known patterns, one of the most studied being the P300 peak, that occurs approximately $300\,ms$ after the stimulus onset. The P300 is one of the strongest neural signatures observable by EEG, especially when targets are presented infrequently [32].

A particular signal from one electrode is too weak and noisy to give useful information alone. Hence, it is necessary to calculate averages over a large number of instances of the same stimulus or the same task and at several locations on the scalp. In practical terms, ERP is the measured brain response, averaged over several trials of the same experiment. Brain activity not correctly synchronized to experimental events is averaged out through phase cancellation. It is important to note that averaging may mask some variability at the level of individual events.

## 2.3 Signal analysis

EEG signals are non-stationary, time-dependent, and because of cumulative electrical activity, most likely multicomponent signals [33][34]. Also, non-invasive EEG signals have a small amplitude and are extremely noisy. These properties are but a few of the reasons raw EEG signals do not provide useful information alone, and dedicated signal analysis is therefore required to extract relevant information contained within the signal. Choosing a suitable signal analysis method is a crucial step when extracting information from EEG data. In general, no particular method will provide the best results. Hence several techniques should be tested. The choice of signal analysis tool depends for instance, on the characteristics of the signal and the aim of the experiment.

### 2.3.1 Fourier transform

There is often much information contained in the frequencies of a signal, and a signal is transformed from the time domain to the frequency domain with the Fourier transform (FT). When dealing with finite sequence of equally-spaced samples, the discrete Fourier transform (DFT) is applicable. The DFT transforms a sequence of N complex numbers $x_n := x_0, x_1, ..., x_{N-1}$ into complex numbers $X_k := X_0, X_1, ..., X_{N-1}$, and is defines as [35]:

$$X_k = \sum_{n=0}^{N-1} x_n \cdot e^{\left(-\frac{2\pi i n k}{N}\right)} \tag{2.1}$$

Eq. 2.1 can be implemented in computers, and software implementations usually employ the fast Fourier transform (FFT) algorithm for faster computation. FFT computes the DFT of a signal by factorizing the DFT matrix into a product of sparse (mostly zero) factors, reducing computation complexity from $\mathcal{O}(n^2)$ to $\mathcal{O}(n \log n)$, where n is the data size.

A significant drawback of all the FT variations mentioned above is the loss of time characteristics and it is therefore not suitable for interpreting time-dependent signals. For this reason, methods based on the time-frequency domain has been developed for feature extraction in non-stationary signals.

### 2.3.2 Short time Fourier transform

STFT preserves information about the time domain by windowing the signal around a particular instant in time and calculating the local FT for each time window. The information obtained from the STFT is presented in a spectrogram. Spectrograms show how the spectral density of a signal varies with time, giving the information about the quantity of the frequency, and at what time this frequency is present.

STFT is limited due to the windowing of the signal, which causes a trade-off between time precision and frequency resolution. Frequency resolution must be sacrificed to detect an event precisely in time, and contrariety. This trade-off between time and frequency resolution makes it essential to choose an appropriate window size to optimize both time and frequency [36].

### 2.3.3 Empirical mode decomposition

EMD is a well-known technique used to analyze non-stationary and non-linear data [37]. EMD does not make assumptions regarding stationary or linearity of data, which motivates it's use for analyzing EEG data [38]. In contrast to FT and STFT, EMD is data-driven, based on the assumption that a signal consists of several intrinsic mode functions (IMFs), that must satisfy two basic conditions:

- Number of zero-crossings must equal or differ by one compared with number of extrema in the signal.
- The mean value of the upper and lower envelope of the signal must be equal to zero at any point.

The EMD algorithm finds all the IMFs through the *Sifting process*. The calculation of the IMFs given a signal $x(t)$ are done as follows [37]:

1. Identify all extrema (maxima and minima) in $x(t)$
2. Interpolate between minima and maxima, generating the upper and lower envelope; $e_{upper}$ and $e_{lower}$

3. Determine the local mean as $a(t) = \frac{e_{upper}+e_{lower}}{2}$
4. Extract the mean from the signal; $h(t) = x(t) - a(t)$
5. Decide whether it is an IMF or not based on two basic conditions for IMFs mentioned above
6. Repeat step 1 to 4 until an IMF is obtained
7. Subtract the IMF from the original signal
8. Repeat steps 1-6 until there are no IMFs left to extract, the last extraction resulting in a residue

The decomposition is complete when the sum of the IMFs and the residue is negligible. Fig. 2.4 and 2.5 visualizes the shifting process. In Fig. 2.4, the upper plot illustrates step $1-2$ in the algorithm, ie. the original signal $x(t)$ with added upper and lower splines. Step $3-4$ is illustrated in the lower plot, the original signal in red, the average (zero) signal in blue, and the residua in green. In Fig. 2.5 the successfully extracted IMF, step $5-6$ is plotted in red, and the residual in green.

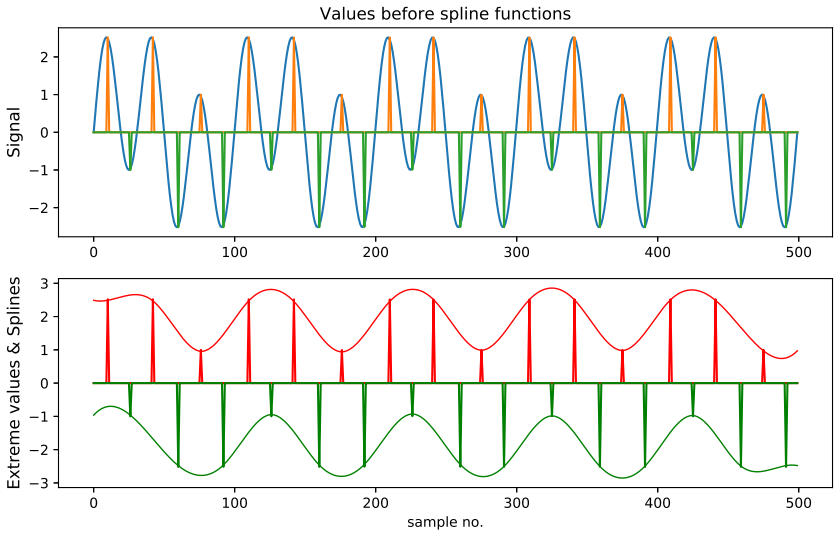


FIGURE 2.4: Illustration of the shifting process and the spline functions.

The major advantage of the EMD algorithm is that the resulting IMFs is well suited for applying the Hilbert transform (HT) to obtain physically meaningful instantaneous frequencies. This method is called the Hilbert-Huang transform (HHT) [37]. A real function $x(t)$ and its HT $H(x(t))$ create a strong analytic signal. The strong analytic signal can be written with an amplitude and a phase

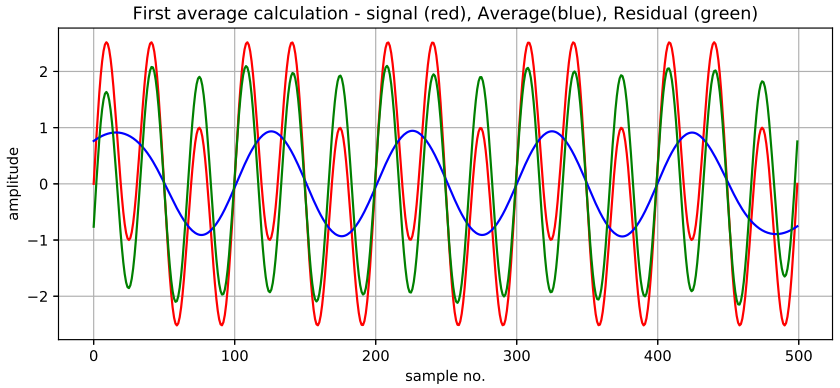


FIGURE 2.5: Extracted IMF (red), average (blue), and residual (green).

where the derivative of the phase can be identified as the instantaneous frequency. A dedicated review of the HHT is given in [39].

#### 2.3.3.1 Limitations of EMD

The end effect problem is a self-inflicted problem on EMD. Unlike the other methods previously mentioned, EMD does not use windows. The use of windows in an analysis of the signal would force the ends to zero, and therefore, mask the end effects. The end effect problem has not been taken into further account here.

Another limitation of the EMD algorithm is mode mixing, which occurs during the sifting process, and can cause the IMFs to lose their physical meaning. Mode-mixing can be summarized by (1) The IMFs contains signals of widely disparate scales and (2) signals of a similar scale reside in different IMF components. A method that can separate neighboring spectral component is proposed in [40] and in [41]. Further, the ensemble empirical mode decomposition (EEMD) algorithm [42] can be used. EEMD uses a large number of noisy signals as masking signals. It is shown that EEMD can resolve the mode mixing problem in some real-life signals. EEMD was used for this purpose in [43].

## 2.4 Feature extraction

The EEG signals are used for further analysis and feature extraction. A feature is an individual measurable property of the process being observed, and any recorded EEG activity includes different features [44]. Researchers, therefore, search for a limited amount of features that can differentiate signals with certainty. The process of selecting only a subset of variables in the input which can efficiently describe the data is called feature selection. Feature selection decreases the effect

of noise, irrelevant or redundant variables reduces, and the predictor performance improved [44][45].

Features can be extracted directly from the raw signals, as well as from the transformations or compositions of the raw signal, for instance by using techniques described in Sec. 2.3. The following sections gives a theoretical description of the features later used in this thesis.

### 2.4.1 Energy features

Energy features provide information regarding instantaneous frequency and amplitude. The instantaneous energy of a signal includes amplitude information, and is found as

$$f = log_{10}\Big(\frac{1}{N}\sum_{r=1}^{N}(IMF(r))^2\Big) \tag{2.2}$$

where $N$ is the length of the IMF, and $IMF(r)$ is the IMF coefficient of an IMF at position $r$.

The teager energy describes changes in frequency and is defined as:

$$f = log_{10}\Big(\frac{1}{N}\sum_{r=1}^{N-1}\big|(IMF(r))^2 - IMF(r-1)\cdot IMF(r+1)\big|\Big) \tag{2.3}$$

### 2.4.2 Fractal features

The fractal dimension gives a complexity index, describing how a curve, or time series such as EEG, changes depending on a scale used as a unit of measurement. There exist several types of fractal dimension, but Petrosian fractal dimensions (PFD) and Higuchi fractal dimension (HFD) have been used in this work.

The PFD translated the signals into a binary sequence and thereby provides a fast computation of the fractal dimension. The PFD is computed as:

$$PFD = \frac{log_{10}(n)}{log_{10}(n) + log_{10}\Big(\frac{n}{n+0.4N_\Delta}\Big)} \tag{2.4}$$

where $n$ is the length of the sequence and $N_\Delta$ is the number of sign changes in the binary sequence [46].

The HFD algorithm approximates the mean length of the curve using segments of k samples and estimates the dimension of a time-varying signal directly in the

time domain [47]. An N-sample data sequence $x(1), x(2), ..., x(N)$ is divided into subsets consisting of k samples:

$$X_k^m;\ X(m),\ X(m+k),\ X(m+2k),\ ...X\Big(m+\Big(\frac{N-m}{k}\Big)k\Big) \tag{2.5}$$

where $m = 1, 2, .., k$ is the initial time, the interval time is $k = 1$, ..., $k_{max}$ and $k_{max}$ is constant parameter. The length $L_m(k)$ for each sub-data set, $X_k^m$, is then computed as:

$$L_m(k) = \frac{1}{k}\left(\sum_{i=1}^{\frac{N-m}{k}} |X(m+i\,k) - X(m+(i-1)k|\right)\left(\frac{N-1}{\frac{N-m}{k}k}\right) \tag{2.6}$$

An array of mean values, $L(k)$, is computed as:

$$L_k = \frac{1}{k}\sum_{m-1}^{k} L_m(k) \tag{2.7}$$

The HFD is then the least square slope of the trajectory:

$$\text{HFD} = \frac{1}{k}\sum_{m=1}^{k} L_m(k) \tag{2.8}$$

### 2.4.3 Statistical features

Also statistical measures can be used to describe a signal. The minimum and maximum are the lowest and highest potential in the time series, respectively. The mean and the median gives information of the central tendency and the 50th—percentile of the signal amplitude. The variance and standard deviation are measures of the dispersion around the mean. Kurtosis is an outlier measure, hence the value of kurtosis for a normal distribution is zero. A kurtosis higher of less than zero indicates more or fewer outliers than a normal distribution, respectively. The skewness, or skew, is an asymmetry measure. For normally distributed data, the skewness is about zero, and a skewness greater than zero means that is more weight in the left tail of the distribution.

## 2.5 Machine learning and classification

ML is a computer's ability to adapt to new circumstances and detect and extrapolate patterns. RGB exposure is hypothesized to provoke patterns in recorded EEG signals, making the use of ML a possibly suitable technique for revealing these patterns. The following section describes the concept of ML and introduces some classification algorithms. The presented information is primarily based on the theory described in [48].

### 2.5.1 Forms of learning

Learning can be supervised, unsupervised, or a combination of these. Features of an observed instance are here referred to as the input, and the label of the class is the output. In this project, the inputs are the signal or the features extracted from the signal, and the output is either red, green, or blue. In supervised learning, example input-output pairs are observed and map a function from input to output. In unsupervised learning, patterns are learned based only on input. As these projects concerned only labeled data, it is a problem for supervised learning. In supervised learning, a classification algorithm will learn a function that predicts the output for new inputs. Given a training set of $N$ input-output example pairs $x_1$, $y_1$), ($x_2$, $y_2$), ...($x_N$, $y_N$), where $y_j$ was generated by an unknown function $y = f(x)$, discover a hypothesis function $h$ that approximates the true function $f$.

There are multiple ways to test the hypothesis and obtain accuracy. The accuracy of the hypothesis is tested on a test set. In $k$-fold cross-validation, the data is split in $k$ subsets of equal length. For $k$ learning rounds, $1/k$ of the data is extracted and used as the test, and the remaining data is used for training. Each subset is held out one time and used to train the model k-1 times. The accuracy is then obtained by averaging the test scores from the $k$ rounds. Statistically accurate results are usually obtained using $k = 5$ or $k = 10$. For novel accuracies, the test set performance should not be used to both find the hypothesis and evaluate it.

A confusion matrix can be used to assess the performance in greater detail. To assess the convergence of neural network (NN), accuracy and loss for both training and test sets can be plotted for each epoch (training round).

### 2.5.2 Classification algorithms

There exist numerous algorithms for classification purposes. A short introduction to the algorithms used in this thesis are described next.

#### 2.5.2.1 Decision tree

Decision tree (DT) builds a classification model in the structure of a tree, branching out in "if-then-else" decision rules. The concept of reducing the entropy of the data samples is used to build the tree structure.

The DT algorithm can in some cases create a large tree, even though there is no pattern to describe the data. In this case, the tree can fully describe the training set but is not capable of generalizing to new examples; a phenomenon referred to as overfitting. Overfitting is a problem not only for DT, but ML algorithms in general.

**Random forest**

The random forest (RF) algorithm constructs several DTs from randomly selected subsets of the training set, and then outputs the aggregate result from the individual trees. RF classifiers correct for decision trees' tendency to overfit to the training set [49].

***k*-nearest neighbors**

The $k$-nearest neighbors (k-NN) algorithm can be used for both classification and regression. An input is classified the the most common among class among its $k$-nearest neighbors, where $k$ is a positive integer. For instance, if $k = 1$, the input is assigned to the class of the single nearest neighbor.

**Support vector machine**

An Support vector machine (SVM) aims to find a hyperplane in an N-dimensional space, where N is the number of features, that distinctly separated the data points. If there are two features, the hyperplane is a one-dimensional line, and with three features it becomes a two-dimensional plane. Higher dimensions naturally exist, but the hyper-plane becomes difficult to imagine. The gap between the hyperplane and the data points should be as wide as possible and is defined by so-called *support vectors*.

In addition to performing linear classification, SVMs can efficiently perform a non-linear classification using what is called the kernel trick. The kernel trick takes data points that are not linearly separable in the N-dimensional space and

transforms it to a higher dimensional space where the data is linearly separable [50].

#### Naive Bayes

Naive Bayes (NB) is a probabilistic classifier, based on utilizing Bayes' theorem, defined as

$$P(A|B) = \frac{P(B|A)P(A)}{P(B)} \tag{2.9}$$

where $P(A|B)$ is the probability of A happening, given B. The model is naive, as it assumes conditional independence between the features (B), given the class (A). The requirement of independent features is often not true for real-life cases, which restricts the performance of the classifier for some applications. The NB classifier is fast and easy to implement, and a well-known classifier in ML.

### 2.5.3 Deep learning

Deep learning (DL) is a type of ML technique that can be used for classification purposes. DL uses multiple processing layers, often arranged in a NN architecture, able to learn representations of data. NN does not require manual feature extraction, as the features are learned while the network trains on a collection of training examples. One common deep NN architecture is convolutional neural network (CNN), which is designed to process data that are arranged in sequential arrays of one or multiple dimensions, such as signals (1D), color images(2D) and videos (3D) [51].

CNNs are especially successful in the field of image classification (as will be outlined in state-of-the-art, Ch. 3).

#### Limitations of deep learning with EEG data

In contrast to image classification, the field of EEG suffers from limited amounts of available training data. Collecting large datasets is time-consuming, and extremely physically demanding on the subject. Advancements in computational power allow for classification of EEG signals without feature extraction. However, results may be limited due to a small amount of training data.

DL with CNN executes end-to-end learning, i.e. learning from the raw data. It becomes difficult to interpret the importance of the features used for classification. With most traditional ML algorithms, it is possible to analyze which features have the highest importance in the classification, and even do causality analysis. Such an analysis is complicated or impossible with NN.

# Chapter 3

# State-of-the-art

*Little work on the design and development of a color controlled BCIs has been carried out. This chapter gives a summary and a short evaluation of the most relevant works.*

## 3.1 Visual color stimulus

The major part of RGB related EEG research is concerned with only offline classification, while one study also assesses performance in real time. A summary including experimental setup, methods, and results of state-of-the-art research is given in Tab. 3.1.

A neural signature of the unique hues (red, yellow, green, and blue), were discovered $230\,ms$ after stimulus onset at a post-perceptual stage of visual processing [52]. The study used ERPs evoked in response to different hues, recorded from 39 EEG electrodes. However, the study does not evaluate the discovered signatures using classification techniques, which makes it difficult to consider its potential use in BCI applications.

A classification study of RGB colors was done in [53]. The dataset used is collected from 14 subjects, and the best accuracy across the 14 subjects was 0.55. The study was done using functional near-infrared spectroscopy (fNIRS), which makes it difficult to compare with EEG experiments.

Classification of EEG signals produced by random visual exposure to RGB colors was presented in [54]. Independent component analysis (ICA) was used to remove artifacts. Event-related spectral perturbations (ERSP) were used as features for a SVM, and the highest classification accuracy reported was 0.98.

However, this work has some drawbacks. Fist, a fully randomized presentation of colors was not applied due, as some colors were presented two consecutive times. Second, all the epochs were used to compute 3 global ERSP matrices used as the feature dataset in the classification stage. Using this method, the classifier knew all the information about the EEG signals. The results are, therefore, thought to be highly overestimated, as the classifier is fitted to both training and test data.

Single-trial classification of RGB using EMD residual is presented in [55]. This study uses various methods of extracting features from EEG signals produced by RGB exposure; ERSP, target mean, auto-regressive and EMD residual. The feature extraction method which gives the highest classification accuracy are target mean and EMD residual, and the study suggested these for a future real-time BCI application. However, the outcomes seem to be overestimated, as they apply feature selection from all available data.

A third offline study to classify EEG signals produced by RGB exposure was done in [56]. The study yields impressive results, but limited documentation of the experiment setup makes it difficult to evaluate the work.

The only known study to test a real-time classification of color related stimuli was done in [57]. Band power features of the EEG signals were used as input for an SVM. The study classifies two colors with $0.7-0.8$ accuracy, using subject-specific models (models trained for each subject individually). Note that the chance level for classifying two colors is 0.5. During the experiment, subjects looked at the two colors by changing their focus from one side of a screen to another. It is therefore plausible that the classification is not directly related to color perception, but rather the focus direction (left or right) of the eyes of the subject.

Learning from the works presented here, a well documented and controlled experiment would be desirable.

Techniques to predict which color a subject is looking at have also been explored using indirect approaches such as analyzing psychological and emotional responses to color [58][59].

## Electrode placement

The positioning of electrodes is essential when a limited number of channels are available. The information and conclusions from related works can serve as a starting point for improved experiment design.

TABLE 3.1: Summary of state-of-art work.

| **Source** | [52] | [53] | [54] | [55] | [56] | [57] |
|---|---|---|---|---|---|---|
| **Method** | EEG | fNIRS | EEG | EEG | EEG | EEG |
| **Colors** | (RYGB) | 3 (RGB) | 3 (RGB) | 3 (RGB) | 5 (RGBWY) | 2 (RB) |
| **no. of channels** | 39 | 30 | 4 | 4 | 14 | 16 |
| **Sampling rate** | 1000 Hz | - | 256 Hz | 256 Hz | 128 Hz | 128 Hz |
| **No. of subjects** | 23 | 14 | 7 | 7 | 10 | 5 |
| **No. of epochs** | 320 | 27 | 180 | 180 | 50 | 32-38 |
| **Pre-processing** | Y | Y | Y | Y | Y | Y |
| **Artif. removal** | Y | N | Y | Y | N | N |
| **Features** | ERP pattern | statistical | amplitude (ERSP) | EMD | ERP (N2, P3, N4) | Band powers |
| **Exposure time** | 0.4 s | 10 s | 3 s | 3 s | 7 s | - |
| **Rest time** | 1.2-1.6 s | 25 s (black) | 3 s (gray) | 3 s (gray) | 5 s | - |
| **Offline/realtime** | offline | offline | offline | offline | offline | real-time |
| **Classification** | - | LDA | SVM | SVM | ANN | SVM |
| **Accuracy** | - | 0.55 | 0.84-0.97 | 0.89 | 0.62 (subject model) | 0.7-0.8 (subject model) |

Surprisingly, one study observed that electrodes placed on the frontal lobe react more than those placed on the occipital lobe when exposed to RGB [53]. Electrode O1 and F7, according to the 10-20 international system, are suggested as most important to record RGB data in [56]. Moreover, a combination of frontal and occipital channels was most relevant when using 39 channels in [52].

## 3.2 Deep Learning and EEG

Although NN have been known for 50 years, recent improvements in computational power and increasing amounts of available data have enlarged the interest and success in the field over the last 10 years. It can be challenging to know which features to extract, but advances in DL opens possibilities to classify data without manual feature extraction. The input to a DL network can be the raw data itself, and the network can extract the most discriminant features by constructing high-level features in the back-propagation step.

DL has revolutionized the field of speech and image classification, achieving state of the art performance, such as automatic speech recognition tasks [60] and learning depth from a moving camera [61]. Image recognition was traditionally a field dominated by feature driven approaches, such as in optical character recognition (OCR) applications for typed text. The number of available pictures is immense, providing the networks with large amounts of training examples, and CNN are successful in challenging image classification problems.

Specifically, deep NN models yield successful results when utilized for the detection of visual-evoked responses in EEG signals. Deep NN has proven an effective tool for single trial P300 classification in [62], and hence the authors encourage the

use of neural networks in EEG tasks. In [63], it is suggested that uniting spatial filtering and classification through the use of a CNN can be more efficient than separating the different steps [63]. A new CNN architecture for generalized multi-class, single-trial EEG classification across subjects was tested in [64]. Usually, subject-specific models yield better results than general models. The proposed CNN in this paper slightly exceeds the performance of the other classifiers despite being trained across subjects.

# Chapter 4

# Method

*The following chapter explains methods used in this thesis for classifying EEG signals produced by RGB stimuli. To accomplish this, the method's main core has 2 elements: pre-processing and classification. The first element, described in Sec. 4.1, looks for the improvement of the signals' quality and its performance is also measured. Whereas the second element, described in 4.2.1 and 4.2.2 used a model to assess both the first element and the capability of a classification algorithm to distinguish the EEG signals recorded during the exposure to RGB colors.*

## 4.1 Pre-processing

The stage consists of improving the signal-to-noise ratio. Noise caused by the subject, the environment, or the electrodes is removed from the raw signals to reveal relevant information.

Also, artifacts produced by involuntary movements can be removed in this stage. Artifacts are noise sources captured in the EEG recording. Noise filtering electronics, special materials, and industrial design techniques are necessary to reduce noise influences. Two typical artifacts are electromyogram (EMG) and electrooculogram (EOG) artifacts. EMG is essentially electrical noise generated by facial muscle activity, and EOG is electrical noise generated by eye movement.

There are numerous ways to prepossess raw EEG data, for instance, by applying a low or high pass filter to remove the influence of line frequency ($50/60\,Hz$). Alternatively, noise is automatically extracted when using EMD or NN with enough data and appropriate number of IMFs. There is no preferred approach, and hence several combinations of pre-processing methods, as well as no pre-processing at all, are explored. Fig. 4.1 illustrates procedures exploited. Finally, the data

are arranged into 3 *sec.* long labeled epochs, for computation of ERP and further analysis.

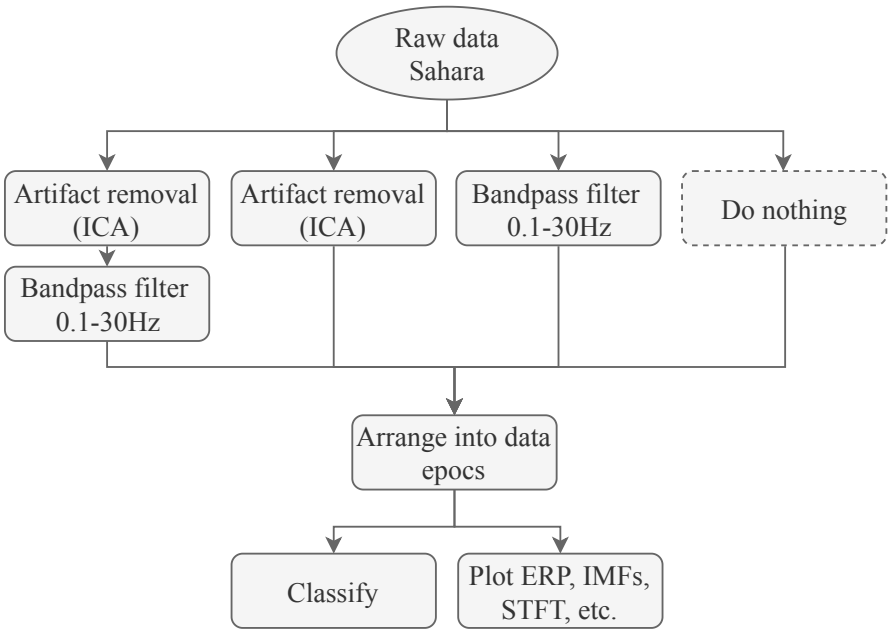


FIGURE 4.1: Overview of exploited procedures for noise reduction and artifact removal.

### 4.1.1 Artifact removal

A dedicated program using ICA and visual inspection was developed to remove artifacts. ICA demands supervised selection of artifact components. A manual selection of which components to extract was implemented by allowing the operator to iterate through all recorded sessions. The signals from each electrode are plotted next to the independent components extracted using ICA. The operator then selects components containing artifacts, which are removed from the data. The operator also has the option to remove full sessions.

### 4.1.2 Bandpass filter

A band-pass filter passes frequencies within a certain range and excludes frequencies outside that range. A band-pass filter from $0.1 - 30\,Hz$ was applied to both the raw data, and the data where artifacts were removed. The implementation of the filter is a much-modified version of the example presented in [65].

### 4.1.3 Epochs

As will be explained later, this work uses two datasets (Dataset 1 and Dataset 2), sampled at $250\,Hz$ and $256\,Hz$ respectively. Both datasets were re-organized in $3\,sec.$ long "epochs". Resulting in 750 and 768 data points for Dataset 1 and Dataset 2, respectively. Each epoch is labeled with the corresponding color.

The epoching of the signals is locking all the events to start at the same position in time. Time-locking the events must be done to analyze the effect of event exposure with respect to time. One epoch contains samples from all channels where the subject is looking at gray for one second, followed by two seconds of looking at one of the RGB colors or a math problem.

## 4.2 Classification

Specifically, two essentially different techniques are used in the second element, as illustrated in Fig. 4.2. First, the combination of feature extraction and supervised classification algorithms, and second, DL, which *learns* the important features directly from sequential data through supervised training and thereby create a classification model. The two methods are explained in Sec. 4.2.1 and 4.2.2, respectively.

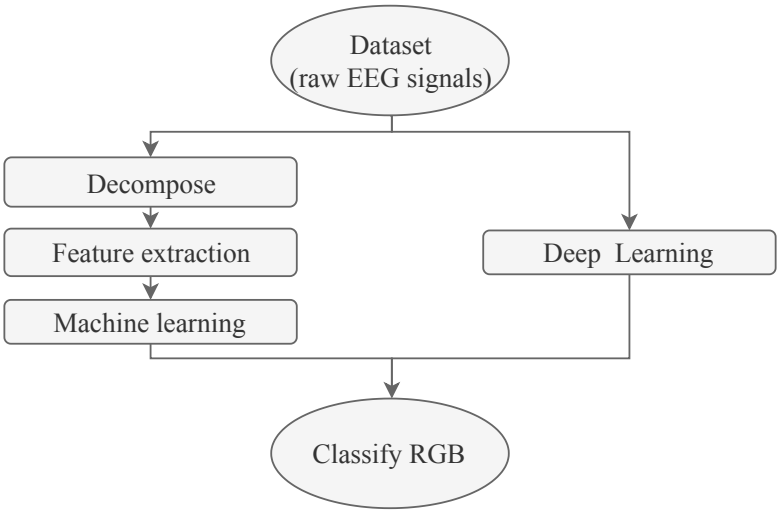


FIGURE 4.2: Flowchart describing the approaches used for creating the classifiers.

### 4.2.1 Classification with feature extraction

The first method (left branch in Fig. 4) applies an initial process of feature extraction to the EEG signals, which are used for the training of classical ML.

The specific method used for *classification with feature extraction* is based on a method developed in [66]. The feature based method was applied to classify EEG data produced by visual exposure to RGB in [67]. The complete article is published as part of this master thesis, and can therefore be found in Appendix C. The method described here is therefore an adapted version of the paper mentioned previously.

One way of classifying RGB colors is by finding a unique descriptor capable of separating the colors from each other. Identifying one or more features for color identification in EEG signals would enable less complex models and reduced computation time for real-time applications. The method used for feature extraction and classification can be described in four steps:

*1. Decompose the individual signals with EMD*
Signals from each channel are decomposed into two IMFs and the corresponding residual, using the EMD algorithm explained in section 2.3.3. Once the IMFs is extracted, certain features are obtained.

*2. Create an array of features for each decomposition*
The feature extraction stage for each electrode consists of the computation of energy and fractal features, but additionally, in this thesis, a set of statistical values are computed for each extracted IMF. This procedure of signal decomposition (1) and feature creation (2) is illustrated in Fig. 4.3. The features are summarized in Tab 4.1.

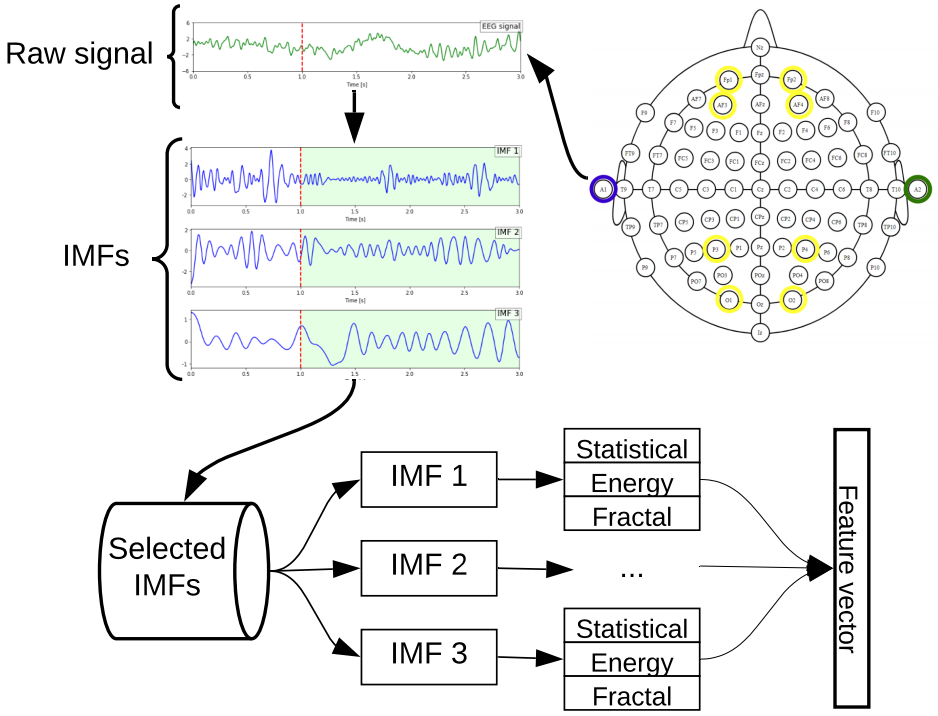


FIGURE 4.3: Flowchart illustrating the feature extraction procedure using EMD. The procedure is the same for each channel.

TABLE 4.1: Summary of features.

| **Feature type** | **Extracted features** |
|---|---|
| **Energy** | instantaneous and teager energy |
| **Fractal** | Petrosian and Higuchi fractal dimension |
| **Statistical** | min, max, mean, median, variance, standard deviation, kurtosis, skew |

*3. Use the feature arrays as inputs to classifiers and obtain the accuracy for each classifier*

The feature vectors obtained for each channel are concatenated to obtain a single vector for each instance and later used as input to the classifiers. As will be explained later, some experiments consist of using all the features shown in Tab. 4.1, while for others, only statistical values were used. For example, using all the 12 features, 3 IMFs and 4 channels, the length of the feature vector for an instance is:

$$\text{Features} \times \text{Channels} \times \text{IMFs} = 12 \times 4 \times 3 = 144 \tag{4.1}$$

Using only statistical features, the length of the feature vector is only 96 for each instance. The features are computed for each IMF, and all experiments are done with 3 IMFs and 4 or 8 channels.

*4. Choose the classifier with the highest accuracy*
Lastly, supervised machine-learning models were created using 10-folds cross validation using the accuracy metric. The ML based algorithms used are, RF, SVM, k-NN,DT and NB.

The experiments were repeated using different parameters to find and select the best parameters for each classifier. The classifier with the highest accuracy was then automatically selected. The set of parameters for each classifier are listed below:

- Depths for RF: 2, 3, 4, 5, 6, 7, 8
- Neighbors for kNN: 2, 3, 4, 5, 6, 7, 8
- Kernels for SVM: linear (lin.), radial basis function (rbf), sigmoid, polynomial (poly.)

A Gaussian distribution is assumed for the NB classifier, and the *GaussianNB* from scikit-learn with default parameters are used. Scikit-learn is an open source machine learning library for Python, providing various built classification algorithms. Unless otherwise stated, default parameters of scikit-learn classifiers are used throughout this work [68].

### 4.2.2 Classification using deep learning

The second method (right branch in Fig. 4.2) directly uses EEG voltages as input for a CNN. The specific architecture of the implemented CNN is based on a publicly available architecture, titled EEGNet. In essence, EEGNet is a compact CNN architecture developed especially for classification of EEG data [69]. A visualization of the EEGNet architecture is given in Fig. 4.4, and shows that it is divided into four main sections after the input.

The first section performs a convolution with several temporal filters (within one channel) with a size of half the sampling rate. The output of these convolutions is a series of signals filtered with bandpass-filters of different sizes.

The second section performs a depth-wise convolution for each of the outputs of the previous layer. This allows for the extraction of spatial features (between channels) for each temporal filter, which means it finds frequency-specific spatial features. This is very important to extract meaningful features from EEG signals.

The third section performs a depthwise convolution followed by a pointwise convolution. The goal of this step is to summarize and combine the output from the previous layers in a meaningful way.

Finally, a softmax layer allows for the final classification.

In summary, this is a CNN network optimized to extract essential features from raw EEG data while limiting the number of parameters.

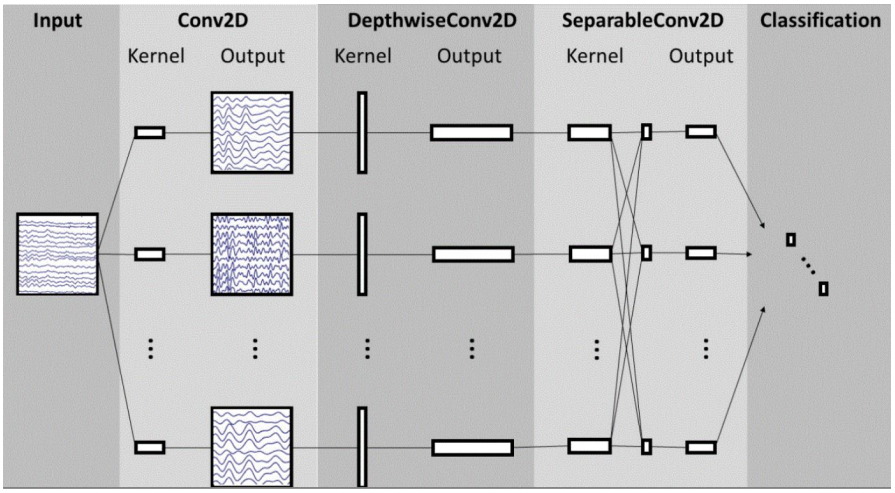


FIGURE 4.4: Overall visualization of the EEGNet architecture.

The hyperparameters and learning rates are, however, optimized for the application in this thesis. The model is fitted using the Adam optimizer with default parameters, minimizing the categorical cross-entropy loss function [70]. 30 or 50 training iterations were used depending on the given dataset. These numbers were obtained from manual testing.

# Chapter 5

# Experiment design and implementation

*The following chapter provides documentation of experiment design and implementation. The reasoning behind design choices will also be presented where relevant. Sec. 5.1-5.2 outlines the experiment, Sec. 5.3 explains how data is acquired and finally some limitations are discussed.*

## 5.1 System overview

An overview of the system implementation is given in Fig. 5.1. A curved screen display events to the subject. Dry electrodes transmit signals recorded from the scalp to the local headset station. Sampled signals are sent to the base station over a local wireless network. The base station is connected to a PC, which runs the server service. The PC display events on the screen, records, and saves EEG data. The following sections explain each system part in detail.

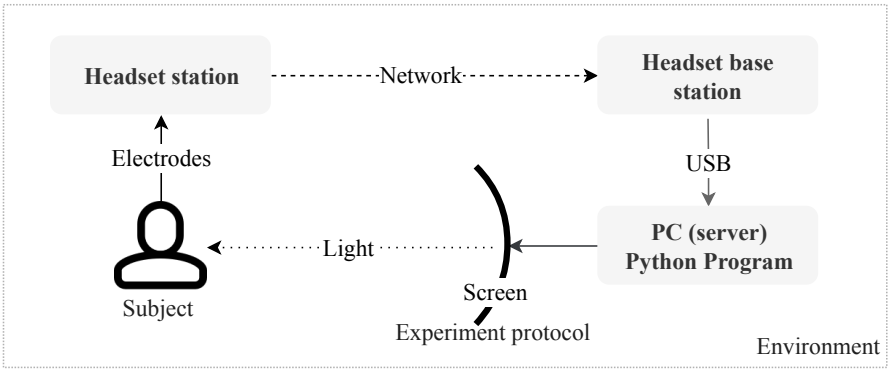


FIGURE 5.1: Experiment setup for RGB data collection.

## 5.2 Experimental paradigm

The following section describes design choices made for the recorded in-house data set, referred to as Dataset 1.

### 5.2.1 Experiment protocol

*Experiment protocol* refers to the scheme the subject experience from beginning to the end of the experiment. The experimental protocol is designed to obtain as many successful short impulse trials of each color as possible without sacrificing subject well being. The protocol was developed by investigating color perception and the dynamics of the eye (Ch. 2), followed by several test experiments with subjects.

Four classes of stimuli, referred to as *events*, were exposed to the subject. The events were red color, green color, blue color, and a math problem. Fig. 5.3 presents the algorithm of the experiment protocol, alongside with an illustration of the respective screen display to the left. Before each exposure, a short break showing uniform gray color was on display for a random duration of $1 - 2\,sec.$, to allow time for blinking. A cross (+) appeared to indicate for the subject to get ready $2\,sec.$ before the next exposure. The exposure step is the display of either event. The colors used are defined in hexadecimal format in Tab. 5.1. Fig. 5.2 gives an illustrative picture of a subject being exposed to RGB colors. Note that the room was dark during actual data collection. The math problem was designed to be solvable in $\approx 3\,sec.$ for an average university student, and is included to serve as a baseline in future research. All events were presented the same number of times, for the same duration ($3\,sec.$). The described procedure was repeated 5 times, before a longer break of $10\,sec.$ This sequence is repeated 3 times, resulting in 15 trials of each event.

FIGURE 5.2: Subject in front of screen displaying RGB colors.

Although more trials would benefit analysis, test experiments suggested that it takes on average eight minutes (time for $15\,trials$) before the light from the screen

cause discomfort or tiredness in the eyes, even when the luminosity is set to minimum.

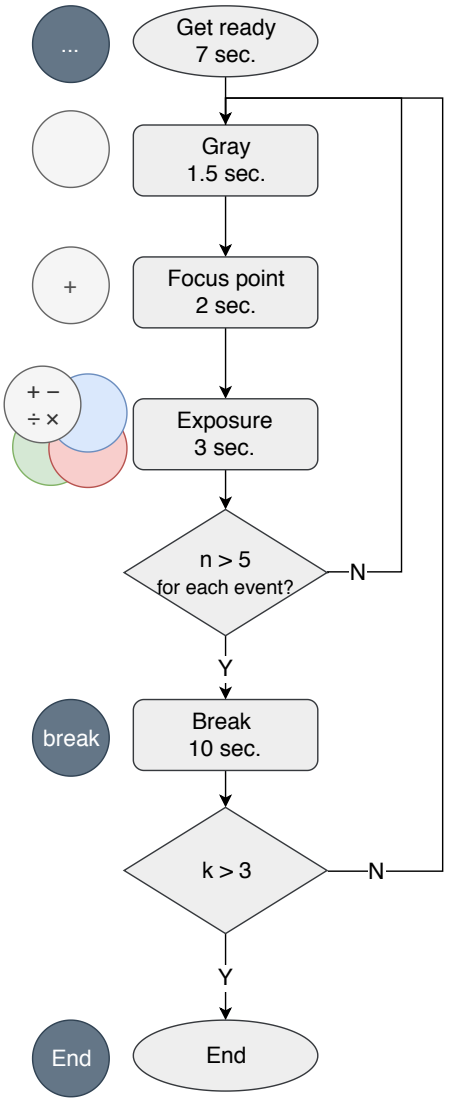


FIGURE 5.3: Experimental protocol; illustration of stimuli (left) and description and length in seconds (right).

The order of the events and the time between each event were both randomized to minimize brain activity due to prediction. No subjects experienced the same pattern or the same break time.

TABLE 5.1: Experiment colors on hexadecimal format.

| **Name** | **Red** | **Green** | **Blue** | **Light gray** | **Medium gray** |
|---|---|---|---|---|---|
| **Hex (RGB)** | FF 00 00 | 00 80 00 | 00 00 FF | c9 c9 c9 | 80 80 80 |

### 5.2.2 Electrodes

Electrodes positioned at a flexible cap measures voltage fluctuations on the subject's scalp. The positions of the electrodes are carefully chosen based on results from related RGB research presented in Ch. 3. The chosen positions according to the $10-20$ international system are [23]:

- Frontal lobe: FP1, FP2, AF3, AF4
- Parietal and occipital lobe: P03, P04, O1, O2

Fig. 5.4 highlights the operative electrodes (yellow), ground (blue) and reference (green) connected to the left and right mastoid respectively.

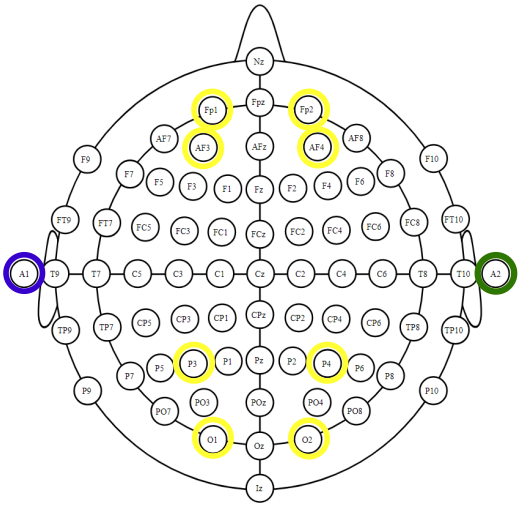


FIGURE 5.4: Operative electrodes (yellow), ground (blue) and reference (green) connected to the left and right mastoid respectively.

### 5.2.3 Screen

A curved computer screen with an active display size of $797 \times 333\,mm$ ($34\,inches$) was used to present the events and interact with the subject. The curved feature of the screen (allowing viewing angle of $178°/178°$) increased the visual exposure area to include the peripheral vision, which is hypothesized to engage greater response to the events. The luminosity of the screen was constantly at $250\,cd/m^2$, chosen to prevent eye pain due to too bright light. The distance from the subject to the screen was $1.5\,m$.

### 5.2.4 Subjects

Twenty healthy volunteers participated in the study, aged in the range 21 − 27 years. Summary of subject details are given in Appendix A, Tab. A.1.

All participants were invited via a written letter explaining the research purpose, what the study will involve, risks, data privacy, and what will happen during the experiment. Participants were asked to follow these instructions before their arrival at the experiment site:

- Do not add gel or any substance to your hair
- Get a good night's sleep the night before
- Refrain from use of recreational drugs and stimulants at least 24 hours before the experiment (coffee, alcohol, medicines)

Subjects shared information regarding their age, gender, BCI experience, handedness, color blindness, and epilepsy. Subjects answered a simple questionnaire regarding mental and physical health before and after the experiment. Questions asked are listed in Appendix A, Tab. A.2. Answers to these questions can complement data analysis and improve the experiment experience for subjects in similar studies in the future.

### 5.2.5 Experiment procedure

Upon arrival, participants signed a consent form and answered the questionnaire described above. Any questions the participant had was answered, and the protocol was carefully explained. Subjects were instructed to sit as comfortable and still as possible, avoid blinking during the events, and when math problems appear; solve them by thinking only. It was made clear that subjects could withdraw from the experiment at any time. However, no one decided to do so.

The skin behind the ears was cleaned with medical alcohol wipes (85 %) for better conductivity from the skin to ground and reference. To protect against electrostatic discharge (ESD), static electricity was discharged from the body of subjects and operator by touching a metal grounded object.

The cap was positioned by measuring the distance between the nasion and inion and the distance between the left and right preauricular points of the subject. The position in the middle of these two locations is the vertex position, Cz. The measured position was aligned with the position Cz of the electrode cap, and

reference and ground were connected. Electrode wires were placed to avoid tension and direct contact with moving parts of the body, and finally, each electrode was twisted to improve contact.

### 5.2.6 Environment

The experiment was conducted in a dark room. An antistatic environment is necessary for high-quality recordings, and as the room at hand did not have antistatic floor (such as antistatic carpet, wood floor or stone floor), an antistatic spray was used to on the floor and furniture.

## 5.3 Data acquisition

The following section describes the software implemented for data acquisition.

### 5.3.1 Recording software implementation

Acquisition of EEG data produced by external events requires carefully timed and reliable software implementation. One main program, referred to as the protocol software, simultaneously handles user interaction, event exposure, as well as data recording and saving.

The protocol software follows sequential steps in two parallel threads, as illustrated in Fig. 5.5. When a user decides to start the experiment, using the "Click to start experiment" button, a separate thread establishes communication with the headset. The recording thread acquires data using the g.NEEDaccess python application programming interface (API). A start and stop recording marker are set using the PC system clock.

The software is designed to run a pre-defined protocol, imported as a `.json` file. This design allows the operator to change the protocol without having to alter the source code, which is especially useful during testing procedures and while developing the final protocol.

Finally, the main thread waits for the recording to complete. Raw data is cut to match the start and stop of color exposure and then saved. In addition to EEG data, metadata (date, time, name, gender, age, handedness, subject no., session no.) is saved.

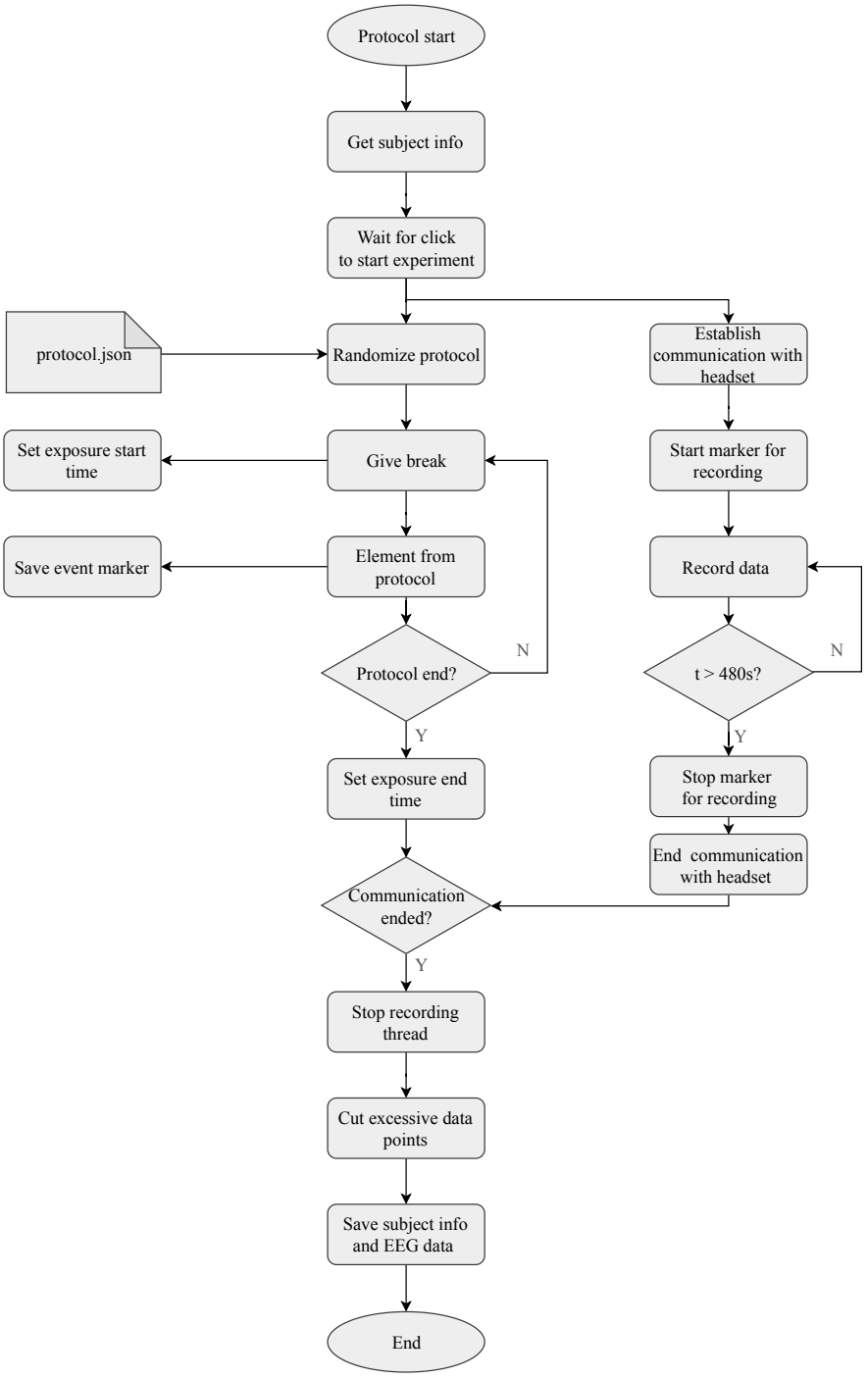


FIGURE 5.5: Program flowchart; software developed for conducting EEG experiments with visual stimuli.

### 5.3.2 g.tec software and hardware

Data acquisition is done using equipment from g.tec (g.Nautilus 8 flexible g.SAHARA). The system comprises 8 active channels with g.SAHARA 7 $mm$ dry EEG electrodes prefixed on a soft cap, with 24-bit resolution, 250 $Hz$ sample rate, built in 3-axis acceleration sensor and lithium ION batteries. The equipment is

developed for research only. The cap has flexible electrode positioning, allowing for case-specific placement of the 8 electrodes.

Wireless data transmission is done using the g.NEEDaccess server and client. The server software runs in the background. A client software, "Python Client API" is used to interact with the server. g.NEEDaccess provides a server service named g.tec Device Service (GDS), which was used to facilitates data acquisition.

A summary of the technical specifications are given in Appendix A, Tab. A.3. For more information regarding g.tec products, consult g.tec product catalogue, g.NEEDaccess Python API and user manual [71][72][73].

## 5.4 Experimental limitations

One common drawback of in BCI experiments is the difficulty of obtaining enough data due to limited subject availability. Besides, in the experiment discussed here, the achieved number of recorded trials in each session were also limited due to unexpected tiredness from looking at bright colors.

The final dataset could be enriched by extended rest- and exposure times, as this would give more options for data analysis.

The lab environment lacked protection against electromagnetic disturbances and acoustic damping, which would be ideal for recording high-quality EEG signals. A possible solution (and suggestion as part of future experiments) is to construct a simple Faraday's cage enclosing the subject, which will shield the electrodes from electromagnetic fields. Even though active electrodes (such as the dry Sahara electrodes used here) are in theory supposed to account for external inference, a Faraday cage can remove external inference without the risk of affecting the raw EEG signals. This is thought to be especially important in research where the features are still unknown, and the researcher must be careful to not remove information from the raw signals by filtering.

The experiment is conducted in a controlled environment with high subject attention level and high color intensity, occupying a large viewing angle. Further experiments and analyses are required to establish reliable algorithms for less than ideal circumstances in a potential real-life application.

## 5.5 Complementary dataset (Dataset 2)

The dataset collected, as explained in this chapter, is referred to as Dataset 1. A second dataset, referred to as Dataset 2, is included to both enrich the analysis and measure the proposed method's performance. The second dataset consists of EEG signals from 7 subjects that were watching RGB colors presented on a screen. The distance from the screen to the subject was $3.5\,m$, and the intensity of the colors was constant at $4.5\,cd/m^2$. Each color was presented 60 times to each subject in a randomized order. Gray was used as the base color between RGB exposure. The signals were recorded from channel P1, P2, O1, and O2, according to the $10-20$ international system. The acquisition system used was BCI200 with g.tec's MOBIlab portable device and a sampling rate of $256\,Hz$ [54]. A summary of the technical specifications is given in Appendix A, Tab. A.4.

In the preprocessing stage, the signals were band-pass filtered from $0.1-30\,Hz$. To reduce the effect of abnormal values, signals crossing $\pm 60\,\mu V$ were removed. Also, some trials were excluded due to EMG and EOG artifacts. The final dataset used in this paper consist of 52 trials for each color to obtain a balanced dataset.

## 5.6 Dataset summary

A summary of the two datasets used in this thesis is given in Tab. 5.2. It is important to highlight that Dataset 1 was recorded during the present work following the process described in this chapter. Whereas Dataset 2 was recorded in [54] and it is described in Sec. 5.5

Table 5.2: Summary of Dataset 1 and Dataset 2.

| **Dataset name** | **no. of sub.** | **trials/sub.** | **no. channels** | **colors** | **epoch length** | **raw signals** | **origin** |
|---|---|---|---|---|---|---|---|
| Dataset 1 | 17 | 30 | 8 | RGB | 3 sec. | yes | in-house |
| Dataset 2 | 7 | 52 | 4 | RGB | 3 sec. | no | external |

# Chapter 6

# Results

*The following chapter first presents the raw data obtained from the experiments presented in Ch. 5. Results from applying signal analysis techniques explained in Ch.2, and methods from Ch.4 are then combined to visualize results and obtain classification accuracies. Two different datasets are used; Dataset 1 and Dataset 2 (See Sec. 5.6). Throughout this chapter, great care is taken not to compare results based on different datasets, as they are fundamentally different, both in processing as well as size (no. of subjects, no. of trials) and experimental setup.*

## 6.1 Raw data

Dataset 1 is recorded completely without any filter or noise reduction. This fact gives greater flexibility to test filtering and analysis techniques, knowing that no information was lost in the recording stage. Such a raw dataset is thought to be necessary when searching for undiscovered features. An example of the raw data from RGB exposure over a duration of ca. $6.5\,min$ is given in Fig. 6.1.

### 6.1.1 Distortions in the occipital and parietal channels

Two distortions are observed in the channels placed between the occipital and parietal lobe (Chan. $5-8$); a slow drift and a high-frequency noise. Both problems were reviled in the testing stage, and attempts were made to reduce the effect.

First, the slow drift of Chan. $4-8$ is clear in 6.1. Several attempts were made to reduce and explain this signal drift. A headband was used to put pressure on the electrodes, without significant improvements. The electrode positions were changed to ensure that the position of the electrodes was the problem, and not the

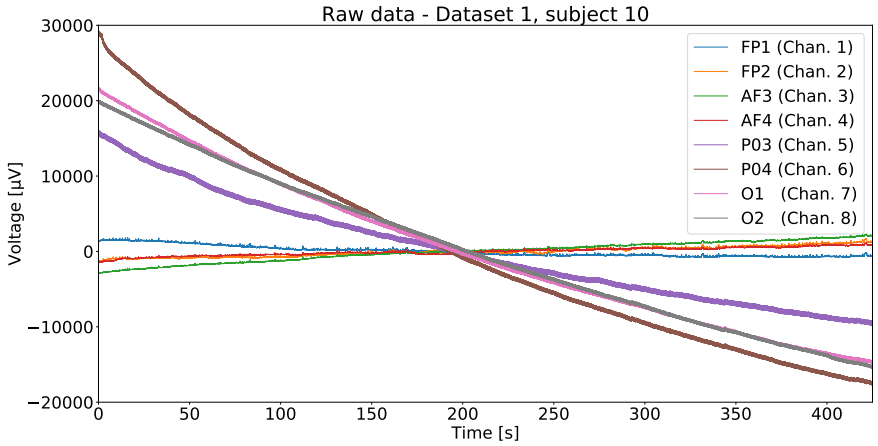


FIGURE 6.1: High levels of noise and a slow drift in raw data from Dataset 1.

electrodes themselves. It was concluded that it is always the electrodes positioned at the occipital and parietal lobe that suffer from drift. In retrospect, it is reasonable to believe that this drift is caused by increased temperature as the hair-covered (and hence temperature isolated) occipital and parietal electrodes slowly reach body temperature, as the same effect is not observed in the electrodes placed on the hairless forehead. It can, however, not be ruled out that poor electrode-skin contact causes the slow drift.

Second, high-frequency noise is observed only in the occipital and parietal channels. Eye blinks are clear in the frontal channels (Chan. $1-4$), plotted in Fig. 6.2, while the occipital and parietal channels (Chan.$5-8$) plotted in Fig. 6.3 clarifies this high-frequency noise. The wireless transmitter is, by design, located close to the occipital electrodes and may very well be the source of this high-frequency noise, perhaps amplified by poor skin contact. It is, however, doubtful that a perfectly functioning transmitter would cause these problems. The reason may perhaps, therefore, be an out-of-spec component in its high-frequency circuit or poor grounding, resulting in unwanted oscillations or harmonics.

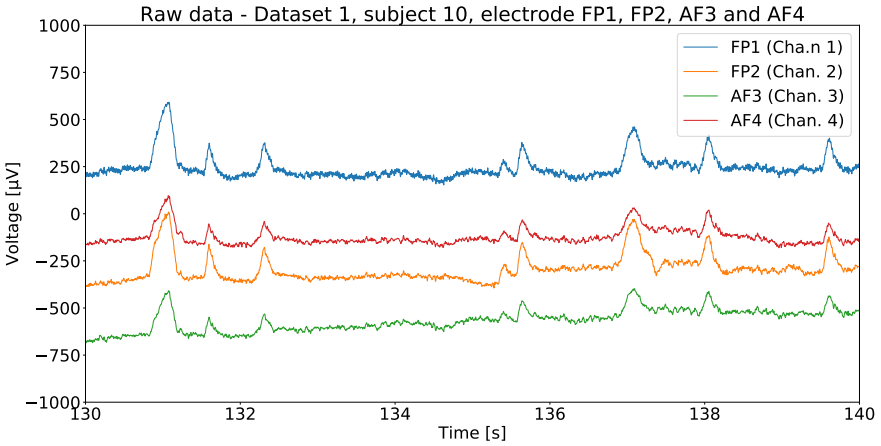


FIGURE 6.2: Raw signals from Chan. $1 - 4$.

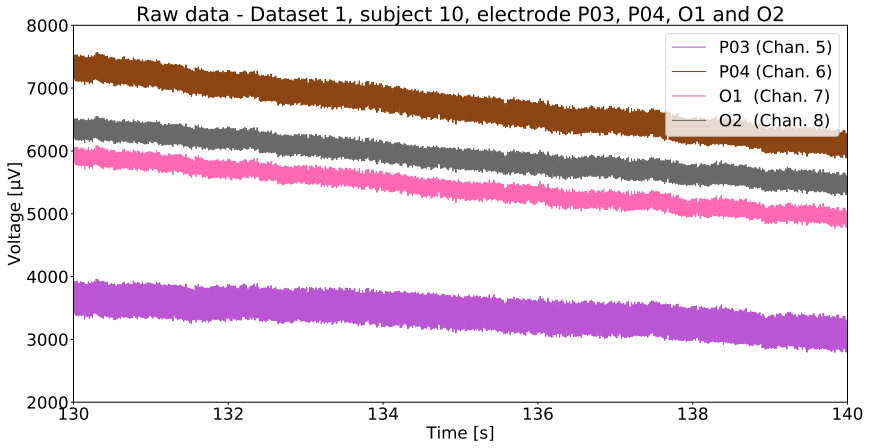


FIGURE 6.3: Raw signals from Chan. $5 - 8$.

### 6.1.2 Possible solutions for noise reduction and detrending

Dedicated research has been done to investigate and propose solutions for noise reduction and detrending in EEG data [74]. Robust techniques for detrending are especially addressed in [75].

High-pass filtering is a simple solution to remove high-frequency noise and a standard method to deal with drifts. Frequencies lower than $0.1\,Hz$ and higher than $30\,Hz$ are considered noise, and hence a bandpass-filter for $0.1 - 30\,Hz$ was applied to the epoched data.

ICA was applied to remove, or reduce, the effect of artifacts such as eye blinks and spices caused by subject movement. As explained in 4.1, manually selected independent components were extracted from each channel.

Alternative solutions exist, such as a notch filter for noise removal, and detrending by extracting the EMD residual. EMD would also be applicable to remove high-frequency noise, usually by extracting the first IMF from the original signal. However, for some tasks, the first IMF can contain useful information. Hence, there is no single solution to the problem, as it depends on the type of experiment. Undoubtedly, the processing is a crucial step to obtain high-quality data. However, an advanced review is out of the scope of this thesis.

## 6.2 Visualization and analysis of EEG signals

The following section address research question #1. ERPs, STFT and EMD were applied to the EEG signals for the two datasets. The next subsections show the computed plots, aiming to find differences between colors.

### 6.2.1 ERP-based Analysis

ERPs are evoked by sudden onset of visual stimuli, containing a negative and a positive peak around $150 - 300\,ms$ and $300\,ms$ respectively. This pattern can be identified in both raw and processed data. In all ERP plots, color exposure starts at $t = 1\,s$, indicated with a black dotted vertical line, and each plot contains samples from $0.2\,sec.$ before color exposure followed by $0.6\,sec.$ of color exposure.

The grand average of ERP hides variability in the waveforms, enabling visual interpretation of the signals. However, it loses accurate information for individual subjects. The ERPs for individual subjects are also investigated.

The response of the brain to experimental events is not fully captured in the averaged ERPs [76]. For this reason, the individual signals (not the average) from each electrode are used as a basis for classification in all the following results. ERP plots from Dataset 1 and Dataset 2 are given next.

#### 6.2.1.1 Dataset 1

All ERP plots from Dataset 1 are plotted after artifact removal with ICA and noise reduction with band-pass filtering.

Signals from frontal and occipital channels are thought to contain different waveforms due to their position. Frontal and occipital channels are averaged

separately not to hide information. Fig. 6.4 plots the response for each color, averaged over all subjects for Chan. 1-4 (left column) and Chan. 5-8 (right column). The average using all channels are included in Appendix B, Fig. B.1. The same plot for one individual subject (subject 10) is given in Fig. 6.5.

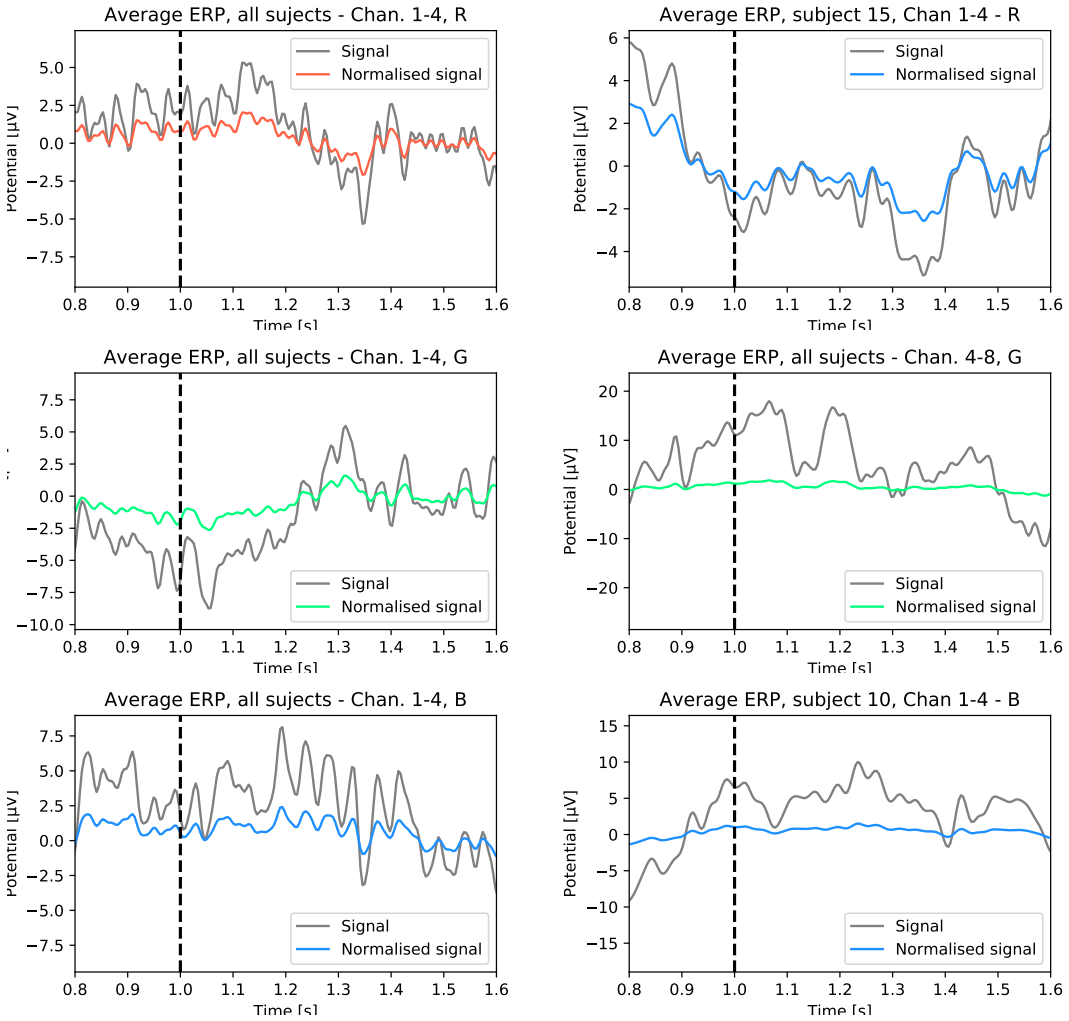


FIGURE 6.4: Dataset 1: Averaged ERP waveform produced by RGB, for all subjects Chan. 1-4 (left) and Chan. 4-8 (right).

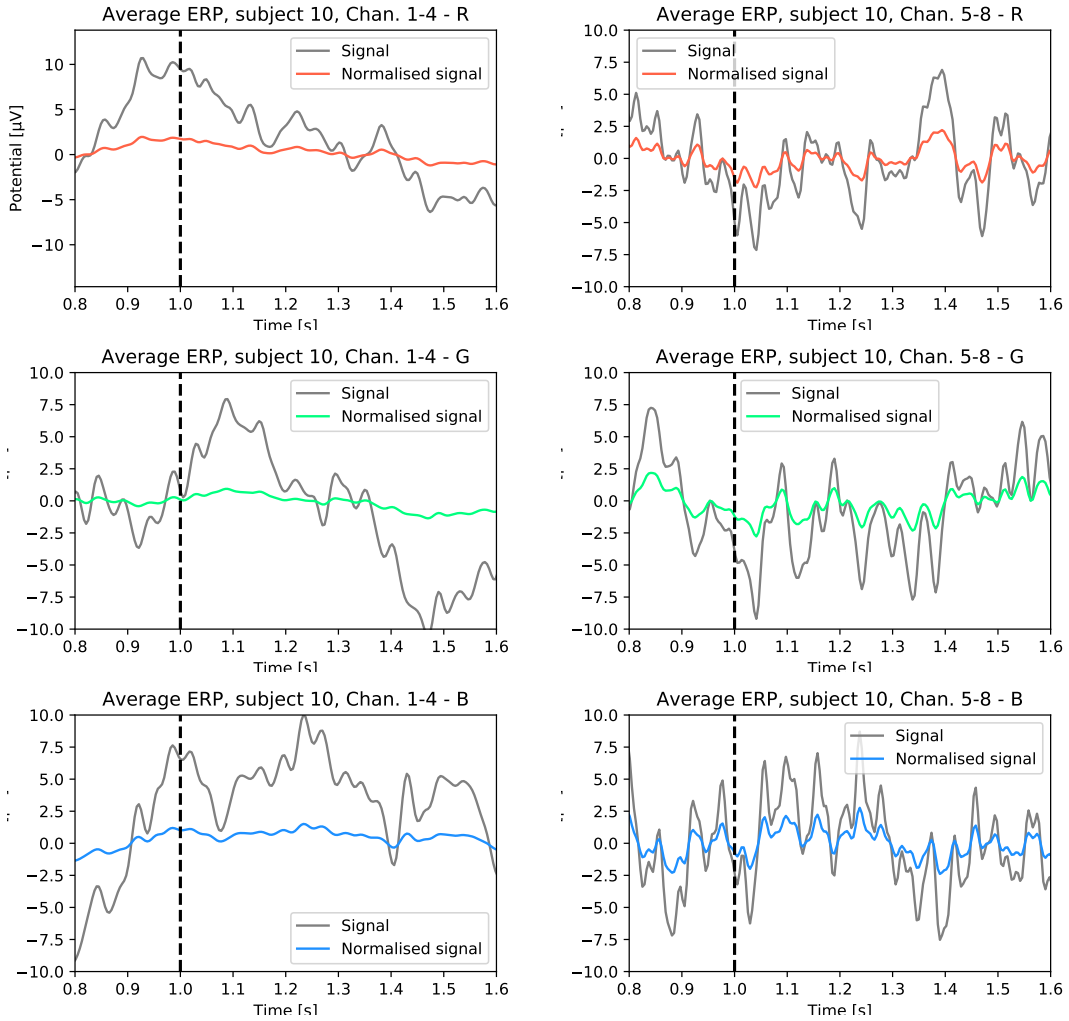


FIGURE 6.5: Dataset 1: Averaged ERP waveform produced by RGB, for subject 10, Chan. 1-4 (left) and Chan. 4-8 (right).

In the search for clear ERP plots, the average response from subject $6, 7, 9, 10$ and 11 are plotted individually in Fig. 6.6. The same plot for the remaining subjects are included in Appendix B, Fig. B.3-B.3.

Limited pre-processing prior to computing ERP plots is one reason why it is challenging to identify a clear ERP in epoched data.

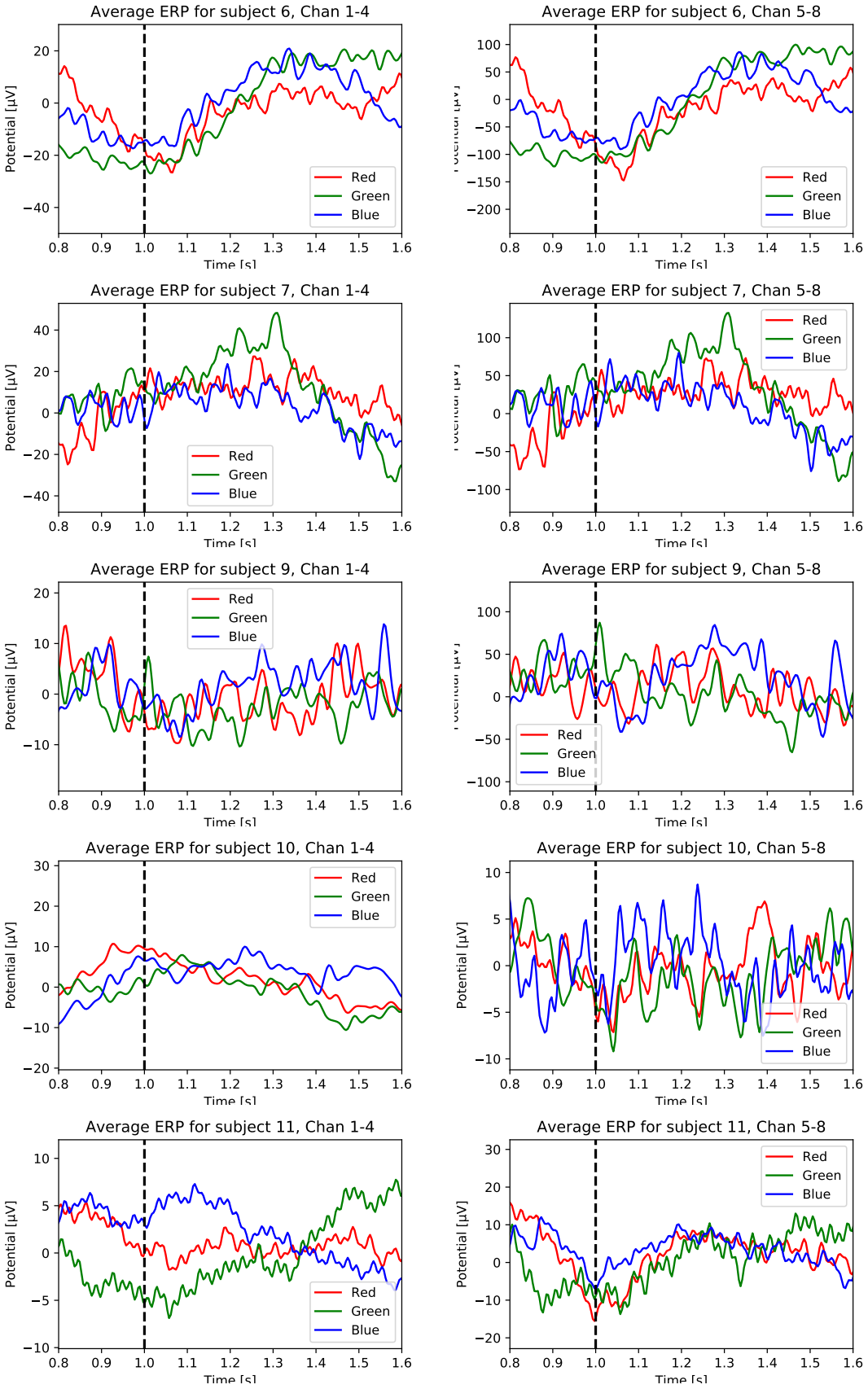


FIGURE 6.6: Dataset 1: Individual averaged RGB plots for Chan. 1-4 (left) and Chan. 5-8 (right).

#### 6.2.1.2 Dataset 2

Fig. 6.7 shows the grand average responses to red, green and blue (first, second and third row respectively) for Dataset 2. The left columns are the grand average ERP for all subjects, averaged over all available channels and instances. The right columns are the grand average ERP for one individual subject.

When averaging over all subjects, the positive peaks around 300 $ms$ are higher for red and blue (around $4\mu V$ in the normalized presentation), when compared to green. When averaging over all subjects, the duration of the negative ($t = 1.2s$) and positive peak ($t = 1.3\,s$) are longer compared to the duration of individual subject response. The reason being that the subject responses happen at slightly different times for different people, or that the light was not turned on at exactly $t = 1.00\,s$ for all subjects.

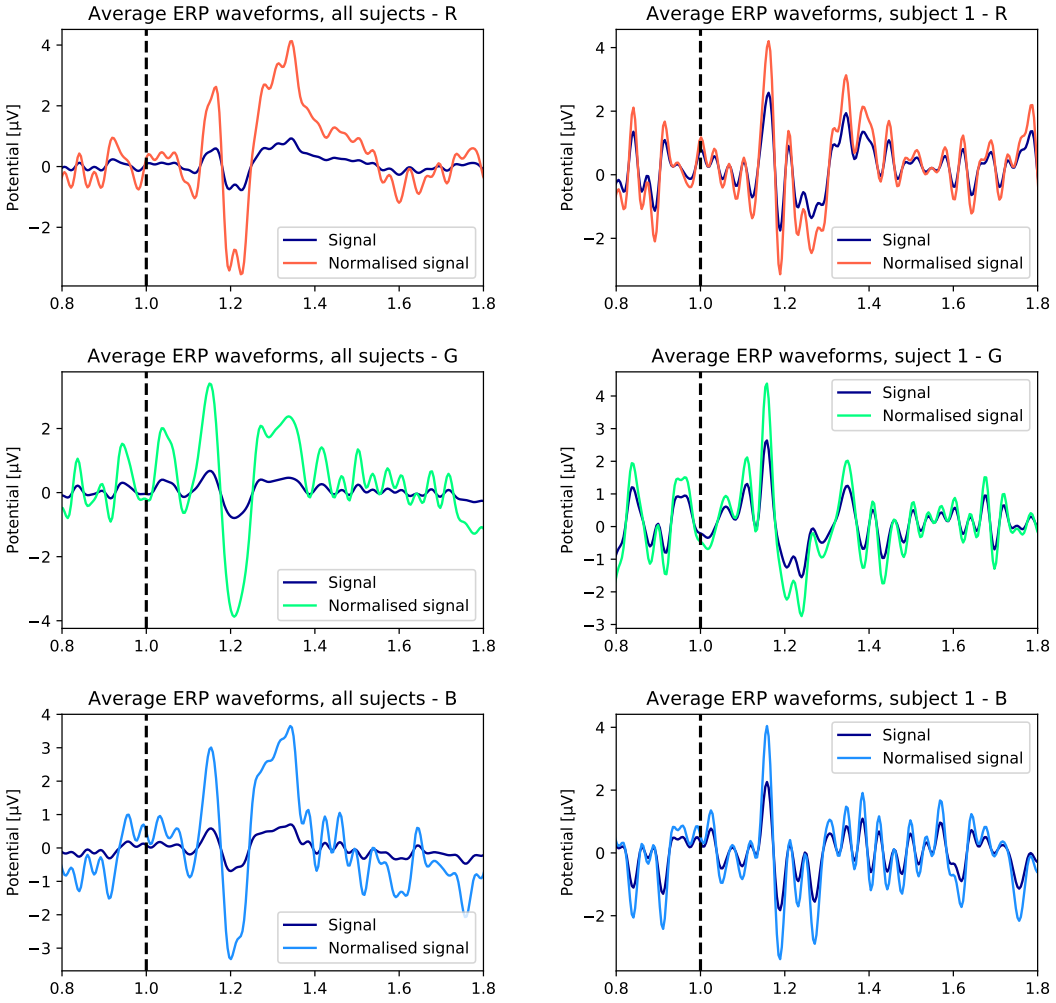


FIGURE 6.7: Dataset 2: Averaged ERP waveform produced by RGB, for all subjects (left) and one subject (right).

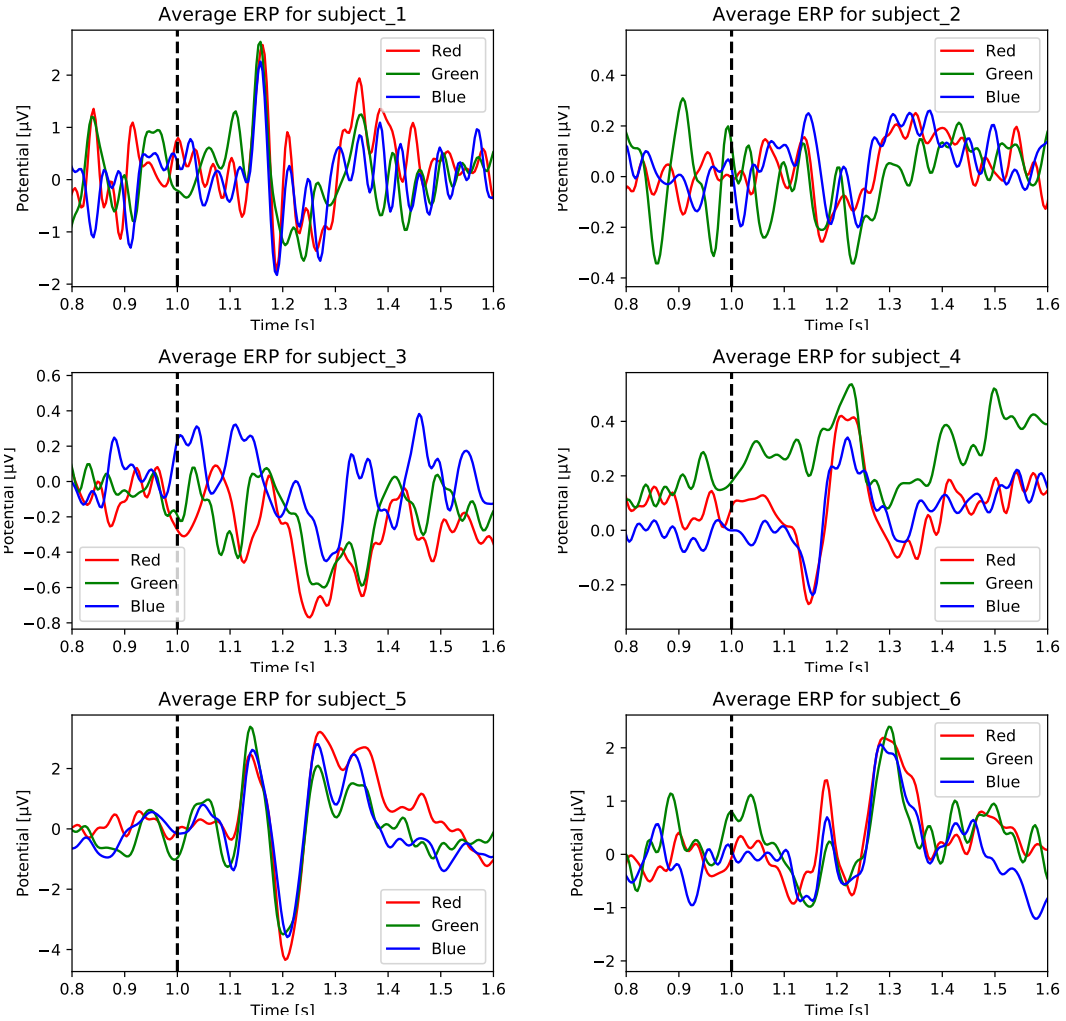


FIGURE 6.8: Dataset 2: Individual differences in averaged ERP waveforms for color exposure to RGB.

There is variation in the ERP waveforms (both in timing and amplitude) among the different subjects, and a small variation on subject level. A unique cortical pattern for each subject can influence the variation among subjects. The shape can, for instance, be affected by age and personality [77].

### 6.2.2 Short time Fourier transform

Another technique employed for visualizing and analyzing the EEG signals in the presented thesis is STFT. Specifically, STFT was applied to both datasets to investigate possible changes of frequencies over the given period. An STFT with a "Hanning" window size of 200 samples and an overlap of 190 samples were used to produce the spectrograms in Fig. 6.9 and Fig. 6.10 for Dataset 1 and Dataset 2 respectively. The spectrogram represents the grand average for RGB from top to bottom.

#### 6.2.2.1 Dataset 1

Despite the apparent prevalence of noise, the information gain from STFT for Dataset 1 is very limited.

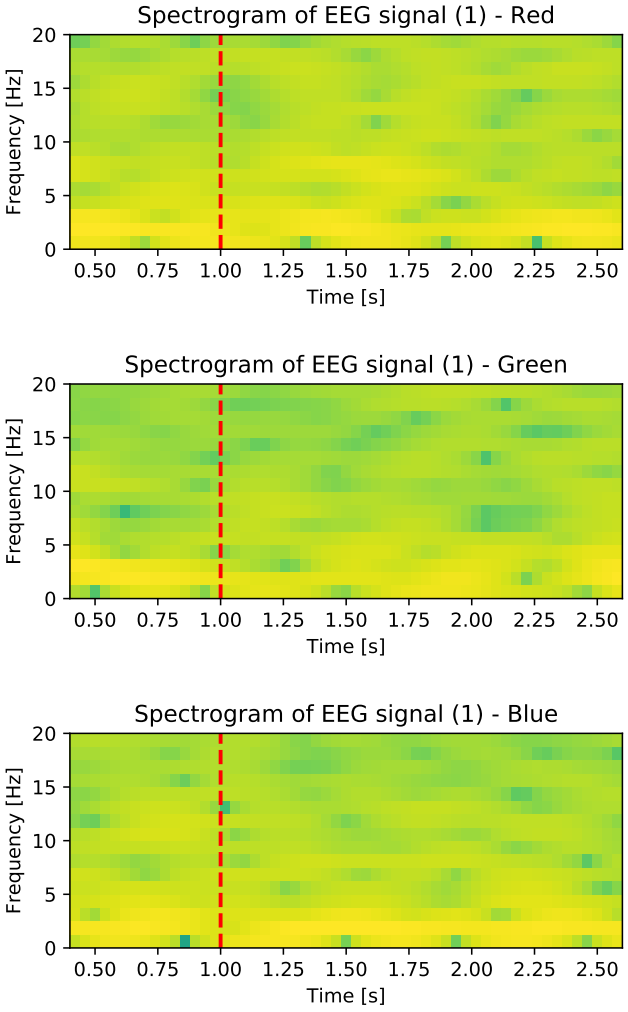


FIGURE 6.9: Dataset 1: Spectrogram of grand average EEG signal for RGB.

#### 6.2.2.2 Dataset 2

There is an amplitude increase in $2-12\,Hz$ for all colors, and for green, there is an amplitude increase for $0-5\,Hz$ in the time frame $1-2\,s$. Hence, averaging data reveals a change caused by visual stimuli from gray to RGB colors $200-300\,ms$ after exposure. However, it is clear from their overlap that frequency alone is not sufficient to separate three colors. In addition, there is no lasting change in frequency, even though all subjects are continuously looking at color from from $t = 1\,s$ to $t = 3\,s$. Information gain from STFT is limited, and doubtfully sufficient to reveal a signal feature specific for each of the colors.

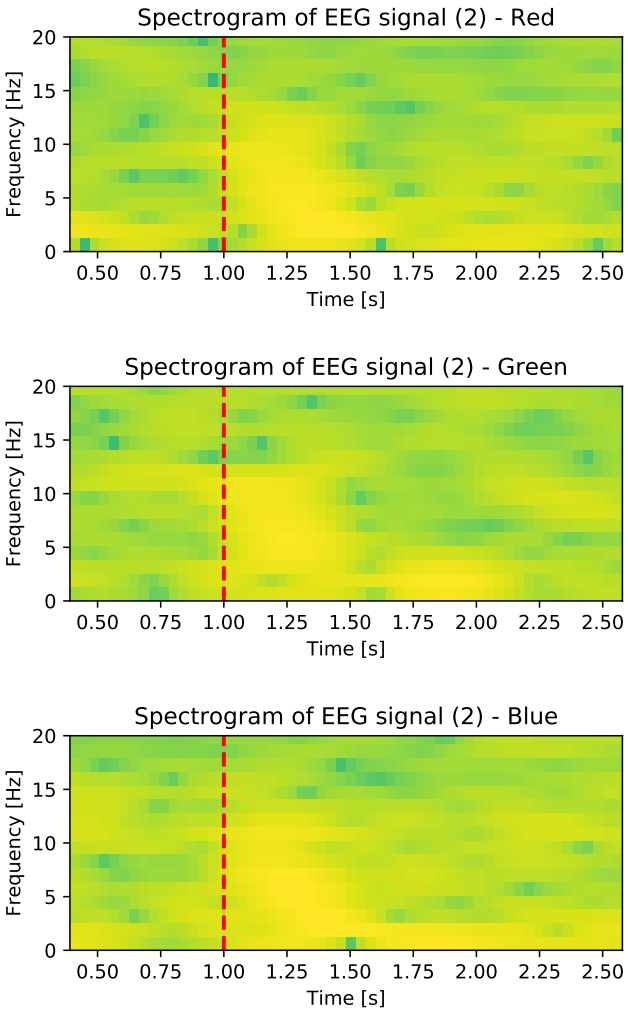


FIGURE 6.10: Dataset 2: Spectrogram of grand average EEG signal for RGB.

### 6.2.3 Empirical mode decomposition

The EMD algorithm was applied on each raw signal, and after ten siftings, the residual fulfills the IMF requirements previously discussed in Sec. 2.3.3. An example of extracted IMFs and the residual are presented in Fig. 6.12 and 6.13 for Dataset 1 and Dataset 2 respectively. The cubic spline is used for the upper and lower envelope. Note, however, that in the feature extraction stage, this procedure is repeated for all the colors and not only green, as in the given examples.

Neither spectrograms nor IMFs reveal distinct color dependent frequency or amplitude related characteristic by visual inspection.

#### 6.2.3.1 Dataset 1

Fig. 6.12 presents the IMFs extracted from instance no. 19 and electrode AF3 (Chan 3), for subject 10. The spectrogram of each IMF from Fig. 6.12 is presented in Fig. 6.11.

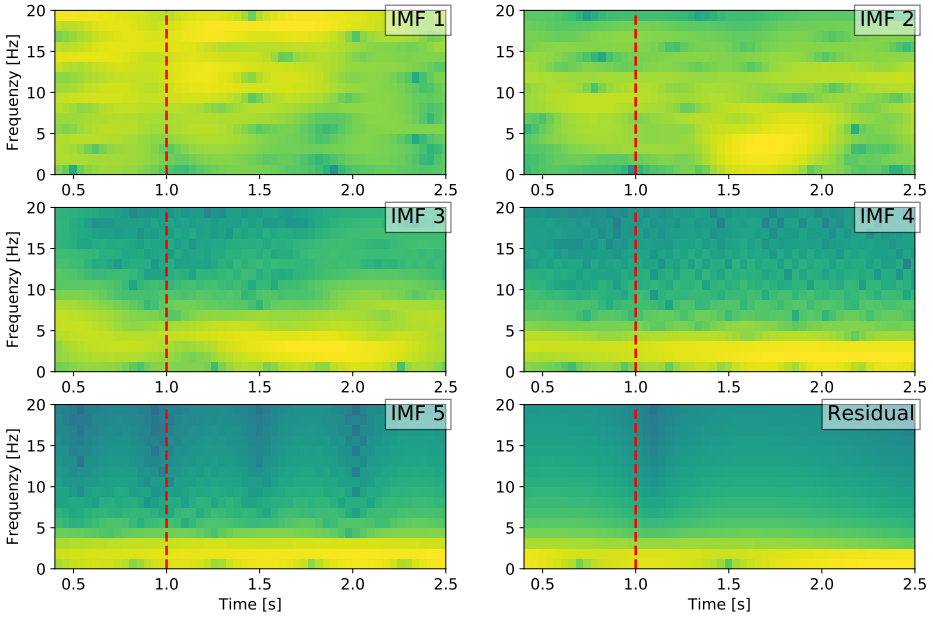


FIGURE 6.11: Dataset 1: Spectrograms of each of the five IMFs and the residual obtained from ten siftings.

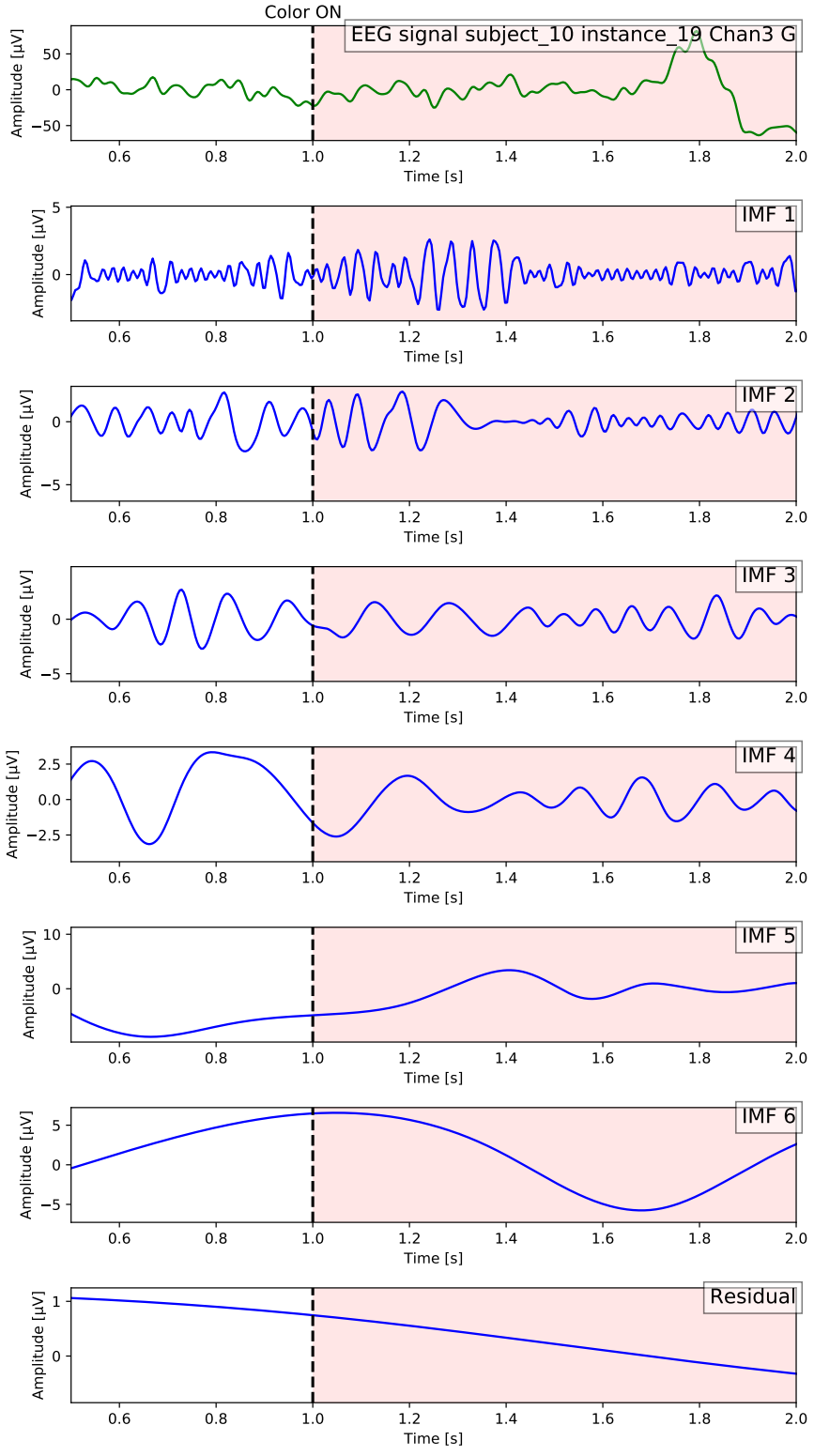


FIGURE 6.12: Dataset 1: EEG signal from one channel, extracted IMFs and the residual. Red background represents red light is on.

#### 6.2.3.2 Dataset 2

Fig. 6.13 presents the IMFs extracted from instance no. 50 and electrode O2 (Chan. 4), for subject 1, looking at green.

By visual inspection, it is not straight forward to identify the P300 peak expected at $t = 300\,ms$ in the decomposed data. IMF1 might be subject to mode mixing. The EMD algorithm finds the next IMF using the residual obtained in the previous iteration. A wrongly extracted IMF will, therefore, influence the rest of the process, resulting in distorted IMFs. It is, therefore, a reason to further explore methods to cope with this problem.

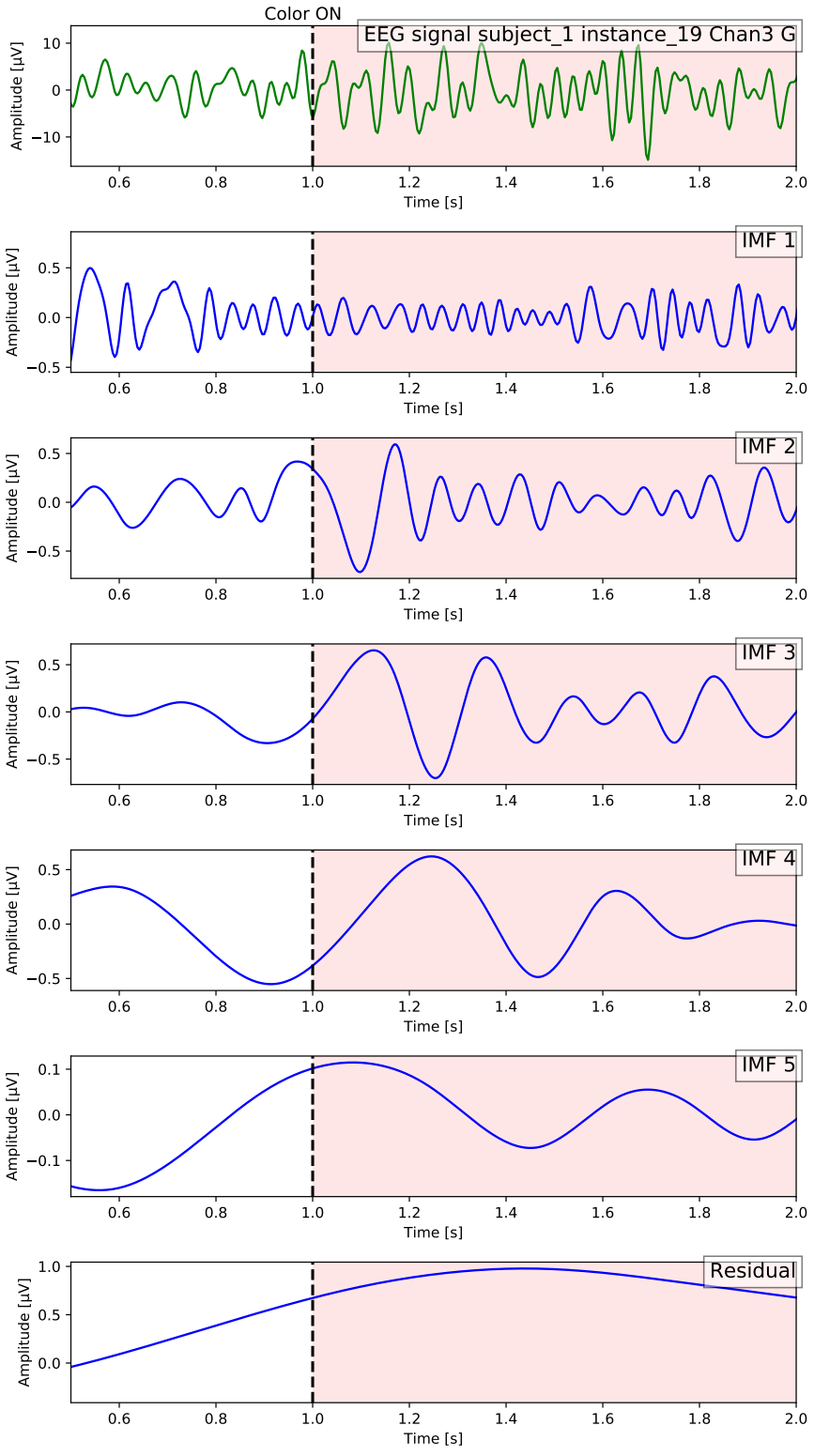


FIGURE 6.13: Dataset 2: EEG signal from one channel, extracted IMFs and the residual. Red background represents red light is on.

Similarly, Fig. 6.14 gives the spectrogram of each of the IMFs from Fig. 6.13. EMD successfully extracts the highest frequency components in the first IMFs.

IMF1 reveals a slight increase in magnitude for all frequencies at $t \approx 1.5\,s$, which might be related to color exposure or change of mental state for the person in the experiment. Extracted IMFs can be representing the physical properties of the process from which the signal is obtained. However, the problem of mode mixing in EMD caused by the presence of adjacent frequencies will cause loss of meaningful information in the IMFs. A new method for separating closely spaced spectral tones using EMD is presented in [78], and could be implemented to improve results.

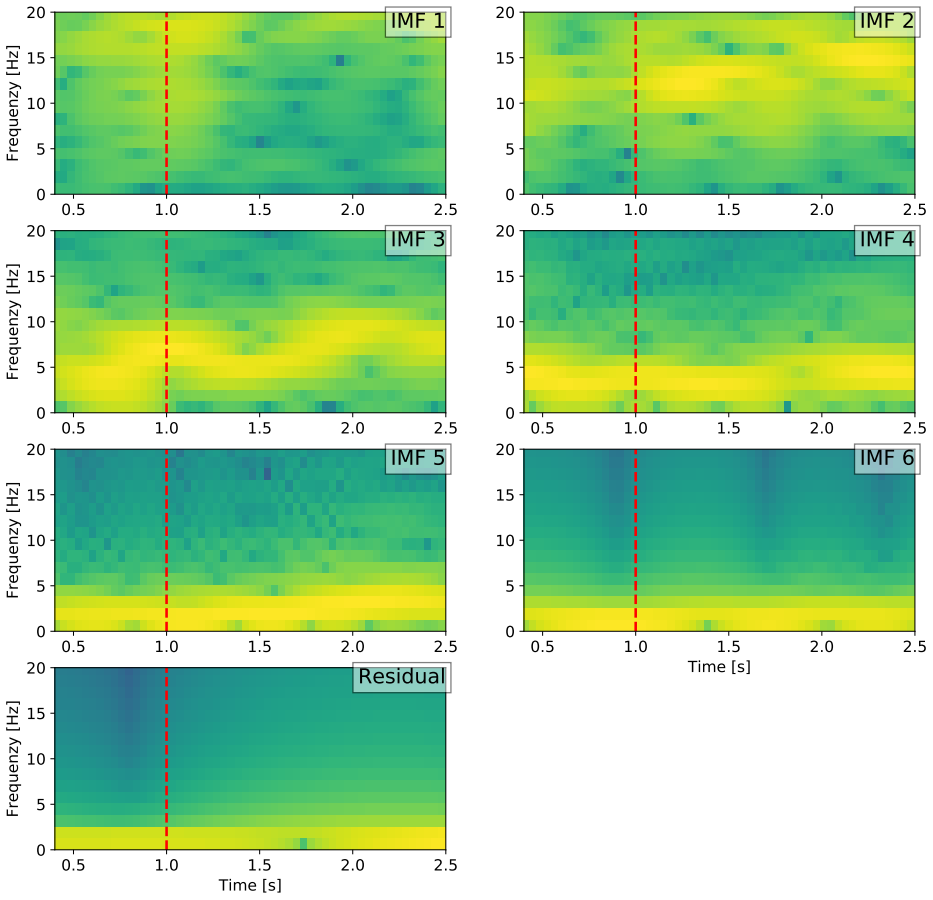


FIGURE 6.14: Dataset 2: Spectrograms of each of the five IMFs and the residual obtained from ten siftings.

## 6.3 Classification with feature extraction

To test if machine-learning models can classify EEG signals evoked by exposure to RGB colors using features based on EMD, the following experiments are proposed:

(I) Classification of exposure to color and gray

(II) Classification of exposure to red, green and blue considering signals across all subjects

(III) Classification of exposure to red, green and blue considering signals individually from each subject

For all experiments, the procedure described for *Feature extraction and classification* in Sec. 4.2.1 is used. The accuracy metric after 10-fold cross-validation is presented. As the classes are balanced in the dataset, accuracy serves as a satisfactory metric for assessing the performance. Note that the chance level accuracy for experiment (I) is 0.5, and 0.33 for both experiment (II) and (III).

The first experiment addresses research question one, presented in Ch. 1, and aims to provide experimental information about the performance of the method and to check if there is a set of features that can separate these two classes; gray and RGB colors.

In the second experiment, the classification consists of three classes; red, green, and blue. This experiment aims to discover if the features proposed are generalizable to all subjects, and hence represent a signature of the RGB colors in EEG recordings.

In the third experiment, the same three-class classification between RGB is done, using models trained and tested on data from the same subject. This test explores the possibility of subject tailored applications.

### Experiment (I); Gray vs RGB

For a possible real-time application, it will be necessary to clearly distinguish if the subject is looking at "nothing in particular", or decisively looking at a color. Uniform gray color is used to simulate "nothing in particular". The complexity of such differentiation was investigated by first classifying if subjects were looking at gray or RGB color using all available data from Dataset 2, referred to as "Dataset 2, complete".

An ERP is expected at approximately 300 $ms$ after the presentation of an infrequent stimulus. The part of the signal where the subject is exposed to the color will contain the P300 component, and it can be distinguished from a signal not containing an ERP. To investigate if the ERP is crucial for the classification between gray and color, a simple test was done where data points from $t = 1$ to $t = 2$ (where the P300 component is expected) was removed. This data is referred to as "Dataset 2, limited". All results, using both the complete and limited dataset, are presented in Tab. 6.1. In addition to using different sized datasets, the importance of features is assessed. The table contains the accuracies (Acc.) obtained for the using all features (all), the statistical features (stat.) and only one statistical feature, the mean (mean). Note that results for experiment I was only computed for Dataset 2.

TABLE 6.1: Dataset 2: Results for gray vs. color classification.

| **Data** | **Feat.** | **Classifier** | | | | | | | |
|---|---|---|---|---|---|---|---|---|---|
| | | **RF** | | **kNN** | | **SVM** | | **DT** | **NB** |
| | | Acc. | depth | Acc. | k | Acc. | ker. | Acc. | Acc. |
| **Dataset 2, complete** | all | **0.99** | 5 | 0.72 | 6 | **0.99** | lin. | 0.98 | 0.98 |
| | statistical. | 0.88 | 4 | 0.72 | 6 | **0.92** | lin. | 0.83 | 0.87 |
| | the mean | 0.89 | 6 | **0.91** | 8 | 0.84 | rbf | 0.87 | 0.89 |
| **Dataset 2, limited** | all | **0.87** | 5 | 0.62 | 4 | 0.85 | lin. | 0.86 | 0.85 |
| | statistical | **0.89** | 6 | 0.62 | 4 | 0.73 | poly | 0.86 | 0.85 |
| | the mean | 0.90 | 6 | **0.92** | 4 | 0.87 | rbf | 0.88 | 0.87 |

The best classification accuracy for each feature set is high, ranging from 0.91 to 0.99 for the complete dataset, and 0.87 to 0.92 for the limited dataset.

Surprisingly, for the limited dataset, the accuracy decreases with 0.12 using all features. An interesting finding is a 0.92 accuracy when using the limited dataset, and only one feature; the mean. A possible explanation can be that redundant features create noise that distorts the model due to limited source data. Further analysis is required to conclude the importance of the different features.

In this experiment, the lowest accuracy obtained is well above the chance level, which in two class classification is 0.5. These results yield a promising first step towards a less complex real-time application for separating between gray and RGB colors.

## Experiment (II); Classification of red, green and blue across all subjects

First, two separate models, including data from all 17 and 7 subjects for datasets 1 and 2 respectively, were developed, and the results are presented in Tab. 6.2. The maximum accuracy is the same for both datasets; 0.37 for Dataset 1, using 7-NN, and 0.37 for Dataset 2 using both RF with depth 2 and Gaussian NB. These results are weak but slightly better than the chance level of 0.33.

The different nature of the datasets makes the results non-comparable. For both datasets, a limited amount of data and individual differences are believed to impair the result, and hence, subject-specific models were developed (III).

TABLE 6.2: Classification accuracies (Acc.) using Dataset 1 and Dataset 2.

| **Dataset** | **Pre-processing description** | **Classifier** | | | | | |
|---|---|---|---|---|---|---|---|
| | | **RF** | | **kNN** | | **DT** | **NB** |
| | | Acc. | depth | Acc. | k | Acc. | Acc. |
| **Dataset 1** | Raw data | 0.36 | 2 | 0.34 | 3 | 0.34 | 0.33 |
| | Filtered data | 0.34 | 6 | 0.33 | 3 | 0.34 | 0.33 |
| | Artifacts removed | 0.35 | 5 | 0.34 | 5 | 0.32 | 0.32 |
| | Filtered and artifacts removed | 0.36 | 5 | 0.37 | 7 | 0.33 | 0.33 |
| **Dataset 2** | Pre-processed | 0.37 | 2 | 0.34 | 6 | 0.35 | 0.37 |

## Experiment (III); Subject specific classification of red, green and blue

The mean accuracy for the subject models is found by obtaining the maximum accuracy for each subject individually and then calculating the mean of these. The best performing classification algorithm differs dependent on the subject, and hence no algorithm, in particular, can be favored.

It should be remarked that the chance level for this experiment is 0.33, and the lowest accuracy obtained is still above that value.

### Results Dataset 1 (III)

Tab. 6.3 gives the average and max classification accuracy when creating subject-specific models. The individual average is based on all individual models, where parameters differ for each subject. None of these models are listed, but are indicated with **. Tab. 6.4 provides further details for each individual subject.

The highest individual accuracy obtained is 0.63 with 2-NN (subject 2 in Dataset 1). This accuracy was obtained using data that was bandpass filtered and stripped of artifacts before classification.

The best average performance across subjects was 0.45 and was also obtained on the filtered and artifact stripped dataset.

TABLE 6.3: Mean and maximum accuracy for subject models from Dataset 1.

| **Description** | **Classifier accuracy** | | | | | |
|---|---|---|---|---|---|---|
| | **raw data** | | **filtered data** | | **filtered and artifacts removed** | |
| **Average** | 0.42 | ** | 0.40 | ** | 0.45 | ** |
| **Best individual** | 0.52 | DT | 0.58 | RF depth 3 | 0.63 | 2-NN |

TABLE 6.4: Classification results for subject models, using raw and processed data from Dataset 1.

| **Subject no.** | **Raw data** | | **Filtered data** | | **Filtered, artif. removed** | |
|---|---|---|---|---|---|---|
| | **Acc.** | **Classifier** | **Acc.** | **Classifier** | **Acc.** | **Classifier** |
| **subject 1** | 0.52 | DT | 0.42 | 4-NN | 0.50 | 2-NN |
| **subject 2** | 0.52 | DT | 0.38 | RF depth 4 | **0.63** | 2-NN |
| **subject 3** | 0.40 | NB | 0.37 | NB | 0.50 | NB |
| **subject 5** | 0.43 | RF depth 2 | 0.37 | RF depth 2 | 0.43 | 2-NN |
| **subject 6** | 0.39 | 10-NN | 0.41 | RF depth 3 | 0.47 | 2-NN |
| **subject 7** | 0.38 | RF depth 2 | 0.39 | RF depth 6 | 0.43 | RF depth 5 |
| **subject 9** | 0.38 | 4-NN | 0.36 | NB | 0.43 | 9-NN |
| **subject 10** | 0.44 | RF depth 4 | 0.49 | NB | 0.49 | NB |
| **subject 11** | 0.39 | DT | 0.44 | RF depth 5 | 0.46 | 3-NN |
| **subject 13** | 0.39 | 10-NN | 0.39 | RF depth 6 | 0.40 | RF depth 4 |
| **subject 14** | 0.43 | 8-NN | 0.39 | 3-NN | 0.38 | RF depth 2 |
| **subject 15** | 0.40 | 9-NN | 0.39 | NB | 0.39 | NB |
| **subject 16** | 0.40 | 2-NN | 0.40 | 5-NN | 0.36 | RF depth 3 |
| **subject 17** | 0.45 | RF depth 5 | 0.43 | RF depth 5 | 0.45 | 9-NN |
| **subject 18** | 0.45 | 9-NN | **0.58** | RF depth 3 | 0.40 | RF depth 4 |
| **subject 19** | 0.38 | RF depth 3 | 0.37 | RF depth 5 | 0.36 | RF depth 6 |
| **subject 20** | 0.37 | 9-NN | 0.38 | RF depth 2 | 0.45 | 2-NN |

### Results Dataset 2 (III)

Concerning Dataset 2, one subject in particular obtained higher accuracy when testing with all classifiers: 0.58 of accuracy using NB, 0.51 using linear SVM, 0.47 with 6-NN, 0.53 using DT, and finally 0.57 using RF with depth 4. In contrast, another subject model classified at chance level. Tab. 6.5 summarizes accuracies of the RGB models for both a general model and considering each subject separately.

TABLE 6.5: Mean and maximum accuracy for subject models from Dataset 2.

| **Description** | **Classifier accuracy** | | | | | | | |
|---|---|---|---|---|---|---|---|---|
| | **RF** | | **kNN** | | **SVM** | | DT | **NB** |
| | **Acc.** | **depth** | **Acc.** | **k** | **Acc.** | **kernel** | **Acc.** | **Acc.** |
| **Individual average** | **0.41** | ** | 0.37 | ** | 0.39 | ** | 0.39 | 0.38 |
| **Best individual** | 0.57 | 4 | 0.47 | 6 | 0.51 | lin. | 0.53 | **0.58** |

### 6.3.1 Discussion - feature extraction

Experiment I shows encouraging results, but some limitations should be mentioned. It is difficult to know if the actual color exposure causes the successful classification, or other factors such as subjects being more focused during RGB exposure compared to a more relaxed state during gray exposure. However, this experiment proves a successful use of the method proposed for decomposition and feature extraction using EMD.

Across both experiments II and III, subject-specific models perform better than models trained across several subjects. To classify RGB correctly within one subject, the model has to learn features that are related to the exposure of a color for that individual, which can both come from actual visual stimuli, but also from other cognitive associations that individual makes. A non-generalizing response would, for instance, be a person that always thinks of the ocean each time the blue color appears on the screen. To classify signals correctly across several individuals, the model needs to learn features that represent the exposure to color in a more general sense. It has to ignore specific features that are strongly linked to specific individuals and pick out those who generalize across subjects. General models are less accurate than subject tailored models as general features are harder to extract. Generalized features are preferred, as they would likely enable less complicated and scaleable real-life applications.

The best results are obtained using pre-processed data. For Dataset 1, the accuracy increases when using data that has been bandpass filtered prior to decomposition and feature extraction, indicating that the proposed method benefits from using bandpass filtered data. Although EMD, in theory, is capable of removing noise, the bandpass filtered and artifact stripped data achieves higher accuracy than the raw data. The reason for this somewhat surprising result is not completely clear, but it could be that signals are not fully decomposed since a constant number of IMFs, and one residual is extracted from each channel. The

first IMF from the raw data hence contains mostly noise, while the first IMF from the filtered data includes more information from the actual brain response.

## 6.4 Classification with deep leaning

To test if DL can classify RGB colors using a time series of sampled EEG voltages as input, one experiment is proposed:

(II) Classification of exposure to red, green and blue considering signals across all the subjects

There is too little data to create individual subject models using DL, and the subject-specific experiments have been excluded in this section.

For all the experiments in this section, the EEGNet CNN model was used. The model is designed explicitly for classifying EEG raw data and has shown state-of-the-art performance in previous experiments.

The following measures are included in reporting the nature of the obtained models: no. of epochs (training rounds) and respective accuracy are presented in a table, the training and validation values are plotted against epoch no. Also, the performance of the corresponding CNN is visualized in a confusion matrix.

The confusion matrices have two dimensions ("true label" and "predicted label"), and identical sets of "classes" in both dimensions (red, green and blue). The content of the matrix is the number of false positives, false negatives, true positives, and true negatives. Particularly in unbalanced datasets, the confusion matrix is a better measure for the actual performance of the classifier than overall accuracy. Both Dataset 1 and Dataset 2 are balanced (same number of trials for each color). However, the confusion matrix is helpful to review if specific colors are more straightforward to classify than others.

A classification report, showing precision, recall and f1-score were also computed, and are included in Appendix B, Tab. B.1 and Tab. B.2 for Dataset 1 and Dataset 2, respectively.

For both datasets, the data is split into a training set and a test set with a test ratio of 0.33. The data is shuffled to ensure an equal distribution of subjects in both the training and test data. A random seed was set in Python to ensure reproducible results.

### 6.4.1 Dataset 1

Results from classification using CNN with Dataset 1 is summarized for each pre-processing technique in Tab. 6.6.

Table 6.6: CNN accuracy (Acc.) results for Dataset 1.

| **Input data** | **Epochs** | **Acc.** |
|---|---|---|
| Raw data | 100 | 0.28 |
| Filtered data | 50 | 0.38 |
| Artifacts removed | 30 | 0.27 |
| Filtered and artifacts removed | 30 | 0.38 |

The model accuracy for Dataset 1 is plotted in Fig. 6.15. The model fails to learn anything on the datasets without filtering. The accuracy has no positive trend for neither the training set nor the test set. For the filtered data, the model manages to fit the model well on the training set. The effect is not as successful on the test set, but there is a slight increase in test accuracy, indicating some generalization of learned features. The model is over-fitting to the training set. This effect could be reduced by adding regularization (for example, dropout or L2-norm), further pre-processing of the data (e.g., filtering and normalization), or by acquiring more data.

The confusion matrix for Dataset 1 is plotted in Fig. 6.16. As indicated in the overall accuracy, the filtered data generally yields better results than the unfiltered data. For the raw data (upper left) the predictions appear random, as the number of true positives is lower than the false positives, indicating no learned features of the different colors. Comparable results are seen for the artifact removed data, which also tend to predict *green* more often than *red* and *blue*. In general, the results using EEGNet with Dataset 1 are well below the accuracies required for any practical purposes.

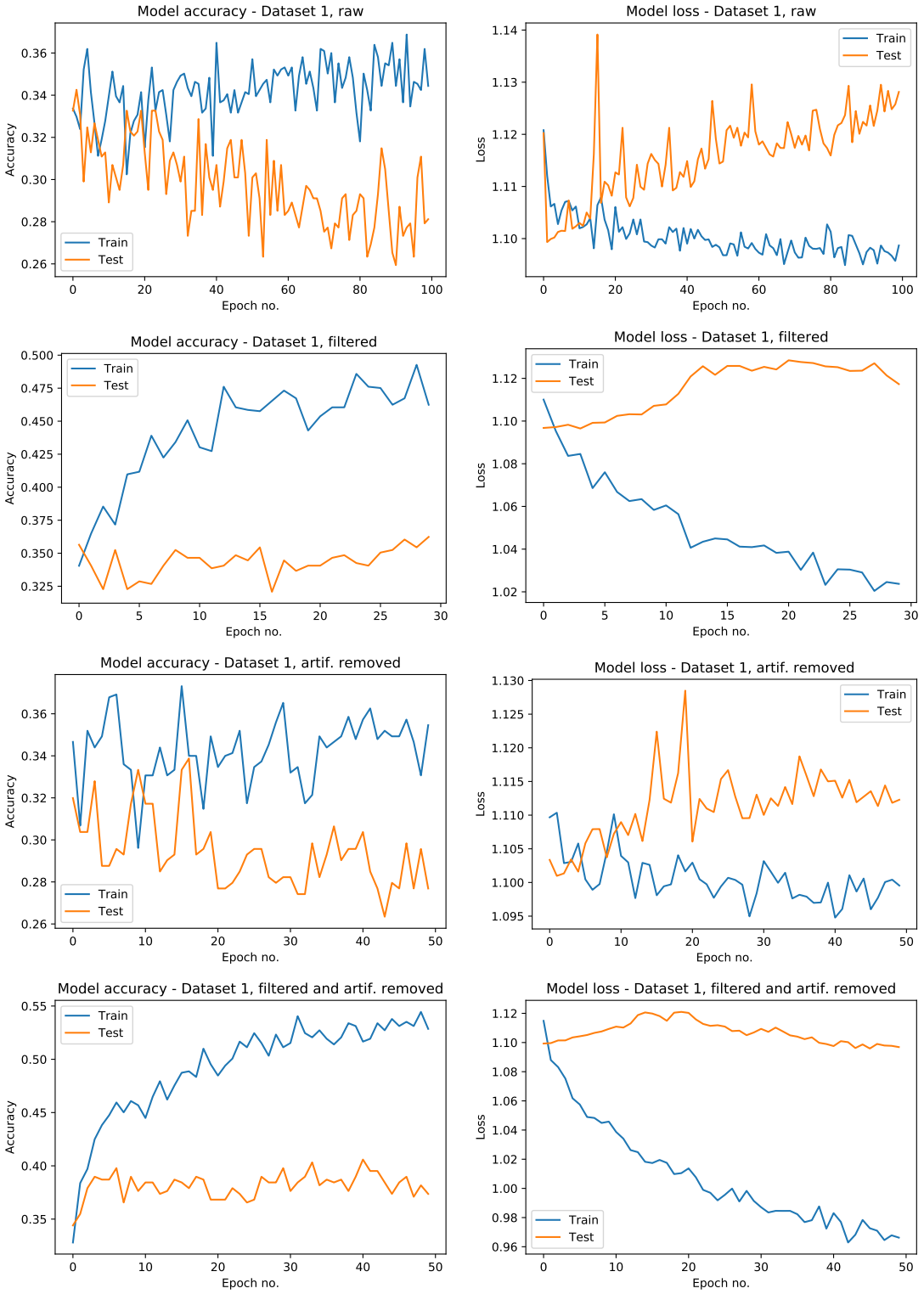


FIGURE 6.15: Left: Training and validation accuracy values. Right: Training and validation loss values. All results from Dataset 1.

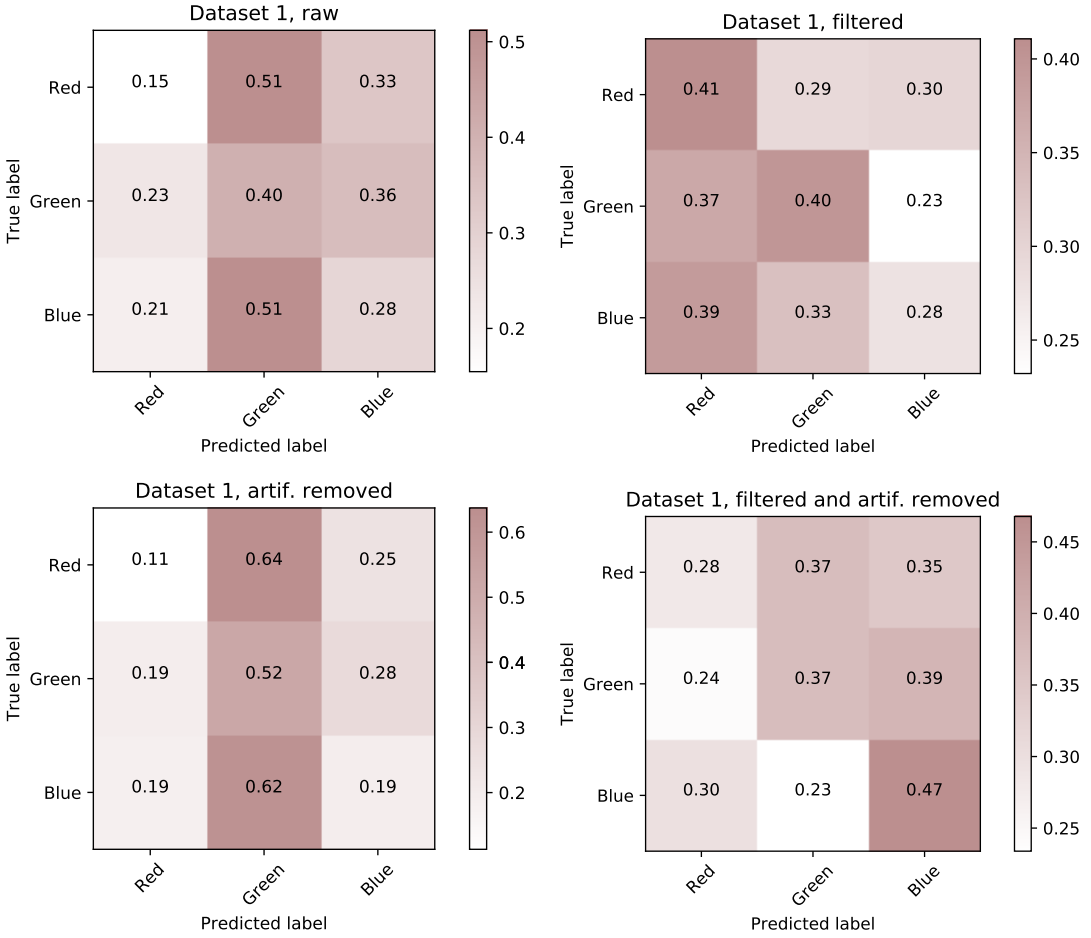


FIGURE 6.16: Confusion matrix for all versions of Dataset 1.

### 6.4.2 Dataset 2

The best accuracy obtained for Dataset 2 is 0.46, as given in Tab. 6.7. The training curves in Fig. 6.17 indicate a better ability to generalize than Dataset 1, due to less overfitting. Both the training and test accuracy, as well as the loss curves, have clear trends that indicate learning.

TABLE 6.7: CNN accuracy (Acc.) results for Dataset 2.

| **Input data** | **Epochs** | **Acc.** |
|---|---|---|
| Pre-processed data | 50 | 0.46 |

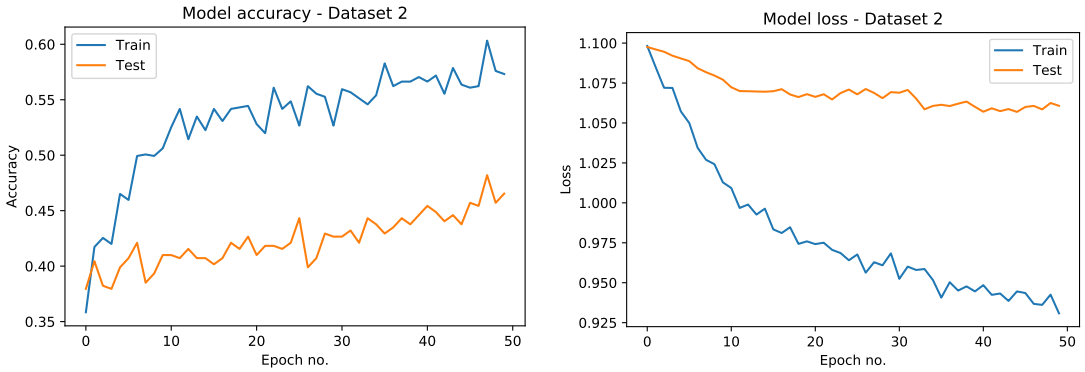


FIGURE 6.17: Confusion matrix for different versions of Dataset 2.

The confusion matrix for Dataset 2 is plotted in Fig. 6.18.

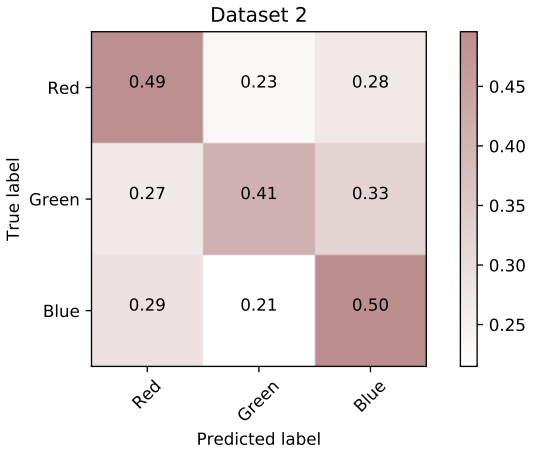


FIGURE 6.18: Confusion matrix for Dataset 2.

### 6.4.3 Discussion - using deep learning

Interestingly, Dataset 2 shows better results using CNN compared to the feature-extraction method. This shows that the automatic feature extraction of the CNN model manages to extract features relevant to the classification better that the features included in the EMD approach. However, it is much harder to analyze features from the CNN afterward, due to the nature of NN. Dataset 1 shows similar results for both methods, given pre-processed data.

The main variations between the two datasets are that Dataset 2 has more data per subject, fewer subjects, and more pre-processing. Fewer subjects reduce the variance in the dataset, and the increased number of trials provides more support for learning essential features. The pre-processing excludes noise, enabling the model to capture features more quickly. This reasoning shows that further

attention should be given to increasing dataset size and doing more pre-processing to get better results with NNs.

# Chapter 7

# Summary

This thesis has investigated the possibility to classify EEG signals produced by visual exposure to RGB, thought to be especially useful for rapid control and decreased learning times for future BCI applications. First, background theory and relevant research are outlined and reviewed. An in-house experiment with 17 participants was designed and conducted, acquiring a dataset of raw EEG signals produced by random visual exposure to RGB colors. The dataset is used together with a complementary dataset for further analysis and classification. The highest accuracies were 0.38 and 0.63 for generic and subject-specific models respectively.

In the signal analysis step, STFT and EMD were studied. The EMD process decomposed the raw signals from each channel into several IMFs. As the IMFs alone did not reveal distinct features, the STFT of each IMF was plotted. None of the methods reveals a lasting unique frequency marker for each of the colors detectable by visual inspection.

Two fundamentally different methods have been explored. The feature driven method uses IMFs as the basis for feature extraction. Features are manually selected and automatically extracted from the IMFs, and finally used as the input for classical ML algorithms. Three experiments were computed; the classification of gray and RGB, general classification of the three RGB colors, and finally, a subject-specific model to classify RGB.

Classification accuracy of gray and any of the RGB colors were up to 0.99 with a general model based on the second dataset, using statistical, energy and fractal features. The results indicate the possibility of deciding if a person is looking at a primary color.

Classification of RGB considering all subjects together gives limited results. The best accuracy is 0.37 for both datasets tested and is obtained using pre-processed data. This number is much lower than the value required for reliable classification. Nevertheless, the accuracy is slightly above the chance level of 0.33 for the 3 class classification, which indicates that the extracted features can partly describe the colors in EEG signals.

In addition to the generic models, the feasibility of subject-specific models was tested. The accuracy vary from 0.36 to 0.63. The reason can be individual differences such as the amount of hair or attention level during data collection. It can be concluded that color classification suffers from subject dependencies, and a subject tailored system should be considered for future work.

A CNN was adopted to classify EEG signals without manual feature extraction, motivated by the success of deep learning in the field of image classification. The method used raw or processed signals as input for a CNN, which learns the relevant features trough supervised training. The datasets had too few trials for each subject to train a CNN for each subject, hence only generic models were tested. The highest accuracy for the two datasets is 0.38 and 0.46. It should be remarked that the second dataset, achieving the highest accuracy, ha only 7 subjects, while the other dataset had 17 subjects. Fewer subjects reduce the variance in the dataset, and as it was previously concluded that subject-specific models benefit accuracy, the 7-subject model naturally achieves better results.

As might have been expected, results using CNN is restrained by limited amounts of data. The pre-processed datasets perform better than the raw signals, although a CNN can learn to eliminate noise and extract relevant features. A possible approach could be to train the classifiers on a global dataset and then add several new instances for one specific subject.

An important issue to resolve for future studies is the limited amount of data. CNN performance is expected to improve if allowed to train on expanded datasets, for example, obtained by data augmentation or ensemble learning.

Color exposure does not produce lasting features in amplitude nor frequency in raw EEG signals. Dedicated methods are required to extract useful information from such noisy and complex signals. It is not clear, however, if EEG signals contain features that reliably can be used to distinguish RGB colors for practical applications. Further investigation of methods is still necessary to find the practical application potential of color controlled BCIs.

# Chapter 8

# Conclusion and future work

Inspection of the raw signals acquired for this thesis reveals slow drift and high-frequency noise on the electrodes placed on the occipital lobe, likely related to the nearby combined amplifier and transmitter, poor electrode-skin contact, or perhaps gradually increasing electrode temperature. ICA and a bandpass filter for $0.1 - 30\,Hz$ was applied in the pre-processing stage, successfully increasing the accuracy in the classification step.

In the signal analysis step, STFT and EMD were studied. None of the methods reveals a permanent unique frequency marker for each of the colors detectable by visual inspection of transformations.

A generic model for classification of RGB colors is challenging using the proposed methods. Subject tailored models obtain considerably higher classification accuracy than the generic models. The highest accuracy for the generic model is 0.37 and 0.48 for the feature driven and DL method, respectively. Using the feature-driven method, the best subject-specific model have an accuracy of 0.63. Limited amounts of data prevented the development of a subject-specific CNN.

Based on the results, it can be concluded that the preferred solution to classify RGB using feature extraction is to select and train subject-tailored models. As the CNN achieves higher classification accuracy, subject-specific CNN models are thought to yield even higher accuracy.

Subject-specific models demand more data, either by data collection, data augmentation, or transfer learning. Alternatively, new features and new methods for feature selection and extraction can be explored using the acquired dataset.

Although the model performances were not ideal, it is still believed that the dataset collected and the results presented constitute an essential first step towards a classification of EEG signals evoked by visual exposure to RGB colors.

Plots of the raw signals, as well as plots of the epoched data, clearly show high levels of noise and artifacts. It is suggested that considerable attention should be given to the pre-processing stage, and in obtaining a version of Dataset 1 that is free for extreme artifacts and high levels of noise.

An improved method for feature extraction could extract the maximum number of IMFs, select the most important ones, and thereby avoid the need for the bandpass filter. There are certain limitations of using a bandpass filter. It can, for instance, remove slow cortical activity, whether spontaneous or stimulus-evoked [75]. Another issue is that transient features can also be distorted in the filtering. Processing that erases such information is not optimal and is a significant limitation.

Alternative solutions exist, such as a notch filter for noise removal, and detrending by extracting the EMD residual. EMD would also be applicable to remove high-frequency noise, usually by extracting the first IMF from the original signal. However, for some tasks, the first IMF can contain useful information. Hence, there is no single solution to the problem, as it depends on the type of experiment. Undoubtedly, the pre-processing is a crucial step to obtain high-quality data.

Also, the feature-driven method uses a large number of features, obtained at a high computational cost. This motivates the application of methods for feature selection or reduction. An analysis of the features' relevance is likely to reveal that some features are less important than others, and hence can be excluded. Decreasing the computational cost of the method is essential as this would allow efficient real-time classification for a real application.

# Bibliography


[1] David Steyrl, Reinmar Kobler, and Gernot Müller-Putz. On similarities and differences of invasive and non-invasive electrical brain signals in brain-computer interfacing. *Journal of Biomedical Science and Engineering*, 9(8):393–398, 6 2016.

[2] Hans Berger. Über das elektrenkephalogramm des menschen. *Archiv für Psychiatrie und Nervenkrankheiten*, 87(1):527–570, 12 1929.

[3] Sheffy Bhayee, Patricia Tomaszewski, Daniel H. Lee, Graeme Moffat, Lou Pino, Sylvain Moreno, and Norman A. S. Farb. Attentional and affective consequences of technology supported mindfulness training: a randomised, active control, efficacy trial. *BMC Psychology*, 4(1):60, 11 2016.

[4] Pouya Bashivan, Irina Rish, and Steve Heisig. Mental state recognition via wearable EEG. 2 2016.

[5] Xinyi Yong and Carlo Menon. EEG classification of different imaginary movements within the same limb. *PloS one*, 10:e0121896, 04 2015.

[6] Sara Åsly. The effect of RGB colour stimuli on the human brain: finding a unique descriptor in EEG recordings. Semester project, Norwegian University of Science and Technology (NTNU), 2018.

[7] S Ogawa, T M Lee, AR Kay, and D W Tank. Brain magnetic resonance imaging with contrast dependent blood oxygenation. *Proceedings of the National Academy of Sciences of the United States of America*, 87:9868–72, 1 1990.

[8] Staff of Blausen Medical. Medical gallery of blausen medical 2014. *WikiJournal of Medicine*, page 31, 8 2014.

[9] Larry Squire, Darwin Berg, Floyd E. Bloom Sascha du Lac, and Anirvan Ghosh Nicholas C. Spitzer. *University Physics; 15 edition.* Academic Press, 11 2012.

[10] Christine A. Evers Cecie Starr and Lisa Starr. *Biology: Concepts and Applications*. Brooks/Cole biology series. Thomson, 2006.

[11] Hugh D. Young and Roger A. Freedman. *University Physics; 15 edition*. Pearson, 2019.

[12] Kim Cooper CJ Kazilek. Rods and cones. *Arizona State University School of Life Sciences Ask A Biologist*, Jan 6, 2010.

[13] David H. Hubel and Torsten N. Wiesel. Brain mechanisms of vision. *Scientific American*, 241:130, 1979.

[14] David H. Hubel. The brain. *Scientific American*, 241:38, 1979.

[15] Nobel Media AB 2019. The Nobel Prize in Physiology or Medicine 1981, 2016. Press release.

[16] Graham Saxby. *The science of imaging*. CRC Press, 2 edition, 2010.

[17] Tom Baden and Thomas Euler. Early vision: Where (some of) the magic happens. *Current Biology*, 23(24):R1096 – R1098, 2013.

[18] Theresa Puthussery, Sowmya Venkataramani, Jacqueline Gayet-Primo, Robert G. Smith, and W. Rowland Taylor. Channels in axon initial segments of bipolar cells augment input to magnocellular visual pathways in the primate retina. *Journal of Neuroscience*, 33(41):16045–16059, 2013.

[19] Stephen Lucian Polyak. *The Retina*. The University of Chicago Press, 1 edition, 1941.

[20] Robert Shapley and V. Hugh Perry. Cat and monkey retinal ganglion cells and their visual functional roles. *Trends in Neurosciences*, 9:229–235, 1986.

[21] Jonathan Wolpaw and Elizabeth Winter Wolpaw. *Brain-Computer Interfaces: Principles and Practice*. Oxford University Press, USA, 2012.

[22] Maureen Clerc, Laurent Bougrain, and Fabien Lotte. *Brain-Computer Interfaces 1: Foundations and Methods*. Wiley-ISTE, 7 2016.

[23] Richard W Homan, John Herman, and Phillip Purdy. Cerebral location of international 10–20 system electrode placement. *Electroencephalography and Clinical Neurophysiology*, 66(4):376 – 382, 1987.

[24] George H. klem, Hans Otto Lüders, H.H. Jasper, and C. Elger. The ten-twenty electrode system of the international federation. the international federation of clinical neurophysiology. *Electroencephalography and clinical neurophysiology. Supplement*, 52:3–6, 2 1999.

[25] Luis F. Nicolas-Alonso and Jaime Gomez-Gil. Brain computer interfaces, a review. *Sensors (Basel, Switzerland)*, 12:1211–79, 12 2012.

[26] Thalía Harmony. The functional significance of delta oscillations in cognitive processing. front. integr. *Frontiers in integrative neuroscience*, 7:83, 12 2013.

[27] Wolfgang Klimesch. EEG alpha and theta oscillations reflect cognitive and memory performance: A review and analysis. *Brain research. Brain research reviews*, 29:169–95, 5 1999.

[28] Wolfgang Klimesch. Alpha-band oscillations, attention, and controlled access to stored information. *Trends in cognitive sciences*, 16, 11 2012.

[29] Kazutaka Takahashi, Maryam Saleh, Richard D Penn, and Nicholas Hatsopoulos. Propagating waves in human motor cortex. *Frontiers in human neuroscience*, 5:40, 4 2011.

[30] Bijan Pesaran, John Pezaris, Maneesh Sahani, Partha P Mitra, and Richard A Andersen. Temporal structure in neuronal activity during working memory in macaque parietal cortex. *Nature neuroscience*, 5:805–11, 9 2002.

[31] Elizabeth Bauer, Rony Paz, and Denis Paré. Gamma oscillations coordinate amygdalo-rhinal interactions during learning. *The Journal of neuroscience : the official journal of the Society for Neuroscience*, 27:9369–79, 9 2007.

[32] John Polich. Updating p300: an integrative theory of p3a and p3b. *Clinical Neurophysiology*, 118:2128 – 2148, 2007.

[33] Hasan Ocak. Optimal classification of epileptic seizures in EEG using wavelet analysis and genetic algorithm. *Signal Process.*, 88(7):1858–1867, 7 2008.

[34] Leon Cohen. What is a multicomponent signal? *Proc. ICASSP*, 5:113 – 116, 4 1992.

[35] John G. Proakis and Dimitris K. Manolakis. *Digital Signal Processing.* Pearson, 4 edition, 2014.

[36] Jont B. Allen. Short term spectral analysis, synthesis, and modification by discrete fourier transform. *IEEE Transactions on Acoustics, Speech, and Signal Processing*, 25(3):235–238, 6 1977.

[37] Nicholas Huang, Z Shen, S.R. Long, M.C. Wu, H.H. Shih, Quanan Zheng, N.C. Yen, Chi-Chao Tung, and H.H. Liu. The empirical mode decomposition and the hilbert spectrum for nonlinear and non-stationary time series analysis. *Proc. R. Soc. A*, 454:679–699, 3 1998.

[38] Farhan Riaz, Ali Hassan, Saad Rehman, Imran Khan Niazi, and Kim Dremstrup. EMD-based temporal and spectral features for the classification of EEG signals using supervised learning. *IEEE Transactions on Neural Systems and Rehabilitation Engineering*, 24:28–35, 2016.

[39] Norden E. Huang and Zhaohua Wu. A review on hilbert-huang transform: Method and its applications to geophysical studies. *Reviews of Geophysics*, 46(2), 2008.

[40] Olav B. Fosso and Marta Molinas. Method for mode mixing separation in empirical mode decomposition. *arXiv preprint arXiv:1709.05547*, 2017.

[41] Baoping Tang, Shaojiang Dong, and Tao Song. Method for eliminating mode mixing of empirical mode decomposition based on the revised blind source separation. *Signal Processing*, 92:248–258, 1 2012.

[42] Zhaohua Wu and Norden Huang. Ensemble empirical mode decomposition: a noise-assisted data analysis method. *Advances in Adaptive Data Analysis*, 1:1–41, 1 2009.

[43] Lars-Erik Notevarp Bjørge and Trond Hübertz Emaus. Identification of EEG-based signature produced by visual exposure to the primary colors RGB. Master's thesis, Norwegian University of Science and Technology, Department of Engineering Cybernetics, Norway, 2017.

[44] G. Chandrashekar and F. Sahin. A survey on feature selection methods. *Computers & Electrical Engineering*, 40(1):16–28, 1 2014.

[45] I. Guyon and A. Elisseeff. Special issue on variable and feature selection. *An Introduction to Variable and Feature Selection*, 3:1157–1182, 2003. cited By 29.

[46] Cindy Goh, Brahim Hamadicharef, Goeff Henderson, and Emmanuel Ifeachor. Comparison of fractal dimension algorithms for the computation of EEG biomarkers for dementia. *CIMED'05: Proc. Computational Intelligence in Medicine and Healthcare*, 6 2005.

[47] T Higuchi. Approach to an irregular time series on the basis of the fractal theory. *Physica D*, 31, 1 1998.

[48] S. Russell and P. Norvig. *Artificial Intelligence: A Modern Approach*. Series in Artificial Intelligence. Prentice Hall, Upper Saddle River, NJ, third edition, 2010.

[49] Trevor Hastie, Robert Tibshirani, and Jerome Friedman. *The Elements of Statistical Learning: Data Mining, Inference, and Prediction, Second Edition (Springer Series in Statistics)*. 02 2009.

[50] Vladimir Vapnik. *Statistical Learning Theory*. Wiley-Interscience, 9 1998.

[51] Yann LeCun, Yoshua Bengio, and Geoffrey Hinton. Deep learning. *Nature*, 521(7553):436 – 444, 2015.

[52] Lewis Forder, Jenny Bosten, Xun He, and Anna Franklin. A neural signature of the unique hues. *Scientific Reports*, 7, 2 2017.

[53] Xiaolong Liu and Keum-Shik Hong. Detection of primary RGB colors projected on a screen using fNIRS. *Journal of Innovative Optical Health Sciences*, 10(3):1750006, 2017.

[54] Saim Rasheed and Daniele Marini. Classification of EEG signals produced by RGB colour stimuli. *Journal of Biomedical Engineering and Medical Imaging*, 2(5):56, 10 2015.

[55] Eman Alharbi, Saim Rasheed, and Seyed Buhari. Single trial classification of evoked EEG signals due to RGB colors. *BRAIN. Broad Research in Artificial Intel ligence and Neuroscience*, 7(1):29–41, 2016.

[56] Je-Hun Yu and Kwee-Bo Sim. Classification of color imagination using emotiv epoc and event-related potential in electroencephalogram. *Journal of Innovative Optical Health Sciences*, 127(20):9711–9718, 2016.

[57] L. Yang and H. Leung. An online bci game based on the decoding of users' attention to color stimulus. In *2013 35th Annual International Conference of the IEEE Engineering in Medicine and Biology Society (EMBC)*, pages 5267–5270, 7 2013.

[58] Ai Yoto, Tetsuo Katsuura, Koichi Iwanaga, and Yoshihiro Shimomura. Effects of object color stimuli on human brain activities in perception and attention referred to EEG alpha band response. *Journal of physiological anthropology*, 26:373–9, 6 2007.

[59] H. Zhang and Z. Tang. To judge what color the subject watched by color effect on brain activity. *IJCSNS International Journal of Computer Science and Network Security*, 11(2):80–83, 2 2011.

[60] Daniel S. Park, William Chan, Yu Zhang, Chung-Cheng Chiu, Barret Zoph, Ekin D. Cubuk, and Quoc V. Le. Specaugment: A simple data augmentation method for automatic speech recognition, 4 2019.

[61] Zhengqi Li, Tali Dekel, Forrester Cole, Richard Tucker, Noah Snavely, Ce Liu, and William T. Freeman. Learning the depths of moving people by watching frozen people, 4 2019.

[62] Ran Manor and Amir B. Geva. Convolutional neural network for multi-category rapid serial visual presentation bci. *Frontiers in Computational Neuroscience*, 9, 12 2015.

[63] Hubert Cecotti, Miguel P Eckstein, and Barry Giesbrecht. Single-trial classification of event-related potentials in rapid serial visual presentation tasks using supervised spatial filtering. *IEEE transactions on neural networks and learning systems*, 25:2030–2042, 11 2014.

[64] Jared Shamwell, Hyungtae Lee, Heesung Kwon, Amar Marathe, Vernon Lawhern, and William Nothwang. Single-trial EEG RSVP classification using convolutional neural networks, 5 2016.

[65] WarrenWeckesser. Butterworth bandpass, 3 2012. .

[66] Luis Alfredo Moctezuma and Marta Molinas. *EEG-Based Subjects Identification Based on Biometrics of Imagined Speech Using EMD*, pages 458–467. Springer, Cham, 12 2018.

[67] Sara Åsly, Luis Alfredo Moctezuma, Monika Gilde, and Marta Molinas. Towards EEG-based signals classification of RGB color-based stimuli. In *Proceedings of the 8th Graz Brain-Computer Interface Conference 2019*, 2019.

[68] F. Pedregosa, G. Varoquaux, A. Gramfort, V. Michel, B. Thirion, O. Grisel, M. Blondel, P. Prettenhofer, R. Weiss, V. Dubourg, J. Vanderplas, A. Passos, D. Cournapeau, M. Brucher, M. Perrot, and E. Duchesnay. Scikit-learn: Machine learning in Python. *Journal of Machine Learning Research*, 12:2825–2830, 2011.

[69] Vernon J Lawhern, Amelia J Solon, Nicholas R Waytowich, Stephen M Gordon, Chou P Hung, and Brent J Lance. EEGNet: a compact convolutional neural network for EEG-based brain–computer interfaces. *Journal of Neural Engineering*, 15(5):056013, 2018.

[70] Diederik Kingma and Jimmy Ba. Adam: A method for stochastic optimization. *International Conference on Learning Representations*, 12 2014.

[71] g.tec Guger technologies. Advanced biosignal acusition, processing and analysis, 2016. product catalogue.

[72] g.tec Guger technologies. g.needaccess CLIENT API V1.16.01, 2016.

[73] g.tec Guger technologies. g.Nautilus RESEARCH instructions for use V 1.18.01, 2016.

[74] G Repovs. Dealing with noise in EEG recording and data analysis. *Informatica Medica Slovenica*, 15:18–25, 1 2010.

[75] Alain de Cheveigné and Dorothée Arzounian. Robust detrending, rereferencing, outlier detection, and inpainting for multichannel data. *NeuroImage*, 172:903 – 912, 2018.

[76] Scott Makeig. Auditory event-related dynamics of the EEG spectrum and effects of exposure to tones. *Electroencephalography and Clinical Neurophysiology*, 86(4):283 – 293, 1993.

[77] Saim Rasheed, Daniele Marini, and Alessandro Rizzi. Recognition of colors in EEG: planning towards brain-computer interface applications, 1 2012.

[78] Yunchao Gao, Guangtao Ge, Zhengyan Sheng, and Enfang Sang. Analysis and solution to the mode mixing phenomenon in emd. *Congress on Image and Signal Processing*, 2008.

# Appendix A

# Experimental setup

## A.1 Subject information

Table A.1: Subject information.

| Subject (no.) | Handedness (L/R) | Gender (M/F) | Age (years) | Color blind (Y/N) |
|---|---|---|---|---|
| 1 | R | M | 26 | N |
| 2 | R | F | 25 | N |
| 3 | R | F | 23 | N |
| 4 | R | M | 24 | N |
| 5 | R | F | 23 | N |
| 6 | R | F | 23 | N |
| 7 | R | M | 26 | N |
| 8 | R | F | 24 | N |
| 9 | R | M | 27 | N |
| 10 | R | F | 21 | N |
| 11 | R | M | 25 | N |
| 12 | R | M | 26 | N |
| 13 | R | M | 25 | N |
| 14 | R | M | 23 | N |
| 15 | R | M | 21 | N |
| 16 | R | M | 22 | N |
| 17 | R | F | 21 | N |
| 18 | R | F | 22 | N |
| 19 | R | M | 23 | N |
| 20 | R | F | 26 | N |

## A.2 Technical specifications for data collection

TABLE A.2: Questionnaire given to all participants.

| | | | | |
|---|---|---|---|---|
| **Before** | How long did you sleep (no. hours)? | | | |
| | Did you drink coffee the past 24 hours (no. hours before)? | | | |
| | Did you drink alcohol the past 24 hours (no. hours before)? | | | |
| | Did you smoked within the past 24 hours? (no. hours before)? | | | |
| **Before and after** | How do you feel? | Relaxed | 1 2 3 4 5 | Anxious |
| | How do you feel? | Exciting | 1 2 3 4 5 | Boring |
| | Physical state | Very good | 1 2 3 4 5 | Very bad/tired |
| | Mental state | Very good | 1 2 3 4 5 | Very bad/tired |
| | Attention level | High | 1 2 3 4 5 | Low |
| **After** | Did you look away from the screen? | | | |
| | Did you close your eyes consciously? | | | |
| | How many trials you miss? | | | |
| | How was this experiment? | | | |
| | Duration | Short | 1 2 3 4 5 | Long |
| | Procedure | Good | 1 2 3 4 5 | Bad |
| | Environment | Comfortable | 1 2 3 4 5 | Uncomfortable |

TABLE A.3: Technical specifications for data collection - Dataset1.

| **Description** | **Specification** |
|---|---|
| Recording device | g.tec's g.MOBIlab+ portable device |
| Recording software | g.Nautilus |
| Sampling rate | $250Hz$ |
| Processed and analyzed | offline, Python |
| Band-pass filter | $0.1 - 30Hz$ |
| Artifact rejection | with manual selection with ICA |
| Electrode placement | [FP1, FP2, AF3, AF4, P03, P04, O1, O2, ] |
| Electrode reference | right ear lobe |
| Electrode ground | left ear lobe |
| Nr. of subjects | 20 |
| Screen - subject distance | $1.5m$ |
| Base color between RGB | gray and gray with cross |
| Luminosity of color | $250cd/m^2$ |

TABLE A.4: Technical specifications for data collection - Dataset 2.

| **Description** | **Specification** |
|---|---|
| Recording device | g.tec's g.MOBIlab+ portable device |
| Recording software | BCI2000 |
| Sampling rate | $256Hz$ |
| Processed and analyzed | offline, EEGlab, MATLAB |
| Band-pass filter | $0.1 - 30Hz$ |
| Artifact rejection | All signals that crossed $\pm 60\mu V$ |
| Electrode placement | [P3, P4, O1, O2] |
| Electrode reference | right ear lobe |
| Nr. of subjects | 7 |
| Screen - subject distance | $3.5m$ |
| Base color between RGB | gray |
| Luminosity of color | $4.5cd/m^2$ |

# Appendix B

# Results

Appendix B includes extensive material forom the results presented in Ch. 6.

## B.1 Event Related Potentials

Additional plots of epoched data are presented in the following section.

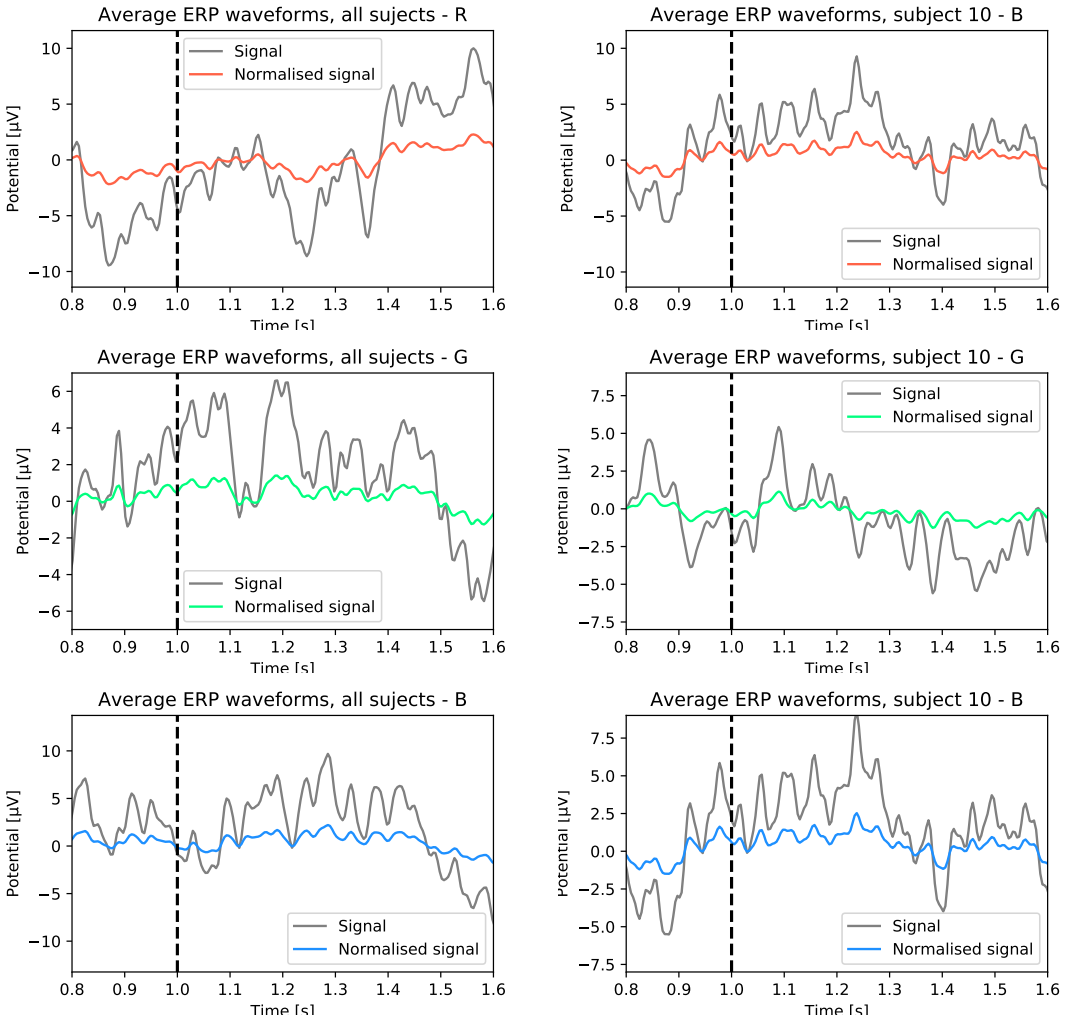


FIGURE B.1: Dataset 1: Averaged ERP waveform produced by RGB, for all subjects (left) and one subject (right).

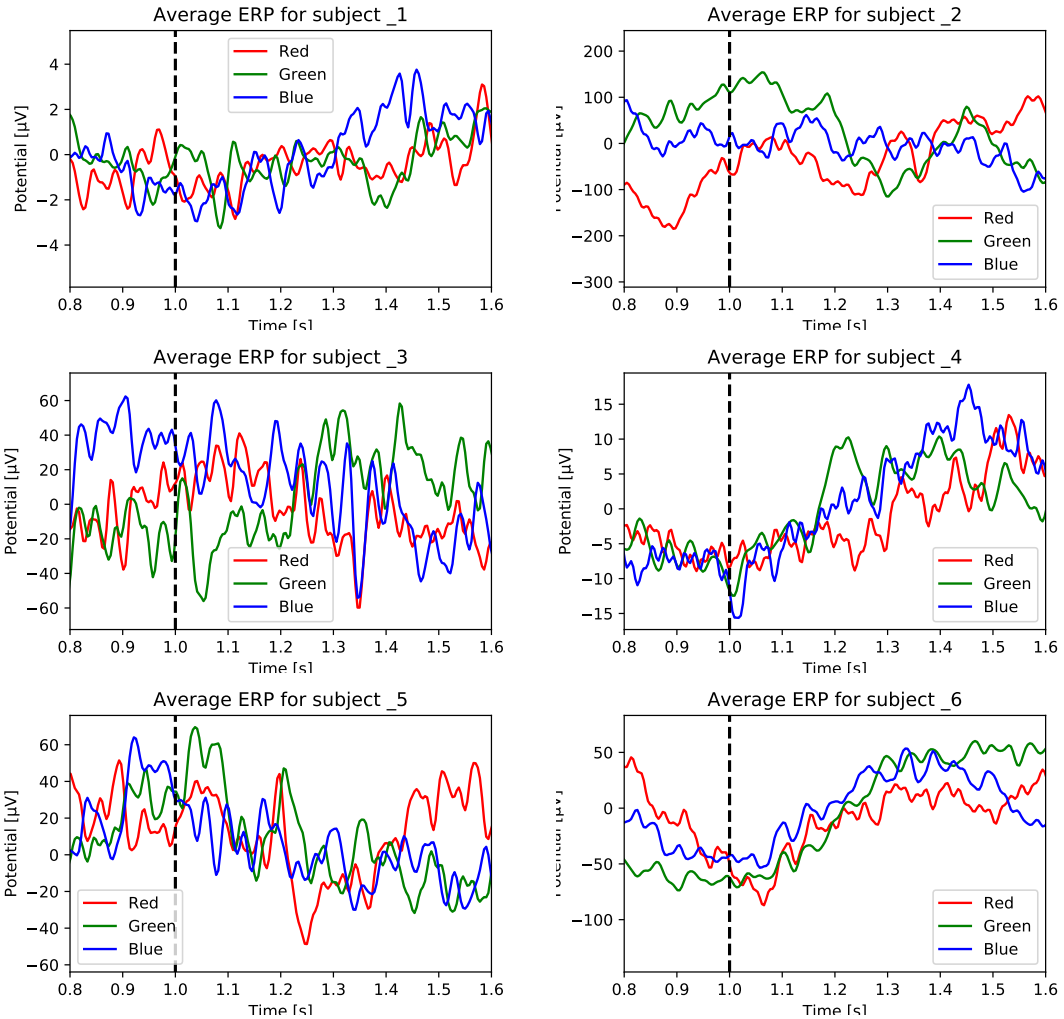


FIGURE B.2: Dataset 1: Individual differences in averaged ERP waveforms for color exposure to RGB.

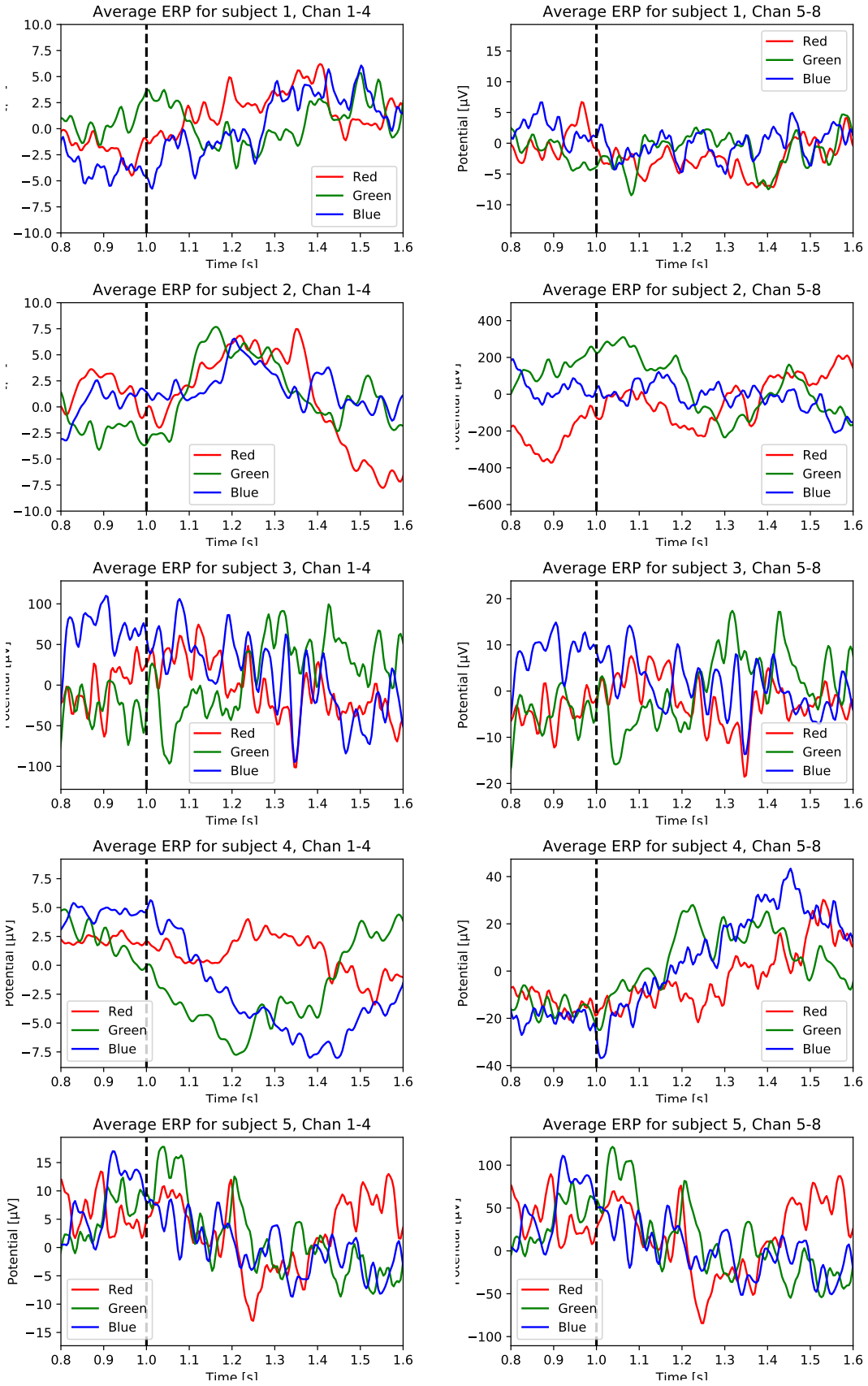


FIGURE B.3: Dataset 1: Individual averaged RGB plots for Chan. 1-4 (left) and Chan. 5-8 (right), part 1.

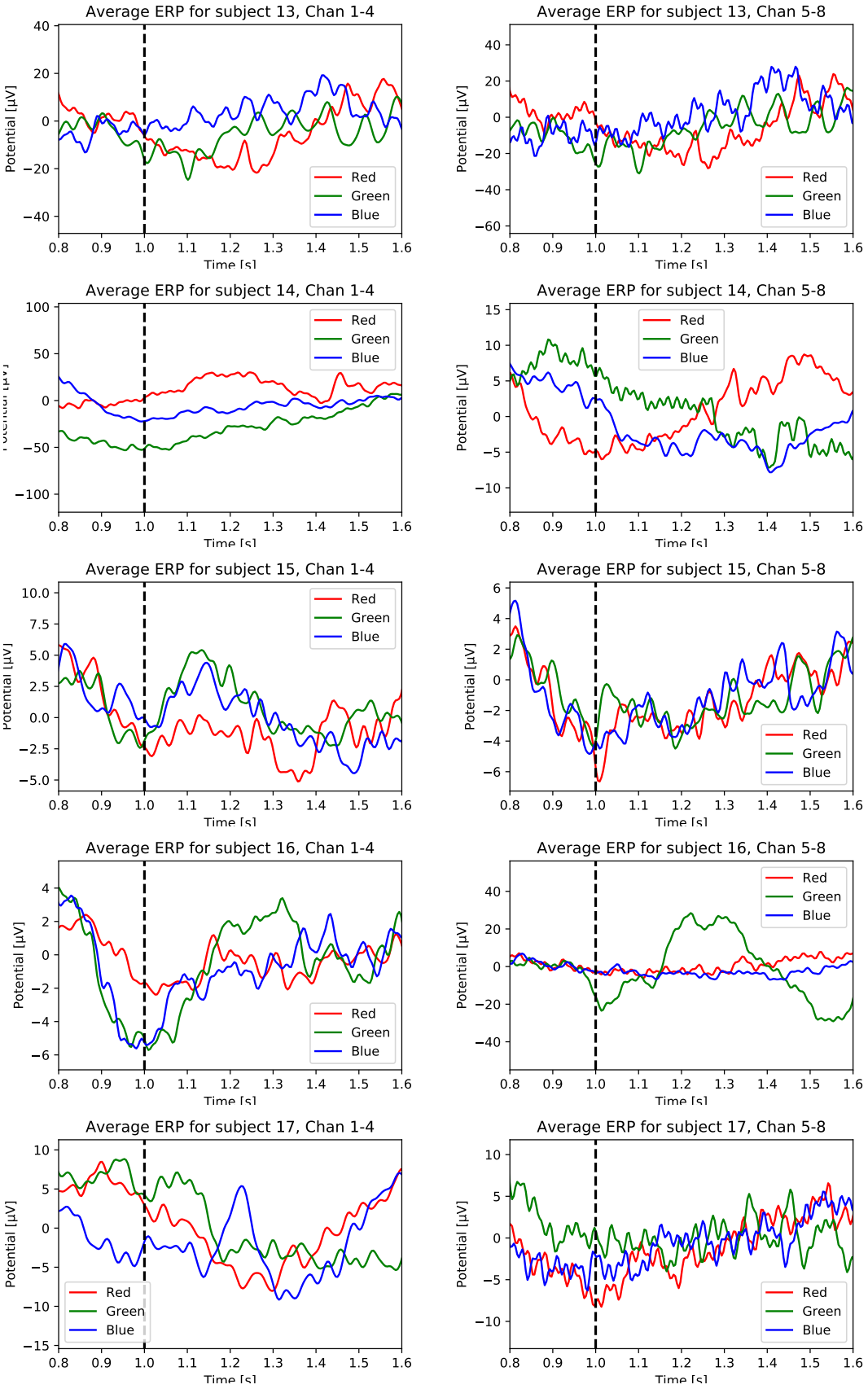


FIGURE B.4: Dataset 1: Individual averaged RGB plots for Chan. 1-4 (left) and Chan. 5-8 (right), part 2.

## B.2 CNN classification reports

The following section includes the classification reports for the CNN presented in Sec. 6.4.

For example, for Tab. B.1, filtering the data slightly benefits the classification using CNN. For the unfiltered Dataset 1, the precision scores are similar for all three classes, while recall is significantly better for one class compared to the others. For the raw data case, the model is relatively good at detecting green but correspondingly bad at detecting the two other colors. This could be an artifact of the NN's random initial state, as no satisfactory learning is observed.

Table B.1: Classification report for CNN - Dataset 1.

| **Input data** | **Epochs** | **Acc.** | **Class** | **Precision** | **Recall** | **f1-score** | **Support** |
|---|---|---|---|---|---|---|---|
| **Raw data** | 100 | 0.28 | R | 0.26 | 0.15 | 0.19 | 168 |
| | | | G | 0.28 | 0.40 | 0.33 | 168 |
| | | | B | 0.29 | 0.28 | 0.29 | 169 |
| **Filtered data** | 30 | 0.36 | R | 0.35 | 0.41 | 0.38 | 168 |
| | | | G | 0.39 | 0.40 | 0.39 | 168 |
| | | | B | 0.35 | 0.28 | 0.31 | 169 |
| **Artifacts removed** | 50 | 0.28 | R | 0.23 | 0.11 | 0.15 | 124 |
| | | | G | 0.29 | 0.52 | 0.38 | 124 |
| | | | B | 0.27 | 0.19 | 0.22 | 124 |
| **Filtered and artifacts removed** | 50 | 0.37 | R | 0.34 | 0.28 | 0.31 | 124 |
| | | | G | 0.38 | 0.37 | 0.38 | 124 |
| | | | B | 0.39 | 0.47 | 0.42 | 124 |

Table B.2: Classification report for CNN - Dataset 2.

| **Input data** | **Epochs** | **Acc.** | **Class** | **Precision** | **Recall** | **f1-score** | **Support** |
|---|---|---|---|---|---|---|---|
| **Pre-processed** | 50 | 0.47 | R | 0.47 | 0.49 | 0.48 | 120 |
| | | | G | 0.48 | 0.41 | 0.44 | 120 |
| | | | B | 0.45 | 0.50 | 0.47 | 121 |

# Appendix C

# Article

Parts of the work done for this master thesis was published as S. Åsly, L.A. Moctezuma, M. Gilde, and M.Molinas, "Towards EEG based signals classification of RGB color based stimuli" at the 8th Graz Brain-Computer Interface Conference 2019. The article is therefore included here as Appendix C.

# TOWARDS EEG-BASED SIGNALS CLASSIFICATION OF RGB COLOR-BASED STIMULI

Sara Åsly[1], Luis Alfredo Moctezuma[1], Monika Gilde[1], Marta Molinas[1]

[1] Department of Engineering Cybernetics, Norwegian University of Science and Technology, Trondheim, Norway

E-mail: sarahaa@stud.ntnu.no

ABSTRACT: This research looks at the possibility to actuate devices by looking at primary colors, thought to be especially useful for individuals having restricted motor control. Analytic and empirical signal analysis methods for analyzing EEG signals produced by subjects exposed to primary colors (RGB) are presented. Methods used are short time Fourier transform (STFT) and Empirical mode decomposition (EMD). Intrinsic mode functions (IMFs) are obtained using EMD, three of which are used for feature extraction. The features are used as inputs for the machine learning algorithms: random forest (RF), support vector machine (SVM), k-nearest neighbors (kNN), decision tree (DT) and naive Bayes (NB). Using data from 7 subjects, a general model classifies RGB with 0.37 accuracy, while the best subject-specific model achieves an accuracy of 0.58, which is above the chance level of 0.33. The classification accuracy between gray and any one of RGB is 0.98 with NB. Results are encouraging and can be improved by further exploring features and classification techniques.

## INTRODUCTION

Electroencephalographic signals (EEG) represent the electrical activity in the brain. By placing electrodes on the scalp, one can record these signals. One electrode records the cumulative electrical activity of neurons. EEG signals are non-stationary, time-dependent, and because of cumulative electrical activity, most likely multi-component signals [1]. Also, non-invasive EEG signals have a small amplitude and are extremely noisy. These properties are but a few of the reasons raw EEG signals do not provide useful information alone, and dedicated signal analysis is therefore required to extract relevant information contained within the signal. Choosing a suitable signal analysis method is a crucial step when extracting information from EEG data. In general, no particular method will provide the best results. The choice of signal analysis tool depends for instance on the characteristics of the signal and the aim of the experiment.

The goal of certain EEG experiments is to classify signals produced by specific brain activity. A feature is an individual measurable property of the process being observed [2], and any recorded EEG activity includes different features [3]. Researchers, therefore, search for a limited amount of features that can differentiate signals with certainty. The process of selecting only a subset of variables in the input which can efficiently describe the data is called feature selection. Feature selection decreases the effect of noise, irrelevant or redundant variables are reduced, and the predictor performance improved [2][4].

Techniques to predict which color a subject is looking at have been explored using indirect approaches such as analyzing psychological and emotional responses to color [5][6]. Classification of EEG signals produced by random visual exposure to primary colors was presented in [7]. Independent component analysis (ICA) was used to remove artifacts. Event-related spectral perturbations (ERSP) were used as features for a support vector machine (SVM), and the highest classification accuracy was 0.97, more information at [3]. In general, empirical mode decomposition (EMD) for feature extraction from color related EEG signals have proven to be successful in several studies [8]. A neural signature of the unique hues (red, yellow, green, and blue) was discovered 230 ms after stimulus onset at a post-perceptual stage of visual processing [9]. The study used ERPs (activity time-locked to an event) evoked in the response to different hues.

In this paper, analytic and empirical signal analysis methods are investigated to evaluate their ability to reveal color specific patterns in EEG signals produced by exposure to RGB. EMD is used as the basis for feature extraction. Identifying a set of features for color identification in EEG signals would enable less complex machine-learning based models, reducing the computational time for real-time color identification. Reliable real-time classification of EEG signals produced by looking at a color could enable physically disabled people with cognitive functions to control their environment. For instance, a user can open and close doors by looking at colored signs. This research is a step towards discovering a combination of signal analysis method, feature extraction technique, and classification algorithm that can be used to determine which color a subject is looking at using EEG signals.

## METHODS AND MATERIALS

*Dataset description:* The dataset consists of EEG signals from 7 subjects that were watching RGB colors presented on a screen. The distance from the screen to the

subject was 3.5m, and the intensity of the colors was constant at $4.5cd/m2$. Each color was presented 60 times to each subject in a randomized order. Gray was used as the base color between RGB exposure. The signals were recorded from channel P1, P2, O1, and O2, according to the 10-20 international system. The acquisition system used was BCI200 with g.tec's MOBIlab portable device and a sampling rate of 256 Hz [7].
In the preprocessing stage, the signals were band-pass filtered from $0.1-30$Hz. To reduce the effect of abnormal values, signals crossing $\pm 60\mu V$ were removed. Also, some trials were excluded due to electromyogram-(EMG) and electrooculogram (EOG) artifacts. The final dataset used in this paper consist of 52 trials for each color, in order to obtain a balanced dataset
Next, the data was re-organized in 3 seconds long "epochs" (768 data points). One epoch contains samples from all channels where the subject is looking at gray for one second, followed by two seconds of looking at one of the RGB colors. The colored light switched on at $t = 1s$ in all the following results.

*Short time Fourier transform (STFT):*
STFT preserves information about the time domain by windowing the signal around a particular instant in time and calculating the local Fourier transform (FT) for each time window. The information obtained from the STFT is presented in a spectrogram. Spectrograms show how the spectral density of a signal varies with time, giving the information about the quantity of the frequency, and at what time this frequency is present.
STFT is limited due to the windowing of the signal, which causes a trade-off between time precision and frequency resolution. Frequency resolution must be sacrificed to detect an event precisely in time, and vice verse. This trade-off between time and frequency resolution makes it essential to choose an appropriate window size to optimize both time and frequency [10].

*Empirical mode decomposition (EMD):*
EMD is a well-known technique used to analyze non-stationary and non-linear data [11]. EMD does not make assumptions regarding stationary or linearity of data, which motivates its use for analyzing EEG data [8]. In contrast to FT and STFT, EMD is data-driven, based on the assumption that a signal consists of several intrinsic mode functions (IMFs), that must satisfy two basic conditions:

- Number of zero-crossings must equal or differ by one compared with the number of extrema in the signal.
- The mean value of the upper and lower envelope of the signal must be equal to zero at any point.

The EMD algorithm finds all the IMFs trough a process called *Sifting*. The calculation of the IMFs given a signal $x(t)$ are done as follows [11]:

1. Identify all extrema (maxima and minima) in $x(t)$
2. Interpolate between minima and maxima, generating the upper and lower envelope; $e_{upper}$ and $e_{lower}$
3. Determine the local mean as $a(t) = \frac{e_{upper}+e_{lower}}{2}$
4. Extract the mean from the signal; $h_1(t) = x(t) - a(t)$
5. Decide whether it is an IMF or not based on two basic conditions for IMFs mentioned above
6. Repeat step 1 to 4 until an IMF is obtained.
7. Subtract the IMF from the original signal
8. Repeat steps 1-6 until there are no IMFs left to extract, the last extraction resulting in a residue

The decomposition is complete when the sum of the IMFs and the residue is negligible.

*Feature extraction and classification:*
The main method used for feature extraction and classification is based on the work presented in [12]. The feature extraction stage for each electrode consists of the computation of energy and fractal features, but additionally, in this paper, a set of statistical values are also computed for each channel. This procedure is illustrated in Fig. 1, and the features are summarized in Tab 1

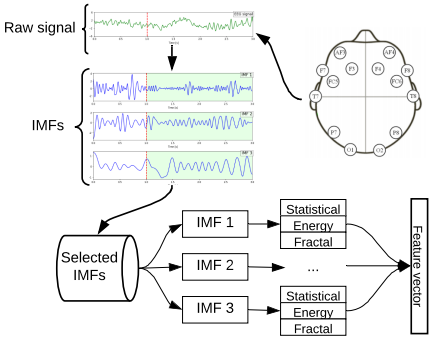


Figure 1: Flowchart illustrating the feature extraction procedure using EMD. The procedure is the same for each channel.

Table 1: Summary of features.

| **Feature type** | **Extracted features** |
|---|---|
| Energy | instantaneous and teager energy |
| Fractal | Petrosian and Higuchi fractal dimension |
| Statistical | min, max, mean, median, variance, standard deviation, kurtosis, skew |

The feature vectors obtained for each channel are concatenated to obtain a single vector for each instance and later used as input to the classifiers. As will be explained later, some experiments consist of using all the features shown in Tab. 1, while for others, only statistical values were used. For example, using all the 12 features, 3 IMFs and 4 channels, the length of the feature vector for an instance is:

$$\text{Features} * \text{Channels} * \text{IMFs} = 12 * 4 * 3 = 144$$

Using only statistical features the length of the feature vector is only 96 for each instance. Note that the features

are computed for each IMF, and all experiments are done with 3 IMFs and 4 channels.
Lastly, supervised machine-learning models were created using 10-folds cross-validation using the accuracy metric. The machine-learning based algorithms used are, random forest (RF), SVM, k-nearest neighbors (kNN), decision tree (DT) and naive Bayes (NB).
To select the best parameters for each classifier, the experiments were repeated using different parameters, thus selecting automatically the classifier with the highest accuracy. The set of parameters for each classifier are listed below:

- Depths for RF: 2, 3, 4, 5, 6, 7, 8
- Neighbors for kNN: 2, 3, 4, 5, 6, 7, 8
- Kernels for SVM: linear (lin.), radial basis function (rbf), sigmoid, polynomial (poly.)

A Gaussian distribution is assumed for the NB classifier, and here the *GaussianNB* from scikit-learn with default parameters are used throughout this work. Unless otherwise stated, default parameters of scikit-learn classifiers are used [13].

RESULTS

*Signal analysis:*
Fig. 2 shows the grand average for each color. The gray background illustrates the duration for which the subject was looking at gray, while the red vertical line indicates the moment of color exposure ($t = 1$).

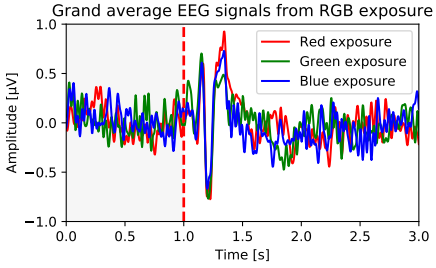


Figure 2: Grand average of all epochs. The colored light is switched on at $t = 1s$

STFT was applied to investigate possible changes of frequencies over the given time period. An STFT with a "Hanning" window size of 200 samples ($\approx 781ms$) overlap off 190 samples ($\approx 742ms$) and sampling frequency of 256 Hz was used to produce the spectrogram in Fig. 3 The spectrogram represents the grand average for RGB respectively. Despite apparent prevalence of noise, there is an amplitude increase in $2-12Hz$ for all colors, and for green there is an amplitude increase for $0-5Hz$ in the time frame $1-2s$. Hence, averaging data reveals a

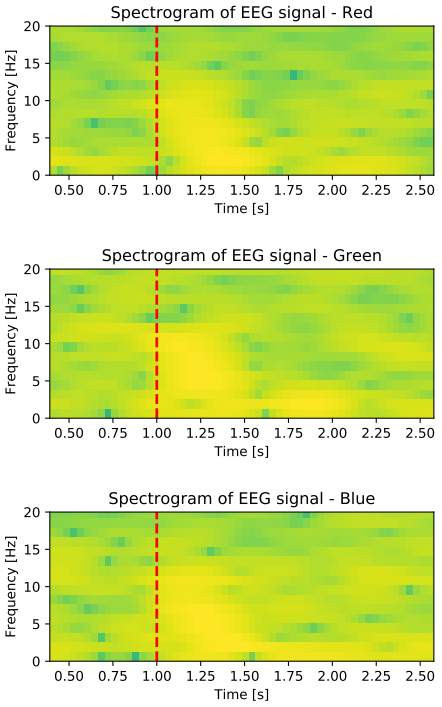


Figure 3: Spectrogram of grand average EEG signal for RGB

change caused by visual stimuli from gray to RGB colors $200-300$ms after exposure. However, is clear from their overlap that frequency alone is not sufficient to separate three colors. In addition, there is no lasting change in frequency, even though all subjects are continuously looking at color from from $t = 1s$ to $t = 3s$. Information gain from STFT is limited, and doubtfully sufficient to reveal a signal feature specific for each of the colors.

For this reason, the EMD algorithm was applied on each raw signal, and after 10 siftings, the residual fulfills IMF requirements discussed in the methodology section. Fig. 4 shows an example of the 5 IMFs and the residual for color green. Note, however, that in the feature extraction stage, this procedure is repeated for all the colors and not only green, as in this example.

EMD does not use windows. Using windows in the analysis of the signal would force the ends to zero, and therefore mask end effects. The end effect problem has not been taken into account in this paper. In Fig. 5 a spectrogram of each of the IMF is plotted. EMD successfully extracts the highest frequency components in the first IMFs. IMF1 reveals slight increase in magnitude for all frequencies at $t \approx 1.5$. This might be related to color exposure or change of mental state for the person in the experiment. Extracted IMFs can be representing the physical prop-

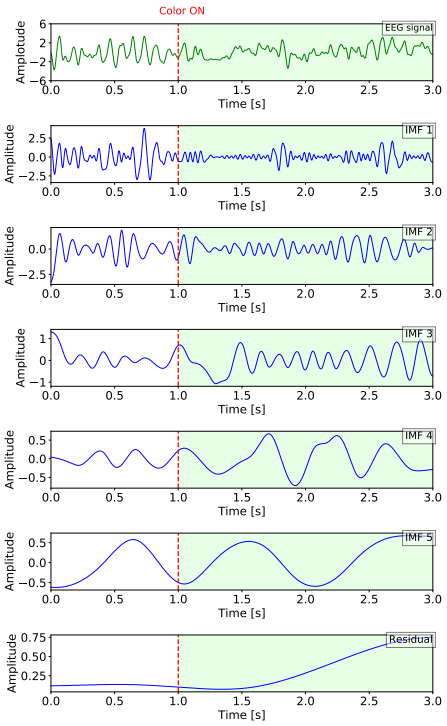


Figure 4: Original EEG signal, extracted IMFs and the residual. Green background represents green light is continuously on

erties of the process from which the signal is obtained. However, the problem of mode mixing in EMD caused by the presence of adjacent frequencies will cause loss of meaningful information in the IMFs. A new method for separating closely spaced spectral tones using EMD is presented in [14][15], and could be implemented to improve results.
Neither spectrograms nor IMFs reveal distinct color dependent frequency or amplitude related characteristic by visual inspection.

*Classification:*
To test if machine-learning models can classify RGB colors from EEG signals using features based on EMD, the following experiments are proposed:

(1) Classify RGB colors from gray color

(2) Classification of red, green and blue considering the EEG signals from all the subjects

(3) Classification of red, green and blue colors for each subject

The first experiment aims to provide experimental information about the performance of the method and to check if there is a feature that can separate these two classes (gray or RGB colors).
In the second experiment mentioned, the classifier consists of three classes (red, green, and blue) intending to check if using the proposed method is possible to differentiate between them. It can be the second step for a real implementation of a BCI based on RGB colors. Since the first step can identify when an RGB color is presented and then recognize the specific color. Following this aim is important to check the feasibility of a general model for the second experiment, that is why the last experiment consists of the same experiment but considering the EEG signals from all the subjects to create the classifier.
For all experiments, the procedure described for *Feature extraction and classification* is used. Accuracy metric after 10-fold cross-validation is presented. All the classifiers are tested with different kernels, the number of neighbors or depth depending on each one, and the best parameters are automatically selected. Note that the chance level for the first experiment is 0.5 of accuracy, and for experiment 2 and 3 it is 0.33

*Experiment (1); gray vs RGB:*
For a possible real-time application, it will be important to clearly distinguish if the subject is looking at nothing in particular, or decisively looking at a color. To simulate "nothing in particular", gray color is used. The complexity of such differentiation was investigated by first classifying if subjects were looking at gray or RGB color. An event-related potential (ERP) (P300) is expected approximately 300*ms* after the presentation of an infrequent stimulus. The part of the signal where the subject is exposed to the color will, therefore, contain the P300 component, and it can easily be distinguished from a signal not containing an ERP. Therefore, classification removing data points between $t = 1-2$ was investigated. Results for gray vs. color classification are presented in Tab. 2.

Table 2: Accuracies (Acc) obtained for the first experiment using all features (all), the statistical features (stat.) and only one statistical feature, the mean (mean).

| **Data** | **Feat.** | **Classifier** | | | | | | | |
|---|---|---|---|---|---|---|---|---|---|
| | | RF | | kNN | | SVM | | DT | NB |
| | | Acc. | depth | Acc. | k | Acc. | ker. | Acc. | Acc. |
| Full | all | **0.99** | 5 | 0.72 | 6 | **0.99** | lin. | 0.98 | 0.98 |
| | stat. | 0.88 | 4 | 0.72 | 6 | **0.92** | lin. | 0.83 | 0.87 |
| | mean | 0.89 | 6 | **0.91** | 8 | 0.84 | rbf | 0.87 | 0.89 |
| Limited* | all | **0.87** | 5 | 0.62 | 4 | 0.85 | lin. | 0.86 | 0.85 |
| | stat. | **0.89** | 6 | 0.62 | 4 | 0.73 | poly | 0.86 | 0.85 |
| | mean | 0.90 | 6 | **0.92** | 4 | 0.87 | rbf | 0.88 | 0.87 |

*Accuracy obtained when removing data points

Surprisingly, when excluding the data samples between $t = 1-2$, the accuracy only decreases with 0.12 using all features. An interesting finding is a 0.92 accuracy when using data without ERP (Limited*), and only one feature; the mean. In this experiment, the lowest accuracy obtained is well above than the chance level, which in two class classification is 0.5. These results yield a promising first step towards a less complex real-time application for separating between gray and RGB colors.

*Experiment (2) and (3); classification of red, green and*

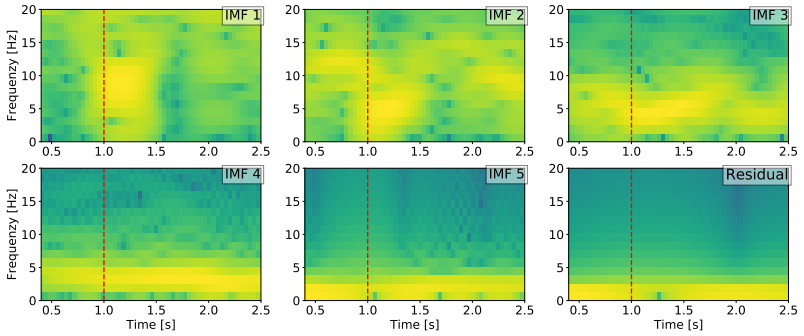


Figure 5: Spectrograms of each of the 5 IMFs and the residual obtained from 10 siftings.

*blue color:*
First, a model including data from all seven subjects was developed (2), reaching a maximum accuracy of 0.37 using both RF with depth 2 and Gaussian NB. A limited amount of data and individual differences are believed to impair the result, and hence, subject-specific models were developed (2). No classifier alone performed better for all subjects, but rather different classifiers yield better results dependent on the subject. There were, in particular, one subject that consistently obtained higher accuracy, when testing with all classifiers: 0.58 of accuracy using NB, 0.51 using linear SVM, 0.47 with 6-NN, 0.53 using DT, and finally 0.57 using RF with depth 4. On the other hand, another subject model classified at chance level. Tab. 3 summarizes accuracies of the RGB models for both a general model and considering each subject separately.

Table 3: Accuracy (Acc) reached for the second and third experiment, classifying red, green and blue colors considering a general model (2) and each subject separately (3)

| Description | **Classifier accuracy** | | | | | | | |
|---|---|---|---|---|---|---|---|---|
| | RF | | kNN | | SVM | | DT | NB |
| | Acc. | depth | Acc. | k | Acc. | kernel | Acc. | Acc. |
| all subjects | **0.37** | 2 | 0.34 | 6 | 0.33 | rbf | 0.35 | **0.37** |
| individual average | **0.41** | ** | 0.37 | ** | 0.39 | ** | 0.39 | 0.38 |
| best individual | 0.57 | 4 | 0.47 | 6 | 0.51 | lin. | 0.53 | **0.58** |

** Average of all individual models. Parameters differs for each subject, hence none of them are listed in particular

The mean accuracy for the subject model is found by finding the maximum accuracy for each subject individually and then performing the mean of these. The best performing classification algorithm differs dependent on the subject, and hence no algorithm, in particular, can be preferred. The maximum accuracy, being 0.58 is the highest individual accuracy obtained for one subject using NB. It should be noted that the chance level for this experiment is 0.33, and the lowest accuracy obtained is still above that value.
The accuracy increase when including only one feature - the mean. A possible explanation can be that redundant features forms the model, due to limited source data.

DISCUSSION

Several methods have been explored in order to check if there exist features that can be useful to describe the EEG data while the subject is looking at gray or RGB colors, and also considering RGB separately. In the signal analysis step, STFT and EMD were investigated.
The EMD method decomposed the original signals from each channel into several IMFs. Since the IMFs alone do not provide any information, they are analyzed further with STFT for visual inspection, and later used as the basis for feature extraction.
None of the methods yields a lasting unique frequency marker sought after for RGB; however, there where clear frequency modulations detected in the spectrogram of each IMF. The frequency modulation after color exposure is confirmed with a successful classification of gray and RGB color with 0.99 of accuracy.
Accuracies from the second experiment, classifying RGB considering all subjects together yields incomplete or inadequate results, considering the chance level of 0.33 for the 3 classes, and with the best accuracy of 0.37 using NB. The highest classification of RGB on an individual subject level was obtained using NB with an accuracy of 0.58. It can be concluded that color classification suffers from subject dependencies. Though NB yields the highest accuracy in the classifications, it should not be concluded as a general preference for RGB classification algorithm.

CONCLUSIONS

These results indicate the feasibility of using the method for feature extraction. Experimental evidence of differences between RGB colors preserved in EEG-data was presented. Further investigation of which features are

best suited to describe the primary colors is suggested as part of the next step towards a less complex classification model.
For a real implementation and future work, ensemble learning should be considered as the best results in this paper were obtained using different classifiers depending on the subject.
Considering the results obtained in this paper and the experiments proposed, it is reasonable to assume that improving the feature extraction stage with a subject tailored system could improve accuracy, which will be tested in future works.

ACKNOWLEDGMENT

This work was supported by Enabling Technologies - NTNU, under the project "David versus Goliath: single-channel EEG unravels its power through adaptive signal analysis - FlexEEG".

REFERENCES

[1] Cohen L. What is a multicomponent signal? Proc. ICASSP. 1992;5:113 –116 vol.5.
[2] Chandrashekar G, Sahin F. A survey on feature selection methods. Computers & Electrical Engineering. 2014;40(No.1):16–28.
[3] Alharbi ET, Rasheed S, Buhari SM. Feature selection algorithm for evoked EEG signal due to RGB colors. 2016 9th International Congress on Image and Signal Processing, BioMedical Engineering and Informatics (CISP-BMEI). 2016:1503–1520.
[4] Guyon I, Elisseeff A. Special issue on variable and feature selection. An Introduction to Variable and Feature Selection. 2003;3:1157–1182.
[5] Yoto A, Katsuura T, Iwanaga K, Shimomura Y. Effects of object color stimuli on human brain activities in perception and attention referred to EEG alpha band response. Journal of physiological anthropology. 2007;26:373–9.
[6] Zhang H, Tang Z. To judge what color the subject watched by color effect on brain activity. IJCSNS International Journal of Computer Science and Network Security. 2011;11(No.2):80–83.
[7] Rasheed S, Marini D. Classification of EEG signals produced by RGB colour stimuli. Journal of Biomedical Engineering and Medical Imaging. 2015;vol. 2(no. 5):p. 56.
[8] Riaz F, Hassan A, Rehman S, Niazi IK, Dremstrup K. Emd-based temporal and spectral features for the classification of EEG signals using supervised learning. IEEE Transactions on Neural Systems and Rehabilitation Engineering. 2016;24:28–35.
[9] Forder L, Bosten J, He X, Franklin A. A neural signature of the unique hues. Scientific Reports. 2017;7.
[10] Allen J. Short term spectral analysis, synthesis, and modification by discrete fourier transform. IEEE Transactions on Acoustics, Speech, and Signal Processing. 1977;25(3):235–238.
[11] Huang NE, Shen Z, Long SR, *et al.* The empirical mode decomposition and the hilbert spectrum for nonlinear and non-stationary time series analysis. Proceedings of the Royal Society A: Mathematical, Physical and Engineering Sciences. 1998;454(1971):903–995.
[12] Moctezuma L, Molinas M. EEG-based subjects identification based on biometrics of imagined speech using emd. Dec. 2018, 458–467.
[13] Pedregosa F, Varoquaux G, Gramfort A, *et al.* Scikit-learn: Machine learning in Python. Journal of Machine Learning Research. 2011;12:2825–2830.
[14] Fosso OB, Molinas M. Method for mode mixing separation in empirical mode decomposition. arXiv preprint arXiv:1709.05547. 2017.
[15] Gao Y, Ge G, Sheng Z, Sang E. Analysis and solution to the mode mixing phenomenon in emd. 2008 Congress on Image and Signal Processing. 2008.